Beyond the SM searches at the LHC: Little Higgs models and Effective Field Theory

Dissertation

zur Erlangung des Doktorgrades

an der Fakultät für Mathematik,

Informatik und Naturwissenschaften

Fachbereich Physik

der Universität Hamburg

vorgelegt von

So Young Shim

aus

Sokcho, Republic of Korea

Hamburg

2018

Gutachter/innen der Dissertation:	Dr. Jürgen Reuter
	Prof. Dr. Gudrid Moortgat–Pick
Zusammensetzung der Prüfungskommission:	Dr. Jürgen Reuter
	Prof. Dr. Gudrid Moortgat–Pick
	Dr. Christophe Grojean
	Prof. Dr. Gregor Kasieczka
	Prof. Dr. Caren Hagner
Vorsitzender der Prüfungskommission:	Prof. Dr. Caren Hagner
Datum der Disputation:	16. April 2018
Vorsitzender des Promotionsausschusses Physik:	Prof. Dr. Wolfgang Hansen
Leiter des Fachbereichs Physik:	Prof. Dr. Michael Potthoff
Dekan der Fakultät MIN:	Prof. Dr. Heinrich Graener

Abstract

In this thesis, we discuss two different approaches to physics beyond the Standard Model.

First, we study a model-independent Effective Field Theory formalism. In particular, we focus on bosonic $\mathcal{CP}$-even six-dimensional operators. We implement them into the Monte Carlo Event Generator `WHIZARD`, which is used to obtain preliminary results on their effect on Higgs production at e^+e^- colliders.

Next, we discuss Little Higgs models as a possible solution to the hierarchy problem. In particular, we detail how the Littlest Higgs model with T-parity (LHT) addresses the hierarchy problem. Quadratically divergent radiative corrections induced by the top quark or electroweak gauge bosons vanish in Little Higgs models by the Collective Symmetry Breaking mechanism. They are forbidden or canceled by loop diagrams mediated by Little Higgs model particles. The T-parity has been introduced to improve on electroweak precision observables and also generates dark matter candidates. As an indicator of naturalness we define the fine-tuning level defined by the size of radiative corrections to the Higgs mass.

To validate our analysis framework, the exclusions limits from LHC data at 8 TeV and electroweak precision observables are reproduced. Then, we recast 13 TeV LHC searches from ATLAS and CMS to determine the limits on the parameter space in a more sophisticated recast framework than that has done before by setting up several different benchmark scenarios in order to scan the parameter space according to mass hierarchies and different patterns of production and decay channels. We show the improvement of 13 over 8 TeV data with also a larger data set, and study the rising tension on fine-tuning. The extrapolated results to the high-luminosity phase of LHC at 14 TeV are shown. Also, we combine the collider results with electroweak precision observables and projections for the LHC high-luminosity phase are given.

Zusammenfassung

In dieser Arbeit diskutieren wir zwei verschiedene Ansätze für Physik jenseits des Standardmodells.

Zunächst betrachten wir einen modellunabhängigen Formalismus mittels effektiver Feldtheorie. Insbesondere studieren wir bosonische, CP-gerade sechsdimensionale Operatoren. Wir implementieren diese im Monte Carlo Eventgenerator WHIZARD, womit wir vorläufige Ergebnisse ihres Effekts auf Higgsproduktion an Elektron-Positron-Collidern erhalten.

Danach betrachten wir das Little-Higgs-Modell als mögliche Lösung des Hierarchieproblems. Insbesondere zeigen wir, wie das Hierarchieproblem im Little-Higgs-Modell mit T-Parität (LHT) gelöst wird. Quadratisch divergente Strahlungskorrekturen auf Grund von top-Quarks oder elektroschwachen Eichbosonen verschwinden im Little-Higgs-Modell auf Grund des kollektiven Symmetriebrechungsmechanismus. Sie sind verboten oder werden durch Schleifendiagramme mit Little-Higgs-Teilchen aufgehoben. Die T-Parität wurde wegen elektroschwachen Präzisionsobservablen eingeführt und erzeugt zudem Teilchen, die als Dunkle Materie in Betracht kommen. Wir führen einen Indikator der Natürlichkeit ein, der den Grad des Fine-tunings als die Größe der Strahlungskorrekturen zur Higgsmasse definiert.

Zur Validierung unserer Analyse reproduzieren wir zunächst die Ausschlussgrenzen auf Grund von LHC-Daten bei 8 TeV und elektroschwacher Präzisionsobservablen. Dann reformulieren wir 13 TeV Suchen von ATLAS und CMS zur Bestimmung des zulässigen Parameterraums in einem besseren Verfahren als bisher verfügbar, indem wir mehrere Szenarien definieren, mittels derer der Parameterraum gemäß Massenhierarchien und verschiedenen Produktions- und Zerfallskanälen durchsucht wird. Wir zeigen die Verbesserung der Ausschlussgrenzen durch Benutzung der 13 TeV Daten im Vergleich zu 8 TeV Daten und betrachten die zunehmenden Einschränkungen des Fine-tunings. Zudem extrapolieren wir unsere Ergebnisse zur Hochluminositätsphase des LHC bei 14 TeV und kombinieren diese mit elektroschwachen Präzisionsobservablen.

List of publications

This thesis is based on the following publications:

- [1] de Florian, D. and others, LHC Higgs Cross Section Working Group, *Handbook of LHC Higgs Cross Sections: 4. Deciphering the Nature of the Higgs Sector*, [1610.07922]
- [2] Dercks, Daniel and Moortgat-Pick, Gudrid and Reuter, Jürgen and Shim, So Young *The fate of the Littlest Higgs Model with T-parity under 13 TeV LHC Data*, [1801.06499]

Contents

Chapter 1.

Introduction

The Large Hadron Collider succesfully started to run in September, 2008 and enormous amount of data have been produced from proton-proton collisions at center-of-mass energies $\sqrt{s} = 7,\ 8,$ and 13 TeV. Predictions of the Standard Model have been corroborated by the experiments at the LHC. In particular, the scalar particle that has been predicted by Robert Brout and François Englert [3], by Peter Higgs [4], and by Gerald Guralnik, Carl R. Hagen and Tom Kibble [5], namely the *Higgs* boson, has been discovered with its mass around 125 GeV and was announced on the 4th of July, 2012.

Since then, the couplings to the Higgs as well as the electroweak quantities of Z boson resonance, have been measured precisely. This not only validates the SM predictions, but also provides severe constraints for physics beyond the SM.

From the fact that the Higgs boson has a mass of 125 GeV we know that the SM vacuum is in the metastable state [6–8], but the Standard Model does not explain the reason why the Higgs boson mass is 125 GeV thereby leading to this metastable state. Not only that, the SM cannot provide answers for such questions as what does dark matter consist of; and why is the amount of matter in the universe asymmetric to that of antimatter?

Also, the fact that the mass of the SM-like Higgs boson is 125 GeV implies a *hierarchy problem* that is originated by the discrepancy between the Fermi scale and the Plank scale. The weak or Fermi scale given by either the Higgs mass of 125 GeV or its vacuum expectation value of 246 GeV is much lower than the Planck scale at 10^19 GeV.

Although these shortcomings are not addressed by the SM, they can guide us in our path to a more fundamental theory. There have been many ideas applied to solve the aforementioned problems. One of the most famous examples is the Minimal Supersymmetric Standard Model. The MSSM resolves the hierarchy problem via cancellations induced by the superpartner's loop diagram.

Another way to resolve the hierarchy problem is the so-called *Collective Symmetry Breaking* mechanism derived from *dimensional deconstruction* [9,10]. The Collective Symmetry Breaking mechanism is a crucial key for *Little Higgs* models. Little Higgs models take the point of view that the Higgs is a Goldstone boson generated by spontaneous symmetry breaking. We study this core mechanism of the Little Higgs models and their variations, and how its discrete symmetry, T-parity, can ease constraints originating from electroweak precision observables e.g. Z boson mass, Fermi coupling constant, and etc.

By making use of Monte Carlo simulation program packages CheckMATE and `WHIZARD`, we test the Littlest Higgs model by comparing several featured processes to LHC Run 2 data at $\sqrt{s} = 13$ TeV. We investigate the bounds in the model's parameter space.

Besides searches for new physics in terms of well-defined models, one can describe deviations from the SM originating from any kind of new physics by the mechanism of effective field

theory. Here, the only assumptions are that the only light degrees of freedom as well as interactions and symmetries among them are those of the SM.

Structure of the thesis

In **Chapter 2**, we review the group structure and symmetry of the Standard Model and how the Higgs acquires the vacuum expectation value via the spontaneous symmetry breaking mechanism. Also, shortcomings of the SM are discussed, in particular the hierarchy problem. In **Chapter 3**, we study the effective field theory formalism is an expansion in inverse powers of the energy scale where new degrees of freedom have been integrated out, parameterizing possible deviations from the SM. In particular, we review the six-dimensional operators and their associated vertices and implement them into `WHIZARD`.

Chapter 4 is dedicated to a self-contained introduction to the Little Higgs model. We describe how the Collective Symmetry Breaking mechanism protects the Higgs mass and how the mechanism is realized in Little Higgs models. We also discuss how a discrete symmetry, T-parity, eases constraints for electroweak precision data. In **Chapter 5**, we scrutinize the phenomenology of the Littlest Higgs model with T-parity. We consider several Little Higgs benchmarks for interesting regions of parameter space and briefly review a Monte Carlo program, CheckMATE. In **Chapter 6**, we use CheckMATE to compare of results for the benchmark Littlest Higgs models LHC RUN 2 data at $\sqrt{s} = 13\,\text{TeV}$. Finally, in **Chapter 7** we summarize the results of Chapter 6 and conclude.

Chapter 2.

The Standard Electroweak Theory

This chapter is a brief introduction to the Standard model of particle physics. We describe fundamental interactions and relevant field contents in the SM. Reviewing the spontaneous symmetry breaking of the SM gauge group gives insight into the SM particle mass terms. We depict a good method to parameterize radiative corrections in the self-energies of the electroweak gauge bosons, so-called S, T, and U. As the corrections are only in loops of these self-energies and not connected to the external fermion lines into which these self-energies are inserted at lepton and hadron collider processes, they are called oblique corrections. We also explain the shortcomings of the SM such as the hierarchy problem. The main resources of this chapter are Refs. [11–15]

2.1. The Standard model

The Standard Model is a gauge theory based on the gauge group $SU(3)_C \times SU(2)_W \times U(1)_Y$. This theory explains how elementary particles interact with each other. The fundamental interactions are considered as two parts: Quantum Chromodynamics explaining the strong interaction and Glashow-Weinberg-Salam theory of the electroweak interaction.

Gauge bosons mediate the interactions. Gluons are mediators of the strong interaction with color charge. Since $SU(3)$ is a dimension-8 group, there are 8 different gluons, according to the 8 traceless combinations of color and anti-color. The $SU(3)_c$ symmetry of the strong interaction is unbroken and can be observed indirectly via quark confinement phenomena.

Because $SU(2)\times U(1)$ is a 4-dimensional group, there are 4 gauge bosons: W^i $(i = 1, 2, 3)$ and B. After the electroweak symmetry breaking W^3 and B mix and become Z boson and photon γ state. $W^\pm$ and Z constitute the weak interaction and A photon γ does in the electromagnetic interaction.

The $SU(2)_L \times U(1)_Y$ symmetry is conserved only if all fermions vanished. Through a spontaneous symmetry breaking, the $SU(2)_L \times U(1)_Y$ symmetry is broken to $U(1)_{em}$, which results in that the gauge bosons states mix and particles get mass terms. We discuss the symmetry breaking mechanism, so-called the Higgs mechanism in the following section.

Particles are classified according to the spin of particles and the statistics they obey; The gauge bosons mentioned above have integer spin number and obey the Bose-Einstein statistics, categorized as *bosons*. *Fermions* have half-integer spin number, which let the particles follow the Fermi-Dirac statistics. We categorize fermions in two groups depending whether they do have a non-vanishing color charge or not. They are called quarks and lepton, respectively.

Quarks have color charge as well as electric charge Q and hypercharge Y. There are three

generations for quarks and their fundamental representations are given as following.

$$Q_L = \begin{pmatrix} u \\ d \end{pmatrix}, \begin{pmatrix} c \\ s \end{pmatrix}, \begin{pmatrix} t \\ b \end{pmatrix}, \qquad u_R,\ d_R, \quad c_R,\ s_R, \quad t_R,\ b_R, \tag{2.1}$$

$$\ell_L = \begin{pmatrix} e \\ \nu_e \end{pmatrix}, \begin{pmatrix} \mu \\ \nu_\mu \end{pmatrix}, \begin{pmatrix} \tau \\ \nu_\tau \end{pmatrix}, \qquad e_R, \quad \mu_R, \quad \tau_R. \tag{2.2}$$

They are the first, second and third generation of quarks and leptons, respectively. Eq. (2.1) are quarks. Leptons of Eq. (2.2) do not carry color charge. And the subscript L refers the to left-handed particle and R to the right-handed one. Note that there is no right-handed neutrinos. Neutrinos are in principle strictly massless in the (original) SM, but have been shown to carry mass by neutrino oscillation experiments. This also serves as a good probe for new physics.

In the SM, the interactions are expressed by the Lagrangian as

$$\mathcal{L} = \mathcal{L}_{\text{gauge}} + \mathcal{L}_f + \mathcal{L}_\phi + \mathcal{L}_{\text{Yuk}}, \tag{2.3}$$

which consists of gauge, fermion, Higgs and Yukawa sector in order. We focus on the electroweak interactions.

The Lagrangian of the gauge sector is given by

$$\mathcal{L}_{\text{gauge}} = -\frac{1}{4} W^i_{\mu\nu} W^{\mu\nu i} - \frac{1}{4} B_{\mu\nu} B^{\mu\nu} \tag{2.4}$$

where $W_{\mu\nu}$ and $B_{\mu\nu}$ are the field strength tensors for $SU(2)$ and $U(1)$ respectively. They are defined as

$$W^i_{\mu\nu} = \partial_\mu W^i_\nu - \partial_\nu W^i_\mu - g\epsilon_{ijk} W^j_\mu W^k_\nu, \quad i,j,k = 1, \cdots, 3 \tag{2.5}$$

$$B^i_{\mu\nu} = \partial_\mu B_\nu - \partial_\nu B_\mu, \tag{2.6}$$

where ϵ_{ijk} are the group structure constants of $SU(2)$. The Lagrangian in Eq. (2.4) contains also three- and four-point self-interactions of W^i. But the gauge boson B of Abelian group $U(1)$ does not have self-interactions.

Because of the chirality of $SU(2)_L \times U(1)_Y$, mass terms for fermions are not allowed yet and the Lagrangian for fermions are given by

$$\mathcal{L}_f \supset \sum (\bar{q} i \not{D} q + \bar{\ell} i \not{D} \ell) \tag{2.7}$$

where q is quark and ℓ is leptons and it sums over the generations. The gauge covariant derivative is given by

$$D_\mu q = \left(\partial_\mu + \frac{ig}{2} \vec{\tau} \cdot \vec{W}_\mu + ig' Y \cdot B_\mu \right) q \tag{2.8}$$

with $\not{D} = \gamma_\mu D^\mu$. g and g' are the gauge coupling constants of $SU(2)_W$ and $U(1)_Y$ respectively. $\vec{\tau}$ refers to Pauli matrices and Y is the hypercharge for $U(1)$. The electric charge Q is related to the hypercharge by Gell-Mann-Nishijima formula as

$$Q = I_3 + \frac{1}{2}Y \tag{2.9}$$

where I_3 is the third component of isospin.

The Lagrangian for scalar fields is

$$\mathcal{L}_\phi = (D^\mu \phi)^\dagger D_\mu \phi - V(\phi), \tag{2.10}$$

where $\phi = \begin{pmatrix} \phi^+ \\ \phi^0 \end{pmatrix}$ is a complex scalar field. The gauge covariant derivative is given by

$$D_\mu \phi = \left(\partial_\mu + \frac{ig}{2}\vec{\tau} \cdot \vec{W}_\mu + \frac{ig'}{2} B_\mu \right) \phi \tag{2.11}$$

$V(\phi)$ is the Higgs potential. Imposing invariance under $SU(2) \times U(1)$ transformations and renormalizability, V is given by

$$V(\phi) = \mu^2 \phi^\dagger \phi + \lambda (\phi^\dagger \phi)^2. \tag{2.12}$$

The coefficient μ^2 of $\phi^\dagger\phi$ gives a condition for spontaneous symmetry breaking; μ^2 has to be smaller than zero. For the case of spontaneous symmetry breaking, the vacuum expectation value (*vev*) of ϕ^0, $< 0|\phi^0|0 >$, generates W and Z boson masses. The λ term is related to the self-interaction $\lambda(\phi^-\phi^+\phi^{0\dagger}\phi)^2$ of the Higgs fields and also related to vacuum stability, $\lambda > 0$ to bound the potential.

Next, we discuss the coupling between the Higgs doublet and the fermions as Yukawa couplings.

$$\mathcal{L}_{\text{Yuk}} \supset - \sum_{m,n=1} \left[Y^u_{mn} \bar{q}_{mL} \tilde{\phi} u_{nR} + Y^d_{mn} \bar{q}_{mL} \phi d_{nR} + Y^\ell_{mn} \bar{\ell}_{mL} \phi e_{nR} \right] + \text{h.c.} \tag{2.13}$$

where $\tilde{\phi} \equiv i\sigma^2 \phi^\dagger$, and m, n are $1, 2, 3$ and it sum over the fermion generation number. Y_{mn} are matrices that are matrices that after SSB yield masses and mixings among the fermions. If the Y's are not real and that phase(s) could not be absorbed in a field redefinition as for two generations, then there will be $\mathcal{CP}$ violation. These represent vertices of Yukawa couplings between fermions and ϕ.

2.2. Spontaneous symmetry breaking: The Higgs mechanism

Gauge invariance of the SM Lagrangian demands the mass terms of gauge bosons to be zero. But from the experiments we know gauge bosons are massive except for the photon. By introducing a scalar field and redefining the minimum point of its potential algebraically, we

can give mass terms to gauge bosons. In the following, we describe the Higgs mechanism.

Consider the Abelian case with the Lagrangian

$$\mathcal{L} \ = \mathcal{L}_{\text{kin}}(\phi, A^{\mu}) \ - V(\phi) \qquad \text{where} \quad V(\phi) = \mu^2\phi^*\phi + \lambda(\phi^*\phi)^2, \tag{2.14}$$

which is invariant under the gauge transformations;

$$\begin{aligned} \phi \rightarrow \ \phi' \ &= e^{ig\chi(x)}\phi \\ A^{\mu} \rightarrow \ A'^{\mu} \ &= A^{\mu} - \partial^{\mu}\chi(x) \\ D^{\mu} &= \partial^{\mu} + igA^{\mu}. \end{aligned} \tag{2.15}$$

Here ϕ is a single-component complex scalar field that is considered for this simpler example, A is a gauge boson and $F^{\mu\nu} = \partial^{\mu}A^{\nu} - \partial^{\nu}A^{\mu}$ is the Abelian field strength of this toy example and an antisymmetric tensor. D^{μ} is the covariant derivative.

The potential $V(\phi)$ has its minimum at

$$\phi = \sqrt{\frac{\mu^2}{2\lambda}} = \frac{v}{\sqrt{2}} \tag{2.16}$$

where v is the vacuum expectation value (*vev*). We redefine the scalar field using the *vev*,

$$\phi \ = \ \frac{(v + h(x))}{\sqrt{2}}, \tag{2.17}$$

where $h(x)$ is a real field. We expand the Lagrangian with this new expression for ϕ,

$$\mathcal{L} \ = \ \frac{1}{2}[(\partial_{\mu} - igA_{\mu})(v + h)(\partial_{\mu} + igA_{\mu})(v + h)] + \frac{1}{2}\mu^2(v + h)^2 - \frac{1}{4}\lambda(v + h)^4 - \frac{1}{4}F^{\mu\nu}F_{\mu\nu}.$$

This expression gives us the mass term of gauge boson A as $(g^2v^2/2)A^{\mu}A_{\mu}$, and that of the scalar boson h as λv^2h^2. Note that we can observe terms that are related with field strength and self-interaction, h^3, h^4, h^2AA, and etc.

If the scalar field is a doublet as in the SM, we can rewrite ϕ as

$$\phi = \begin{pmatrix} \phi^+ \\ \phi^0 \end{pmatrix} = \begin{pmatrix} \frac{1}{\sqrt{2}}(\phi_1 + i\phi_2) \\ \frac{1}{\sqrt{2}}(\phi_3 + i\phi_4) \end{pmatrix} \tag{2.18}$$

which consists of four real fields. Then, the Higgs potential Eq. (2.12) turns into

$$V(\phi) = \frac{1}{2}\mu^2\left(\sum_{i=1}^{4}\phi_i^2\right) - \frac{1}{4}\lambda\left(\sum_{i=1}^{4}\phi_i^2\right)^2, \tag{2.19}$$

which is invariant under $SU(2) \times U(1)$. Finding minimum, setting the *vev* and redefining the

scalar field as in Eqs. (2.16) and (2.17), we get

$$v = \sqrt{\frac{-\mu^2}{\lambda}}, \qquad \phi = \frac{1}{\sqrt{2}} \begin{pmatrix} 0 \\ v + H \end{pmatrix} \tag{2.20}$$

in the unitary gauge. H is the physical Higgs boson field.

2.3. SM Lagrangian after spontaneous symmetry breaking

Gauge and Higgs sectors

After spontaneous symmetry breaking (SSB), the SM Lagrangian can be expanded using the re-defined fields in the unitary gauge.

The *vev* terms of the Higgs covariant kinetic Lagrangian term generate the mass terms of gauge bosons W and Z. The Higgs kinetic term in the Lagrangian is

$$(D_\mu \phi)^\dagger D^\mu \phi \supset \frac{1}{2}(0\ v) \left[\frac{g}{2} \tau^i W_\mu^i + \frac{g'}{2} B_\mu \right]^2 \begin{pmatrix} 0 \\ v \end{pmatrix} \tag{2.21}$$

$$= \frac{g^2 v^2}{4} W^{+\mu} W_\mu^- + \frac{1}{2}(g^2 + g'^2) \frac{v^2}{4} Z^\mu Z_\mu. \tag{2.22}$$

To go from Eq. (2.21) to Eq. (2.22), we used

$$W^\pm = \frac{W^1 \mp i W^2}{\sqrt{2}}, \qquad \tau^\pm = \frac{\tau^1 \pm i \tau^2}{2}, \tag{2.23}$$

$$Z \equiv \frac{-g' B_\mu + g W_\mu^3}{\sqrt{g^2 + g'^2}} = -\sin\theta_W B + \cos\theta_W W^3, \tag{2.24}$$

where $\theta_W = \tan^{-1}(\frac{g'}{g})$ and Z is a linear combination of W_μ^3 and B_μ. Its orthogonal combination is the photon, $A = \cos\theta_W B + \sin\theta_W W^3$. The complex charged gauge bosons $W^\pm$ mediate the charged current interactions, while Z mediates the neutral current interaction.

The first term of Eq. (2.22) is a mass term for the W bosons and the second term is that for the Z boson,

$$M_W = \frac{gv}{2}, \qquad M_Z = \frac{\sqrt{g^2 + g'^2} v}{2} = \frac{M_W}{\cos\theta_W}, \qquad M_A = 0 \tag{2.25}$$

which yield the relations

$$\sin^2\theta_W = 1 - \frac{M_W^2}{M_Z^2}. \tag{2.26}$$

$$\tag{2.27}$$

The Higgs potential implies *custodial symmetry*, which originates from the fact that the

Higgs potential has larger symmetry than the gauge symmetry of the SM. The Higgs can be represented as a doubletand there is $SU(2)_W$ symmetry that acts on the Higgs doublet in the SM. In addition, another global $SU(2)$ symmetry can be introduced, namely $SU(2)_R$, such that the $SU(2)_R$ symmetry acts on the Higgs doublet. When we replace W with L, the Higgs doublet has a representation of the $SU(2)_L \times SU(2)_R$. Under the $SU(2)_L \times SU(2)_R$ symmetry, the kinetic term $D^\mu H^\dagger D_\mu H$, the mass term $H^\dagger H$, and the self-interaction term $(H^\dagger H)$ are invariant. But, we can infer the fact that this symmetry is not exact and should be broken from the Yukawa couplings of fermions. If the $SU(2)_L \times SU(2)_R$ symmetry is exact, the up-type and the down-type quarks have the same Yukawa couplings, which is not true. The hypercharge $U(1)_Y$ of the SM has a small gauge coupling constant. With an assumption that the gauge coupling is zero, the $SU(2)_R$ can be left unbroken. But, the $U(1)_Y$ is weakly gauged and the gauge coupling constant is not vanished. Thus, the $SU(2)_R$ is broken explicitly. As the Higgs doublet gains the vacuum expectation value, the $SU(2)_L \times SU(2)_R$ symmetry is broken the diagonal subgroup $SU(2)_c$ and this approximate symmetry is called the custodial symmetry. The custodial symmetry is parameterized with ρ as

$$\rho = \frac{M_W^2}{M_Z^2 \cos^2 \theta_W}. \tag{2.28}$$

At the tree level, the relation, $\rho = 1$, is kept.

Before SSB, 4 massless EW gauge bosons exist with 2 helicities for each as well as 4 Hermitian scalars. After the symmetry breaking, 3 scalars are eaten by gauge bosons as longitudinal components, and thus the gauge bosons become massive $W^\pm$, Z bosons with 3 helicities, although the photon, γ, remains massless with 2 helicities. The Total number of degree of freedom, 12, remains unchanged.

The weak scale *vev*, v is given as

$$v = \frac{2M_W}{g} \simeq (\sqrt{2}G_F)^{-1/2} \simeq 246\,\text{GeV} \tag{2.29}$$

where the Fermi constant is determined by the muon lifetime.

The full Higgs Lagrangian is therefore

$$\begin{aligned} \mathcal{L}_\phi =& (D^\mu \phi)^\dagger D_\mu \phi - V(\phi) && (2.30) \\ =& M_W^2 W^{\mu+} W_\mu^- \left(1 + \frac{H}{v}\right)^2 + \frac{1}{2} M_Z^2 Z^\mu Z_\mu \left(1 + \frac{H}{v}\right)^2 + \frac{1}{2} (\partial_\mu H)^2 - V(\phi). && (2.31) \end{aligned}$$

In the unitary gauge, the Higgs potential can be written as

$$V(\phi) = -\frac{\mu^4}{4\lambda} - \mu^2 H^2 + \lambda v H^3 + \frac{\lambda}{4} H^4. \tag{2.32}$$

In the potential, the Higgs mass term at tree level $\sim \sqrt{-2\mu^2} = \sqrt{2\lambda} v$. Before the Higgs was observed at around 125GeV, λ was open to all values $(0, \infty)$. Theoretically lower limits from vacuum stability and upper limit from unitarity and perturbativity were expected, but there was no direct prediction. λ as in the last two terms of Eq. (2.30) is related to cubic and quartic

self-interactions of the Higgs.

Yukawa sector

After EW symmetry breaking, fermion sectors get mass terms through Yukawa couplings. The arbitrary matrices Y in Eq. (2.13) become mass and mixing matrices for fermions.

$$\begin{aligned} -\mathcal{L}_{\text{Yuk}} \supset & \sum_{m,n=1} \bar{q}_{mL} Y^u_{mn} \left(\frac{v+H}{\sqrt{2}} \right) u_{nR} + \text{h.c.} \\ & = \bar{q}_L (M^u_{mn} + y^u_{mn} H) u_R + \text{h.c.} \end{aligned} \tag{2.33}$$

where $\bar{q}_L$ is a column vector for the left-handed quarks and M^u is fermion mass matrix with

$$M^u = Y^u_{mn} \frac{v}{\sqrt{2}}, \tag{2.34}$$

$$y^u_{mn} = \frac{M^u_{mn}}{v} = \frac{g M^u_{mn}}{2 M_W}. \tag{2.35}$$

y^u is the Yukawa coupling matrix that is given by

To identify the physical particle content, we need to diagonalize the matrix M with unitary transformations V_L and V_R such that

$$V_L^{u\dagger} M^u V_R^u = M^u_{diag} = \begin{pmatrix} M_u & 0 & 0 \\ 0 & M_c & 0 \\ 0 & 0 & M_t \end{pmatrix}. \tag{2.36}$$

The diagonalization cannot be done simultaneously for up- and down-type quarks, and that the mismatch between the two is the CKM matrix. There are now especially some flavor anomalies at LHC.

2.4. Electroweak Precision observables

The predictions of the SM agree to the observations to high precision. This gives rise to constraints on physics beyond the SM. Prominent SM precision observables are, for example, the W boson mass, the weak mixing angle $\sin\theta_W$, forward-backward and left-right asymmetries for various SM fermions measured on the Z pole resonance. and the anomalous muon magnetic moment, $g_\mu - 2$.

Also, the self interactions of electroweak gauge bosons triple and quartic gauge couplings of the electroweak fill in this class of electroweak precision measurements.

The Peskin-Takeuchi S, T and U parameters [16]. express the (oblique) radiative corrections to these EWPO. New physics effects such as new heavy gauge bosons can impact such observables.

In the following we have a look these so called oblique corrections in the SM and later how new physics impacts them.

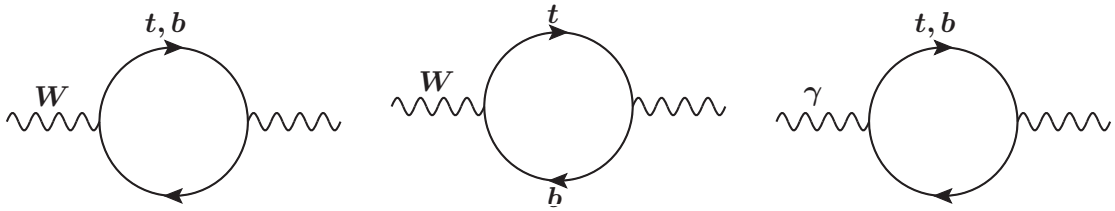

Fig. 2.1.: Examples of one-loop corrections to weak interaction observables

S, T, and U parametrization

In electroweak precision measurements, vacuum-polarization effects is one of the important ways to calculate precision observables and to take into account new physics effects. S, T, and U are defined through the measurements and parameterize the (oblique) radiative corrections to these electroweak precision observables like Fig. 2.1.

When considering bubbles of the $SU(2) \times U(1)$ gauge bosons, we denote the vacuum polarization amplitudes as one particle irreducible propagator,

$$\Pi_{IJ}^{\mu\nu}(q) = \Pi_{IJ}(q^2) g^{\mu\nu} - \Delta(q^2) q^\mu q^\nu, \tag{2.37}$$

where I, J refer to gauge bosons. q^μ, q^ν produce light lepton masses which are negligible. If those vacuum polarization diagrams are inserted in or sandwiched between conserved on-shell light-fermion currents like e.g. in $ee \to jj$ or so, then by means of the Dirac equation q^μ generates a term proportional to the mass term of the electron of the quark.The two pieces Π and Δ are the longitudinal and transversal part of the self-energy, respectively.

For example, the one-loop self-energy correction of W bosons are denoted by $\Pi_{WW}(q)$ and add up to the mass of W boson as

$$M_W^2 = g^2 \frac{v^2}{4} + \Pi_{WW}(M_W^2). \tag{2.38}$$

Part of the renormalization of the kinetic terms of the gauge bosons. can be denoted in the Lagrangian of the form:

$$\mathcal{L}_{V^2} = -\frac{1}{2} W_3^\mu \Pi_{33}(p^2) W_{3\mu} - W_3^\mu \Pi_{3B}(p^2) B_\mu - \frac{1}{2} B^\mu \Pi_{BB}(p^2) B_\mu - W_+^\mu \Pi_{+-}(p^2) W_{-\mu} \ , \tag{2.39}$$

where $\Pi(p^2)$ is the vacuum polarization amplitudes. In Eq. (2.39), each loop amplitude can be affected by both SM and new physics contributions.

Assuming q^2 is small, the amplitude of the vacuum polarizations can be expanded as

$$\Pi(p^2) \ = \ \Pi(0) + p^2 \Pi'(0) + \frac{p^4}{2} \Pi''(0) + \mathcal{O}(p^6). \tag{2.40}$$

Then terms of Eq. (2.39) generate 12 form factors. Three of them are fixed by experimental measurements; $\Pi'_{+-}(0) = \Pi'_{BB}(0) = 1$ for the normalization of the gauge coupling constants and $\Pi_{+-}(0) = -M_W^2$ for the renormalized W boson mass. Also, $\Pi_{Z\gamma}(0)$ and $\Pi_{\gamma\gamma}(0)$ are zero

since the photon is massless.

We define other form factors, $\hat{S}$, $\hat{T}$, $\hat{U}$, $\hat{V}$, $\hat{X}$, $\hat{Y}$ and $\hat{W}$ as defined in Ref. [17]:

$$\hat{S} = \frac{g}{g'}\Pi'_{3B}(0), \quad \hat{T} = \frac{\Pi_{33}(0) - \Pi_{+-}(0)}{M_W^2}, \quad \hat{U} = \Pi'_{+-}(0) - \Pi_{33}(0)' \tag{2.41}$$

$$V = \frac{M_W^2}{2}\left(\Pi''_{33}(0) - \Pi''_{+-}(0)\right), \qquad X = \frac{M_W^2}{2}\Pi''_{3B}(0), \tag{2.42}$$

$$Y = \frac{M_W^2}{2}\Pi''_{BB}(0), \qquad W = \frac{M_W^2}{2}\Pi''_{33}(0). \tag{2.43}$$

They are related to the original S, T, and U parameters defined in Ref. [16] as follows

$$S = \frac{4s_W^2\hat{S}}{\alpha_W}, \qquad T = \frac{\hat{T}}{\alpha_W}, \qquad U = -\frac{4s_W^2\hat{U}}{\alpha_W}. \tag{2.44}$$

In the Higgs one-loop self-energy correction, there are logarithmic divergence contributions and they can be canceled by loops of other degree of freedom in the SM. In the research for new physics, if there is modifications on the Higgs sector and other degrees of freedom, the Higgs coupling would also change. In the paper Ref. [18] that modified a Higgs-top sector in the context of a *composite* Higgs model, we can find the modification for Higgs coupling as generating contributions to the oblique corrections as

$$S_H = -\frac{1}{6\pi}(1 - y_W^2)\log\frac{M_H}{\Lambda}, \qquad T_H = \frac{3}{8\pi c_W^2}(1 - y_W^2)\log\frac{M_H}{\Lambda}, \tag{2.45}$$

where y_W refers to the variation of the couplings of the Higgs to gauge bosons in comparison with that of SM and Λ is a cut-off scale of the effective theory. Oblique corrections usually get non-negligible contributions from new physics, and thus new physics models receive severe constraints from EWPO.

2.5. Challenges of the SM

In this section, we list some of the theoretical or experimental shortcomings of the SM.

Dark matter is proved its existence from gravitational interactions, however, the SM does not have candidate particles for it. There is $\mathcal{CP}$-violation. In particle physics, there are charge conjugation symmetry ($\mathcal{C}$-symmetry) that transforms a particle into its antiparticle, and parity symmetry ($\mathcal{P}$-symmetry) that transforms spatial coordinates of a particle. Although the $\mathcal{CP}$-symmetry is not broken very much in the SM, there are huge discrepancy between the amount of matter and that of antimatter.

Hierarchy problem

The hierarchy problem originates from a huge difference between the energy scale of the Fermi constant for the weak force and Newton's constant for gravity.

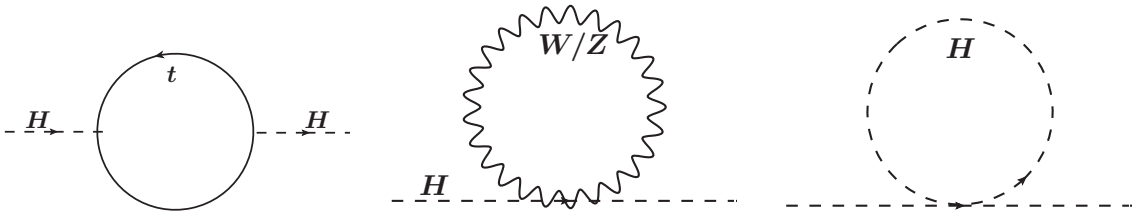

Fig. 2.2.: Quadradically divergent contributions to the Higgs mass

The Higgs mass term gets corrections from fermions and gauge bosons as

$$\begin{aligned} M_H^2 &= \left(M_H^2\right)_{bare} + \mathcal{O}\left(\lambda, g^2, H^2\right)\Lambda^2 \\ &= \left(M_H^2\right)_{bare} + \delta\left(M_H^2\right) \end{aligned} \tag{2.46}$$

where the term with $\mathcal{O}(\lambda)$ refers to the contributions from Yukawa couplings of fermions to the Higgs and the term with $\mathcal{O}(g^2)$ and $\mathcal{O}(H^2)$ indicate the contributions from the loop contributions induced by gauge bosons and the Higgs itself, respectively.

A typical problematic correction to the Higgs mass is generated by fermionic contributions, namely the heaviest quark, the top quark. The Lagrangian of its Yukawa coupling is given by

$$\mathcal{L}_{\text{Yuk}} \supset -\lambda_t \bar{t}_L t_R \phi + \text{h.c.} \tag{2.47}$$

$$= -\frac{\lambda_t}{\sqrt{2}} H\bar{t}t - \frac{\lambda_t v}{\sqrt{2}}\bar{t}t. \tag{2.48}$$

After electroweak symmetry breaking, the last term of Eq. (2.48) appears as a mass term for top quarks at tree level. The loop diagram contributing to the Higgs mass induced by top quarks can be written as

$$\begin{aligned} \Pi_{HH}^{\text{top}}(0) =& (-1)\int \frac{d^4k}{(2\pi)^4}\text{Tr}\left(-i\frac{\lambda_t}{\sqrt{2}}\right)\frac{i}{\not{k} - M_t}\left(-i\frac{\lambda_t}{\sqrt{2}}\right)\frac{i}{\not{k} - M_t} \\ =& -2\lambda_t^2 \int \frac{d^4k}{(2\pi)^4}\frac{k^2 + M_t^2}{\left(k^2 - M_t^2\right)^2} \\ =& -2\lambda_t^2 \int \frac{d^4k}{(2\pi)^4}\left[\frac{1}{\left(k^2 - M_t^2\right)} + \frac{2M_t^2}{\left(k^2 - M_t^2\right)^2}\right], \end{aligned} \tag{2.49}$$

where λ_t is the Yukawa coupling constant and k is the momentum running in the loop with $\not{k} = \gamma_\mu k^\mu$. The term with $1/\left(k^2 - M_t^2\right)$ is quadratically divergent. The divergent term does not contain any dependence on the Higgs mass. Even if we set the Higgs mass to zero there is no symmetry recovered. The Higgs mass is not protected by any symmetry.

The quadratic divergence is not consistent with other theoretical criteria. For example, the perturbative unitarity from the $W^+W^- \to W^+W^-$ scattering amplitude suggested the Higgs

mass to be less than $\mathcal{O}(700\,\text{GeV})$ [19, 20];

$$M_H \leq \left(\frac{4\pi\sqrt{2}}{3G_F}\right)^{1/2} \sim 700\,\text{GeV}. \tag{2.50}$$

The bound from the s-wave unitarity is of the order of roughly $M_H < 1.2\text{TeV}$ depending on literatures, but it depends how to define the cut-off.

If we assume to cut off the integral with a scale Λ at the Planck mass scale $M_p \sim 10^{19}\,\text{GeV}$ because the next relevant physics scale might be gravity then the Higgs mass would be of order $\mathcal{O}(M_p)$, which is much larger than the observed Higgs mass $\sim 125\,\text{GeV}$. If new degrees of freedom either at the tree- or loop-level couple to the Higgs boson, the $H^\dagger H$ operator is driven to that new mass scale.

Chapter 3.

Effective Field Theory: Dimension-6 Operators

This chapter describes an Effective Field Theory (EFT) comprised of the SM with additional dimension-six operators. We study an EFT to test physics beyond the SM at the LHC in a model-independent way. Using a special basis for the operators, the GIMR basis [21], we implemented the complete set of dim-6 operators into the Monte Carlo Event Generator `WHIZARD`*. The resources for this chapter are [21–26]*

3.1. Effective Field Theory Formailsm

To solve the problems that cannot be answered with the SM as pointed out in Chapter 2, there exist numerous extension of the Standard model. To describe physics of both the SM and BSM, one common approach to create BSM theories are effective field theories [25–28]. Physics beyond the SM suggests particles with multi-TeV mass, which are not easy to be detected in experiments because of kinematical constraints. Ways to approach for EFT to phenomena is to separate scale. such as bottom-up or top-down approach. A model can be described in top-down approach of EFT. The original one and the EFT one share the same degrees of freedom with the same set of low-energy interactions and symmetries including accidental symmetries and have the same low-energy physics. At the low energy scale, heavy degrees of freedom are integrating out, as leaving traces as irrelevant and higher-dimensional operators.

In regard of particles that have multi-TeV mass, it is plausible that some heavy particles would be too heavy to be produced. On the other hand, too small masses have a negligible effect on observables. In EFTs, both effects are taken into account by either introducing a large parameter $\Lambda \to \infty$ or assuming $m = 0$. This is the idea of *effective theory*. It helps us to concentrate on the relevant phenomena and makes it easy to calculate quantities. Effective theory describes interactions between degrees of freedom accessible at a given energy scale.

Effective field theory requires ultraviolet regularation, which is so-called renormalization. As the result of the ultraviolet regulation, the renormalization group running coupling constant appears. The running coupling constant also manages the logarithmic dependence of heavy particles masses.

To remove heavy particles from a theory, one can integrate out the heavy fields. Also, one can understand the nontrivial effect of heavy particles by studying Feynmann diagrams or by solving Euler-Lagrange equation for the heavy fields. The nontrivial effects of heavy particles remain in the theory as higher dimensional operators interaction. Their effects are illustrated by non-renormalizable theory. So, the heavy particles processes are replaced by this interaction

as giving the same physics to the low energy theory. The validity of the EFT is constrained up to the certain energy level.

We need to relate the two theories; effective theory and the original theory. Specifically, a coupling constant at the leading order should be continuous around boundary. Also, heavy particles and loop effects should be taken into account. This condition to describe the same physics for the theories is called a matching condition. The coefficients of effective Lagrangian can be measured by experiments procedure or calculated from the underlying theory.

In order to set up a valid EFT with the SM as low-energy limit and a tower of higher-dimensional operators, the following features are desirable [24]:

- Any extension of the standard model should satisfy the S-matrix axioms of unitary, analyticity, *etc.*
- The symmetries of the standard model, namely Lorentz invariance and $SU(3)_C \times SU(2)_L \times U(1)_Y$ gauge symmetry, should be respected.
- It should be possible to recover the standard model in an the low-energy limit.
- It should be possible to calculate radiative corrections at any order in the standard-model interactions in the extended theory.
- It should be possible to calculate radiative corrections at any order in the new interactions of the extended theory.

Since the SM is considered as renormalized theory, we can add higher dimensional operators to the SM as

$$\mathcal{L}_{\text{total}} = \mathcal{L}_{\text{SM}} + \sum_k \left[\frac{1}{\Lambda} C_k^{(5)} \mathcal{O}_k^{(5)} + \frac{1}{\Lambda^2} C_k^{(6)} \mathcal{O}_k^{(6)} + \mathcal{O}\left(\frac{1}{\Lambda^3}\right) \right], \tag{3.1}$$

where $\mathcal{L}_{SM}$ is the Lagrangian of the SM and Λ is the cutoff scale at which the SM is matched to the full theory. The dimensionless coefficients C_k^i are called Wilson coefficients. Because of renormalization conditions, the dimension of $\mathcal{L}_{\text{SM}}$ has 2 or 4 space-time dimension. However, as considering the Standard Model as the low energy effective theory, we can build up higher-dimensional operators such as 5- and 6-dimensional operators.

In Eq. (3.1), $\mathcal{O}^{(n)}$ corresponds to n-dimensional operator and $C_k^{(n)}$ is its dimensionless coupling constant that will be determined by matching after integrating out the heavy fields. Higher-dimensional operators are already derived in many literatures such as Buchmüller and Wyler paper.

3.2. Six-dimensional Operators

We use the operators in Ref. [21], so called "GIMR basis", because some operators considered as duplicated physicswise are removed by the Equations of Motion and do not give contributions to on-shell matrix elements. We discuss six-dimensional operators that are bosonic and $\mathcal{CP}$-even. As well as using GIMR basis, we follow the notation and the way to categorize operators as in Ref. [21].

To form higher-dimensional bosonic operators, an even number of scalar field ϕ should be included for multiplying to $SU(2)_L$ representation tensors. And an even number of covariant derivatives D^μ are needed for contracting all Lorentz indices. The spacetime dimension of the scalar field and the covariant derivative is one and that of the gauge field strength is two. Thus, any five-dimensional operator is absent in the purely bosonic sector. The possible combinations of bosonic fields for six-dimensional operators are

$$X^3, \quad X^2\phi^2, \quad X^2D^2, \quad X\phi^4, \quad XD^4, \quad X\phi^2D^2, \quad \phi^6, \quad \phi^4D^2 \text{ and } \phi^2D^4, \tag{3.2}$$

where X is the gauge boson strength fields with 2 spacetime dimension.

In fact, $X\phi^4$ in Eq. (3.2) vanishes after contracting all Lorentz indices because of the anti-symmetric feature of the gauge field strength tensors. Also, XD^4 is skipped because the contraction for all indices generates the commutator of the covariant derivatives, $[D^\mu, D^\nu] \sim X^{\mu\nu}$, which is already taken into account with X^2D^2.

We consider the bosonic six-dimensional operators after having reduced them to a minimal set by application of the EOMs. Then, this leads us to the following list of six-dimensional bosonic operators:

$$\begin{aligned}
&1.\ \mathcal{O}_6 = (\Phi^\dagger\Phi)^3 && \text{(3.3a)}\\
&2.\ \mathcal{O}_\Phi = \partial_\mu(\Phi^\dagger\Phi)\partial^\mu(\Phi^\dagger\Phi) && \text{(3.3b)}\\
&3.\ \mathcal{O}_T = (\Phi^\dagger D_\mu\Phi)(\Phi^\dagger D^\mu\Phi) && \text{(3.3c)}\\
&4.\ \mathcal{O}_{DW} = (\Phi^\dagger\tau^I i\overleftrightarrow{D}^\mu\Phi)(D^\nu W_{\mu\nu})^I && \text{(3.3d)}\\
&5.\ \mathcal{O}_{DB} = (\Phi^\dagger\overleftrightarrow{D}^\mu\Phi)(\partial^\nu B_{\mu\nu}) && \text{(3.3e)}\\
&6.\ \mathcal{O}_{D\Phi W} = i(D^\mu\Phi)^\dagger\tau^I(D^\nu\Phi)W^I_{\mu\nu} && \text{(3.3f)}\\
&7.\ \mathcal{O}_{D\Phi B} = i(D^\mu\Phi)^\dagger(D^\nu\Phi)B_{\mu\nu} && \text{(3.3g)}\\
&8.\ \mathcal{O}_{\Phi B} = (\Phi^\dagger\Phi)B_{\mu\nu}B^{\mu\nu} && \text{(3.3h)}\\
&9.\ \mathcal{O}_{\Phi G} = (\Phi^\dagger\Phi)G^A_{\mu\nu}G^{A\mu\nu} && \text{(3.3i)}\\
&10.\ \mathcal{O}_G = f^{ABC}G^{A\nu}_\mu G^{B\rho}_\nu G^{C\mu}_\rho && \text{(3.3j)}\\
&11.\ \mathcal{O}_W = \epsilon^{IJK}W^{I\nu}_\mu W^{J\rho}_\nu W^{K\mu}_\rho && \text{(3.3k)}
\end{aligned}$$

Hereby, in Eqs. (3.3a) - (3.3k), the following notations are used:

$$\begin{aligned}
&(D_\mu q)^{\alpha j} = [\delta_{\alpha\beta}\delta_{jk}(\partial_\mu + ig'Y_qB_\mu) + ig\delta_{\alpha\beta}S^I_{jk}W^I_\mu + ig_s\delta_{jk}T^A_{\alpha\beta}G^A_\mu]q^{\beta k},\\
&\phi^\dagger i\overleftrightarrow{D}_\mu\phi \equiv i\phi^\dagger(D_\mu - \overleftarrow{D}_\mu)\phi\ ,\\
&\phi^\dagger i\overleftrightarrow{D}^I_\mu\phi \equiv i\phi^\dagger(\tau^I D_\mu - \overleftarrow{D}_\mu\tau^I)\phi.
\end{aligned} \tag{3.4}$$

Next, we construct vertices for Feynman diagrams from the bosonic dimension-six operators in Eqs. (3.3a) - (3.3k) and their Lorentz structures for the implementation into `WHIZARD`.

	WWZ	WWA	$WWWW$	$WWZZ$	$WWZA$	$WWAA$
$\mathcal{O}_W$	✓	✓	✓	✓	✓	✓
$\mathcal{O}_{DW}$	✓	✓	✓	✓	✓	✓
$\mathcal{O}_{D\Phi W}$	✓	✓	✓	✓	✓	-
$\mathcal{O}_{D\Phi B}$	✓	✓	-	-	-	-

(a) Anomalous gauge couplings

	HHH	$HHHH$
$\mathcal{O}_6$	✓	✓
$\mathcal{O}_\Phi$	✓	✓

(b) Anomalous Higgs self couplings

	HWW	HZZ	HZA	HAA
$\mathcal{O}_{DW}$	✓	✓	✓	-
$\mathcal{O}_{D\Phi W}$	✓	✓	✓	-
$\mathcal{O}_{DB}$	-	✓	✓	-
$\mathcal{O}_{D\Phi B}$	-	✓	✓	-
$\mathcal{O}_{\Phi B}$	-	✓	✓	✓

(c) Anomalous couplings of Higgs to two gauge bosons

	$HWWZ$	$HWWA$	$HHWW$	$HHZZ$	$HHZA$	$HHAA$
$\mathcal{O}_{DW}$	✓	✓	✓	✓	✓	-
$\mathcal{O}_{D\Phi W}$	✓	✓	✓	✓	✓	-
$\mathcal{O}_{DB}$	-	-	-	✓	✓	-
$\mathcal{O}_{D\Phi B}$	✓	✓	-	✓	✓	-
$\mathcal{O}_{\Phi B}$	-	-	-	✓	✓	✓
$\mathcal{O}_T$	-	-	-	✓	-	-

(d) Anomalous quartic couplings

Table 3.1.: Vertices from the six-dimensional operators.

3.2.1. Possible Vertices

We move on to the vertices generated by the operators in Eq. (3.3), calculating Feynman Rules for the six-dimensional operators making use of the Mathematica package FeynRules [29]. The vertices caused by the bosonic six-dimensional operators are categorized in Table 3.1

3.3. WHIZARD

WHIZARD is an automated event generator performing in automatized ways for calculating cross sections and event generation at collider experiments in the high energy colliders [30–33]. WHIZARD can handle not only leading order perturbation theory in the automatized way, but also next-to-leading order calculations [34–40].

Physics from hadron colliders such as the LHC to linear colliders such as the Tevatron, LEP,

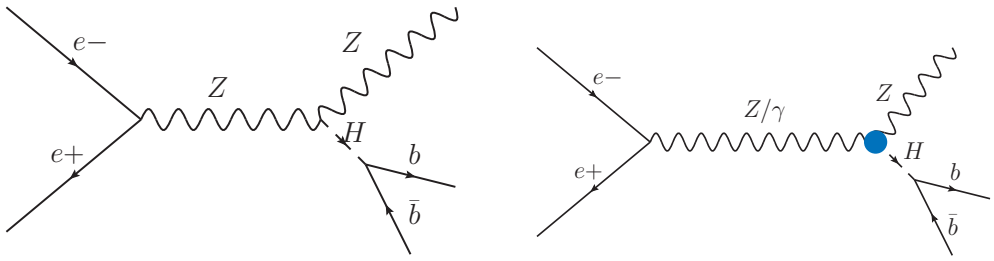

Fig. 3.1.: Feynman diagrams for possible Higgs productions in the e^-e^+ collider. Left one is only with regard to dimension-four operators in the SM. Right one is with dimension-six operators as well.

ILC can be considered at the elementary particle level with this program. Parton distributions functions for hadron collisions at the LHC as well as hadronization can be handled by interfaces to external packages. Regarding lepton collider physics, `WHIZARD` has many options for beam descriptions such as beam spread, beamstrahlung, and etc. `WHIZARD` comes with its in-house (tree-level) matrix element generator `O'Mega`, which has a large number of hard-coded physics models. `WHIZARD` is compatible with UFO model files of FeynRules interface.

`WHIZARD` comes with its own highly-configurable scripting language, `SINDARIN`. Via `SINDARIN` script, one can choose one of the models which are supported by `WHIZARD`. The models available in the `WHIZARD` are described in Ref. [30]. In the `SINDARIN` script, we define processes then `WHIZARD` generates the matrix elements for the corresponding partonic processes using `O'Mega`. It is possible that the processes is set very concretely; the intermediate states can be fixed as certain states and several processes can be combined as summing up the same initial or final states. The beam structure to be used to collider can be specified. Parameters for running or scanning and cuts for the process can be set. For example, when we simulate for the Higgs production, we scan for the invariant mass of $b\bar{b}$ as well as center-of-mass energy. After integration the processes, it can be analyzed and shown as histograms.

The technical detail for the implementation new operators are in Appendix A.1. An example application to the SM with dimension-6 operators, namely `SM_dim6`, is shown in Appendix A.2.

3.3.1. Preliminary Result

We discuss how dimension-six operators could contribute to collider results.

We consider the Higgs production in a electron-positron collider as in Fig. 3.1. The Higgs boson can be produced by $H-Z-Z$ vertex in the SM. $H-Z-\gamma$ vertex becomes available taking into account six-dimensional operators. As in Table 3.1c, operators $\mathcal{O}_{DW}$, $\mathcal{O}_{D\Phi W}$, $\mathcal{O}_{DB}$, $\mathcal{O}_{D\Phi B}$, and $\mathcal{O}_{\Phi B}$ can generate such vertices and enhance the Higgs production.

Since the Higgs decays into $b\bar{b}$ most, we scan on the invariant mass of $b\bar{b}$ and set if for x-axis. The Wilson coefficients of operators is set manually when `WHIZARD` running.

We observe much enhanced effects in Figs. 3.2 and 3.3. Detail script for running is in Appendix A.2.

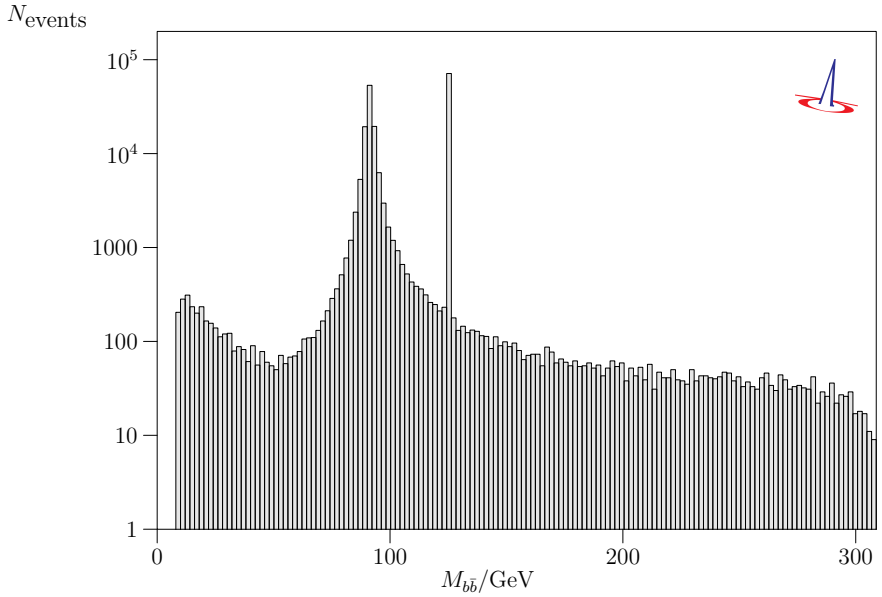

Fig. 3.2.: WHIZARD running for $e^+e^- \to Z \to ZH$ without six-dimensional operators

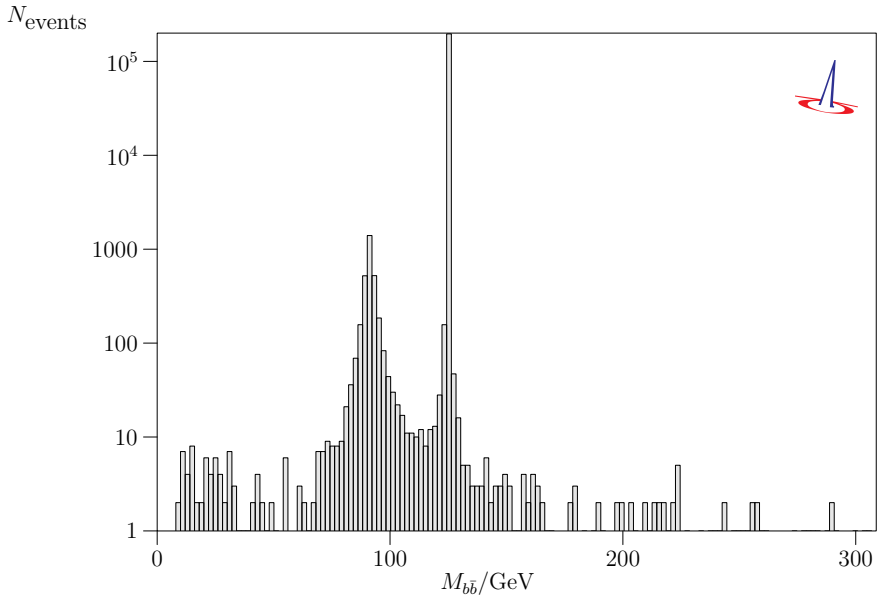

Fig. 3.3.: WHIZARD running for $e^+e^- \to Z \to ZH$ with six-dimensional operators

Chapter 4.

Little Higgs Models

This chapter is a self-contained introduction to Little Higgs models having the Collective Symmetry Breaking mechanism to address the hierarchy problem. We detail the Collective Symmetry Breaking mechanism and its application to a Little Higgs model, the Littlest Higgs model. Without introducing a discrete symmetry, so-called T-parity, the Littlest Higgs model is strongly constrained by the constraints of the electroweak precision observables. By bringing in the T-parity, bounds by the electroweak precision observables become relaxed. We discuss the model with the T-parity in detail. The resources for this chapter are [9, 10, 41–47].

Higgs boson as a Nambu-Goldstone boson

For physics beyond the SM, it is possible that the SM is extended as a weakly interacting theory or a strongly interacting theory. But, we discuss an strongly coupled extension of the SM. This implies the Higgs boson is different from the $SU(2)$ doublet of the SM and consists of constituters that are strongly coupled at above a scale Λ.

This approach for the Higgs boson as a pseudo-Nambu-Goldstone boson (pNGB) is similar to low-energy QCD. There is a compositeness scale Λ_{QCD} and bound states with masses of particles in the same order as Λ_{QCD}. Pions appear naturally much lighter than baryons or vector resonances. It is possible because pions appear as Nambu-Goldstone boson of the spontaneous breaking of the approximate $SU(3)_L \times SU(3)_R$ chiral symmetry.

For constructing a theory in this context, there are severe requirements; To recreate the SM Higgs boson, four Goldstone bosons are needed from spontaneous breaking of G/H. G must embed the SM gauge group $SU(2)_L \times U(1)_Y$ because there are the couplings of the Higgs field to the gauge boson fields. The $SU(2)_L \times U(1)_Y$ as a subgroup of G should be misaligned to the diagonal H to trigger electroweak symmetry breaking. Lastly, in oder to avoid large radiative corrections, the strong sector should respect to the custodial symmetry of the SM.

If the global symmetry G is exact symmetry, the Higgs field remains massless and electroweak symmetry breaking is not triggered. Thus, G should be an approximate symmetry and make the Higgs field massive. G is explicitly broken by gauged subgroups, the Higgs potential is generated effectively by radiative correction terms.

For dividing clearly the scale between the electroweak scale v and the compositeness scale $\Lambda = 4\pi f$, the fine-tuning is demanded for the terms in the Higgs potential. This is so-called *little hierarchy* problem. Additional structure is introduced for Little Higgs models. This helps to split naturally the scale between the electroweak scale and the scale Λ and it causes the electroweak symmetry breaking to happen *collectively*.

4.1. Little Higgs mechanism

Collective Symmetry Breaking

This additional structure imposed on a pNGB-model is the intertwining of tow different symmetries, each of them explicitly broken to generate the mass term and the terms for potential of the Higgs boson. If only one of them is broken and the other global symmetry left unbroken, the Higgs boson field is transformed non-linearly and would be still massless. Since the global symmetry is explicitly broken at the scale $\Lambda = 4\pi f$, there are still quadratically divergent terms for the Higgs boson mass, but they are suppressed by the two-loop level. After spontaneous symmetry breaking of the larger global group, under the remaining symmetry the Higgs potential generated such as

$$V(h) \sim \left[\begin{array}{c} \text{small} \\ \text{w.r.t. } f^2 \end{array} \right] h^\dagger h + \mathcal{O}(1)|h^\dagger h|^2, \tag{4.1}$$

where the coefficient of $h^\dagger h$ is supposed to be small to resolve the little hierarchy problem. Now, we describe how the $h^\dagger h$ terms are suppressed by the Collective Symmetry Breaking mechanism, forbidding or canceling quadratically divergent contributions to the Higgs mass in a toy model.

As a pseudo-Goldstone boson, the Higgs field has a shift symmetry:

$$h \to h + \epsilon. \tag{4.2}$$

This prevents any Higgs potential. However, as another degree of freedom ϕ is suggested operators can be introduced to the potential by radiative corrections of the Coleman-Weinberg potential as

$$V \supset \lambda_1 f^2 \left| \phi + \frac{h^2}{f} \right|^2 + \lambda_2 f^2 \left| \phi - \frac{h^2}{f} \right|^2. \tag{4.3}$$

Then, ϕ field gets mass term as $M_\phi = f\sqrt{\lambda_1 + \lambda_2}$.

To be invariant under the shift symmetry of the Higgs field for the potential, transformations for ϕ are required when the Higgs field is transformed as its shift symmetry:

$$\lambda_1 : \begin{cases} h \to & h + \epsilon \\ \phi \to & \phi - \frac{h\epsilon + \epsilon h}{f} \end{cases} \quad \text{or} \quad \lambda_2 : \begin{cases} h \to & h + \epsilon \\ \phi \to & \phi + \frac{h\epsilon + \epsilon h}{f} \end{cases}. \tag{4.4}$$

As the Higgs field transforms under a shift symmetry, ϕ transforms differently in the two different terms corresponding to the couplings λ_1 and λ_2. Each physical quartic terms of the Higgs can vanish by redefining ϕ fields as

$$\lambda_1 : \phi_+ \equiv \phi + \frac{h^2}{f} \quad , \qquad \lambda_2 : \phi_- \equiv \phi - \frac{f^2}{f}. \tag{4.5}$$

But, since the ϕ field cannot transform in two different way simultaneously, the shift symmetry in the potential is approximately broken. After integrating out the ϕ field, the operators of Eq. (4.3) turn into

$$V_{\text{eff}} \supset \frac{4\lambda_1\lambda_2}{\lambda_1+\lambda_2}h^4 \equiv \lambda_{\text{eff}}h^4. \tag{4.6}$$

Only the terms involving both couplings λ_1 and λ_2 can contribute to radiative corrections for the Higgs mass with a logarithmic sensitivity to the scale Λ as

$$\Delta M_h^2 \sim \frac{1}{16\pi^2}\lambda_{\text{eff}}M_\phi^2 \log\frac{\Lambda^2}{M_\phi^2}. \tag{4.7}$$

As a result, the potential now shows with the scale separation between the electroweak scale and the composite scale Λ. The degree of freedom contributing to cancel the quadratic divergence, such as ϕ here, is called a *quarticon* or a *cancellon*. Its specific features are different depending on the model set-up.

4.2. The Littlest Higgs Model

4.2.1. Gauge and Scalar sector

The Littlest Higgs model is based on the non-linear sigma model with global $SU(5)/SO(5)$ symmetry breaking structure. A vacuum expectation value (*vev*) breaks $SU(5)$ to $SO(5)$ at the scale f, and the *vev* is given by $\langle\Sigma\rangle$ in the form of the following 5×5 matrix

$$\langle\Sigma\rangle = \begin{pmatrix} & & \mathbf{1}_{2\times2} \\ & 1 & \\ \mathbf{1}_{2\times2} & & \end{pmatrix}. \tag{4.8}$$

The sigma field parameterizes the coset space $SU(5)/SO(5)$, and can be expressed in exponential form as

$$\Sigma \;=\; e^{i\Pi/f}\,\langle\Sigma\rangle\,e^{i\Pi^T/f} \;=\; e^{2i\Pi/f}\,\langle\Sigma\rangle, \tag{4.9}$$

with $\Pi = \pi^a X_a$ and X are generators of $SU(5)$. π^a refer to Nambu-Goldstone bosons (NGBs) that parameterize the coset space according to Callan-Coleman-Wess-Zumino (CCWZ) formalism [48,49] and we will classify them according to their quantum numbers in the following sections.

Under an $SU(5)$ transformation, the exponential of NGBs transforms with $V\in SU(5)$ as

$$\Sigma \;\to\; V\Sigma V^\dagger \;=\; V\Sigma V^T. \tag{4.10}$$

The vacuum is invariant under the unbroken $SO(5)$ symmetry:

$$U\,\langle\Sigma\rangle\,U^T = \langle\Sigma\rangle, \qquad \forall U\in SO(5). \tag{4.11}$$

Here, the transformation matrix U can be represented as $U = \exp[i\theta^a T_a]$ where T^a are unbroken generators. We can express $\langle\Sigma\rangle$ in another form with regard to U and θ by expanding Eq. (4.11) as follows,

$$\langle\Sigma\rangle = \langle\Sigma\rangle + i\theta^a(T_a\langle\Sigma\rangle + \langle\Sigma\rangle T_a^T) + \mathcal{O}(\theta^2). \tag{4.12}$$

From the relations above, we obtain conditions for the broken generators X_a and unbroken ones T_a which are the commutator relations,

$$\{T_a, \langle\Sigma\rangle\} = 0, \tag{4.13}$$

$$[X_a, \langle\Sigma\rangle] = 0. \tag{4.14}$$

The global symmetry group $SU(5)$ has two $SU(3)$ groups as its subgroups. One $SU(3)$ is embedded in the 3×3 *upper-left* corner of 5×5 matrix of $SU(5)$ and the other $SU(3)$ is in the 3×3 *lower-right* corner of $SU(5)$.

The gauge group structure of the Littlest Higgs model is $G_1 \times G_2 = (SU(2)_1 \times U(1)_1) \times (SU(2)_2 \times U(1)_2)$, which is embedded in $SU(5)$ and the subgroups $SU(3)$ of $SU(5)$ contain G_1 and G_2, respectively. By the spontaneous symmetry breaking at the scale f, $G_1 \times G_2$ is broken to the SM gauge group $SU(2)_L \times U(1)_Y$. The generators of $G_1 \times G_2$ are

$$Q_1^a = \frac{1}{2}\begin{pmatrix} \sigma^a & \mathbf{0}_{2\times3} \\ \mathbf{1}_{3\times2} & \mathbf{0}_{3\times3} \end{pmatrix}, \qquad Q_2^a = \frac{1}{2}\begin{pmatrix} \mathbf{0}_{3\times3} & \mathbf{0}_{2\times3} \\ \mathbf{0}_{3\times2} & -\sigma^a \end{pmatrix} \tag{4.15}$$

$$Y_1 = \frac{1}{10}\mathrm{diag}\,(-3,-3,2,2,2), \qquad Y_2 = \frac{1}{10}\mathrm{diag}\,(-2,-2,-2,3,3), \tag{4.16}$$

where $Q_{1,2}$ are the generators of $SU(2)_{1,2}$ each; $Y_{1,2}$ are of $U(1)_{1,2}$; and σ^a are Pauli matrices. When the gauge group breaks into the diagonal subgroup, the unbroken SM gauge group $SU(2)_L \times U(1)_Y$ generators are

$$Q^a = \frac{1}{\sqrt{2}}(Q_1^a + Q_2^a), \qquad Y = Y_1 + Y_2 \tag{4.17}$$

which satisfy Eq. (4.14).

Since this model is based on a non-linear sigma model, the kinetic Lagrangian of the scalar fields is

$$\mathcal{L}_\Sigma = \frac{f^2}{8}\mathrm{Tr}|\mathcal{D}_\mu\Sigma|^2, \tag{4.18}$$

where the covariant derivative is given by

$$\mathcal{D}_\mu\Sigma = \partial_\mu\Sigma - i\sum_j \left[g_j W_{\mu j}^a (Q_j^a\Sigma + \Sigma Q_j^{a^T}) + g_j' B_{\mu j}(Y_j\Sigma + \Sigma Y_j)\right]. \tag{4.19}$$

Because of the symmetry breaking at scale f, there is mixing between G_1 and G_2 and under

the rotation, the mass eigenstates of the gauge fields are given by

$$\begin{aligned} W &= sW_1 + cW_2, \qquad & W_H &= -cW_1 + sW_2 \\ B &= s'B_1 + c'B_2, \qquad & A_H &= -c'B_1 + s'B_2 \end{aligned} \tag{4.20}$$

where the mixing coefficients are

$$c = \frac{g_1}{\sqrt{g_1^2 + g_2^2}}, \qquad s = \frac{g_2}{\sqrt{g_1^2 + g_2^2}}, \tag{4.21}$$

$$c' = \frac{g_1'}{\sqrt{g_1'^2 + g_2'^2}}, \qquad s' = \frac{g_2'}{\sqrt{g_1'^2 + g_2'^2}}, \tag{4.22}$$

where primed quantities belong to $U(1)$ and unprimed belong to $SU(2)$. The gauge bosons eat the NGBs and become massive. Their masses are

$$M_{W_H^\pm} = M_{Z_H} = \frac{gf}{2sc}, \qquad M_{A_H} = \frac{g'f}{2\sqrt{5}s'c'}. \tag{4.23}$$

Furthermore, g and g' are coefficients of the SM electroweak gauge group $SU(2) \times U(1)$ and are given as

$$g = g_1 s = g_2 c, \qquad g' = g_1' s' = g_2' c'. \tag{4.24}$$

In the Littlest Higgs model, there are two consecutive symmetry breaking steps; one is the spontaneous symmetry breaking of $SU(5)/SO(5)$ at the scale f. From this symmetry breaking $24 - 10 = 14$ Nambu-Goldstone bosons (NGBs) appear. They can be parameterized as:

$$\Pi \equiv \pi^a X_a = \begin{pmatrix} \frac{1}{2}X & \frac{1}{\sqrt{2}}H^\dagger & \Phi^\dagger \\ \frac{1}{\sqrt{2}}H & \frac{2}{\sqrt{5}}\eta & \frac{1}{\sqrt{2}}H^* \\ \Phi & \frac{1}{\sqrt{2}}H^T & \frac{1}{2}X \end{pmatrix} \tag{4.25}$$

where

$$X = \begin{pmatrix} \chi^0 - \frac{1}{\sqrt{5}}\eta & \sqrt{2}\chi^\dagger \\ \sqrt{2}\chi^- & -\chi^0 - \frac{1}{\sqrt{5}}\eta \end{pmatrix}, \quad \Phi = \begin{pmatrix} \phi^{++} & \frac{1}{\sqrt{2}}\phi^+ \\ \frac{1}{\sqrt{2}}\phi^+ & \phi^0 \end{pmatrix}, \quad H^T = \begin{pmatrix} \pi^+ \\ \frac{h+i\pi^0}{\sqrt{2}} \end{pmatrix}. \tag{4.26}$$

The NGBs are decomposed under $SU(2) \times U(1)$ as $\mathbf{1_0} \oplus \mathbf{3_0} \oplus \mathbf{2}_{\pm\frac{1}{2}} \oplus \mathbf{3}_{\pm\mathbf{1}}$. Among them, the one corresponding to the SM-like Higgs field is complex doublet $\mathbf{2}_{\pm\frac{1}{2}}$ H. Φ is the complex triplet of $\mathbf{3}_{\pm\mathbf{1}}$, η is the real singlet of $\mathbf{1_0}$ and χ refers to the real triplet of $\mathbf{3_0}$, which are eaten by the heavy gauge bosons.

The second symmetry breaking is the electroweak symmetry breaking (EWSB) that gives rise to the mass terms for the SM gauge bosons. After EWSB, another mixing occurs between

the light gauge bosons $W,\ Z$ and the heavy gauge bosons $W_H,\ Z_H$ from the gauge-kinetic terms of the Higgs boson. As a result, the mass terms of gauge bosons differ from the SM gauge bosons masses by terms suppressed by order $\mathcal{O}(v^2/f^2)$ as follows

$$M_{W_{SM}} = M_W \left[1 - \frac{1}{2}\frac{v^2}{f^2}\left(\frac{1}{6} + \frac{1}{4}(c^2 - s^2)\right) + 2\frac{v'^2}{v^2} + \mathcal{O}\left(\frac{v^4}{f^4}\right)\right],$$
$$M_{Z_{SM}} = M_Z \left[1 - \frac{1}{2}\frac{v^2}{f^2}\left(\frac{1}{6} + \frac{1}{4}(c^2 - s^2) + \frac{5}{4}(c'^2 - s'^2)^2\right) + 4\frac{v'^2}{v^2} + \mathcal{O}\left(\frac{v^4}{f^4}\right)\right]. \tag{4.27}$$

Here, $M_W = gv/2,\ M_Z = gv/(2cw)$. By the corrections in Eq. (4.27), we observe that the custodial symmetry $SU(2)_c$ is obviously broken. As discussed in Section 2.3, the custodial symmetry $SU(2)_c$ is broken already in the SM by the effect of the hypercharge $U(1)$. The Littlest Higgs model has doubled symmetry $U(1)_1 \times U(1)_2$ of which both can break the custodial $SU(2)$. In other words, there is additional $U(1)$ that violates the custodial $SU(2)$ and thus, the effects of the violation of the custodial $SU(2)$ is enhanced and the oblique corrections parameterizing it are not negligible.

4.2.2. Collective Symmetry Breaking

As we discussed the group structure of the Littlest Higgs model, there is $SU(5)$ embedding two $SU(3)$, of which each contains one $SU(2) \times U(1)$. Generators $Q_1,\ Y_1$ of $SU(2)_1 \times U(1)_1$ and generators of $SU(3)$ embedded in *right-lower* parts of $SU(5)$ commute. And $Q_2,\ Y_2$ of $SU(2)_2 \times U(1)_2$ and generators of $SU(3)$ embedded in *left-upper* parts of $SU(5)$ commute. In other words, a $SU(3)$ symmetry embedded in *right-lower* parts of $SU(5)$ remains as an exact symmetry even if $SU(2)_1 \times U(1)_1$ spanned by generators $Q_1,\ Y_1$ is broken, and similarly, the other $SU(3)$ embedded in *left-upper* parts of $SU(5)$ remains exact when $SU(2)_2 \times U(1)_2$ with the generators $Q_2,\ Y_2$ is broken. If the gauge couplings, g_1, g_1', of $SU(2)_1 \times U(1)_1$ are zero, a global symmetry $SU(3)$ is left unbroken when the global symmetry $SU(5)$ is broken by the vacuum expectation value $\langle\Sigma\rangle$, the Higgs field appearing as one of NGB fields. The exact $SU(3)$ symmetry keeps the Higgs field as an exact NGB field. To give rise to the radiative correction to the Higgs mass, both gauge couplings should be non-zero in order to break both $SU(3)$s. The quadratically divergent one-loop diagram that usually causes the fine-tuning problem involves one gauge coupling, and thus this cannot be produced in the Littlest Higgs model. Note that another scalar field, Φ, is not protected and gains TeV mass of order $\mathcal{O}(f)$ from the quadratically divergent one-loop diagram.

For gauge boson fields, the Collective Symmetry Breaking works as following: Possible quartic couplings consisting of two Higgs and two gauge boson fields can be found from the kinetic Lagrangian of the scalar fields as

$$\frac{1}{4} H H^\dagger \left(g_1 g_2 W_1^{\mu a} W_{2\mu}^a + g_1' g_2' B_1^\mu B_{2\mu}\right). \tag{4.28}$$

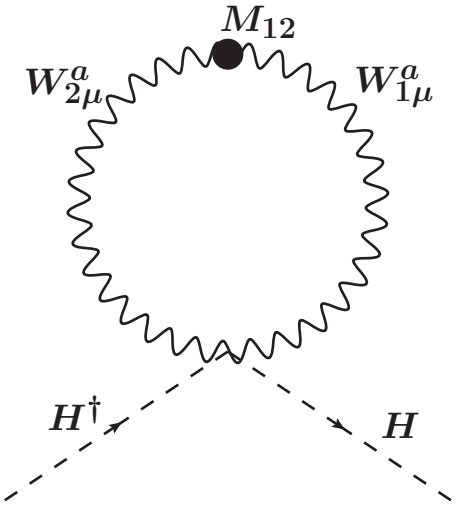

Fig. 4.1.: Mixing W_1, W_2 changes the quadratic divergence to the logarithmic divergence

Note that there is no coupling that may cause the diagonal couplings such as $g_1^2 W_1^2 HH$ and $g_2^2 W_2^2 HH$ in Eq. (4.28), generating the quadratically divergent diagrams. In the Littlest Higgs model, these terms are prevented by the Collective Symmetry Breaking. Thus, no such divergent diagrams exists. The only remaining loop correction contributions are the mixing diagram of $W_1,\ W_2$ and $B_1,\ B_2$ as in Fig. 4.1 and they are logarithmically divergent.

The cancellation of the quadratically divergent one-loop corrections can be understood with the mass eigenstates, which is expressed as

$$\begin{aligned}\frac{1}{4}H^\dagger H(g^2(W^a_{L\mu}W^{\mu a}_L - W^a_{H\mu}W^{\mu a}_H - 2\cot 2\psi W^a_{H_\mu}W^{\mu a}_L)\\ +g'^2(B_{L\mu}B^\mu_L - B_{H\mu}B^\mu_H - 2\cot 2\psi' B_{H\mu}B^\mu_L)),\end{aligned} \tag{4.29}$$

where the gauge boson fields are replaced by their mass eigenstate from Eq. (4.28). Now there are operators that generate the quadratically divergent loop induced by gauge bosons. But, the coupling involved in the loop of the light states has the same magnitude but opposite sign compared to that of the heavy states because of the group symmetry of the Littlest Higgs model. Thus, they cancel each other as in Fig. 4.2.

With regards to fermions, due to the large top Yukawa couplings, the Collective Symmetry Breaking has to be implemented only for the top sector. Because Yukawa couplings of other fermions are negligible, their one-loop contributions to the Higgs mass is not very large. The Collective Symmetry Breaking mechanism for top sector is based on a distinct group structure. There are two Yukawa terms with coupling constants: λ_1 and λ_2. The Yukawa interaction between the top quark and the Goldstone bosons are proportional to λ_1 or λ_2. λ_1 is determined by the explicit breaking of the *upper-left* $SU(3)$ in the global $SU(5)$ symmetry and λ_2 is by that of the *lower-right* $SU(3)$.

The Collective Symmetry Breaking mechanism is quite obvious in Eq. (4.30). If we turn off the Yukawa coupling λ_1, of $SU(2)_1 \times U(1)_1$, the Higgs becomes irrelevant to the top sector. On

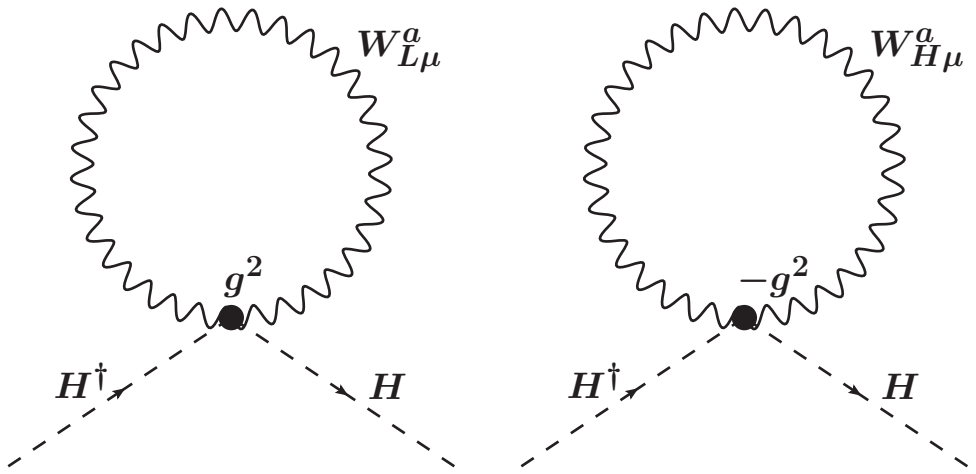

Fig. 4.2.: Loop of *light* gauge boson is cancelled by that of *heavy* gauge boson.

the other hand, if we set λ_2 as zero, the global $SU(3)$ symmetry of the upper-left corner is exact and the Higgs is guaranteed as an exact NGB. Thus, to give rise to the loop contribution to the Higgs mass mediated by the top sector, both λ_1 and λ_2 have to be involved in the interaction. As a result of the Collective Symmetry Breaking mechanism, the quadratically divergent term has been turned to logarithmically divergent terms.

4.2.3. Fermion sector

In the Littlest Higgs model, a pair of weak-singlet Weyl fermion U_L and U_R with electric charge $+2/3$ is introduced additionally. They can couple to the third generation quark doublet $q_{3L} = (t_L, b_L)^T$ and to the singlet t_R as following:

$$\mathcal{L}_{\text{top}} = -\frac{\lambda_1}{2} f \chi^\dagger_{L_i} \epsilon_{ijk} \epsilon_{mn} \Sigma_{jm} \Sigma_{kn} t_R - \lambda_2 f U^\dagger_L U_R + \text{h.c.}, \tag{4.30}$$

where

$$\chi_L = \begin{pmatrix} \sigma_2 q_{3L} \\ U_L \end{pmatrix} \tag{4.31}$$

is the "royal" the $SU(3)$ triplet [41]. Σ_{jm} refers to the 3×2 upper-right block of the Σ field in Eq. (4.9). The indices $i,\ j,\ k$ sum over $1,\ 2,\ 3$ and $m,\ n = 4, 5$. Expanding the Σ field, we see the interactions of the top quark and its partners. After the spontaneous symmetry breaking at the scale f, but without the mixing by EWSB, their mass eigenstates are given by

$$\begin{aligned} t_L &= u_L, & t_R &= \frac{\lambda_2 u_{3R} - \lambda_1 U_R}{\sqrt{\lambda_1^2 + \lambda_2^2}}, \\ T_L &= U_L, & T_R &= \frac{\lambda_1 u_{3R} + \lambda_2 U_R}{\sqrt{\lambda_1^2 + \lambda_2^2}}, \end{aligned} \tag{4.32}$$

with the mass of the top-partner

$$M_T = \sqrt{\lambda_1^2 + \lambda_2^2} f, \tag{4.33}$$

while the SM top quark remains massless yet. The couplings of the top sector to the Higgs field with the mass eigenstates can be written as

$$\begin{aligned} &\lambda_1 \left(\sqrt{2} q_L^\dagger \tilde{H} - \frac{1}{f} H^\dagger H U_L^\dagger \right) u_{3R} + \text{h.c.} \\ &= \lambda_t q_L^\dagger \tilde{H} t_R + \lambda_T q_L^\dagger \tilde{H} T_R - \frac{1}{\sqrt{2} f} (H^\dagger H) T_L^\dagger (\lambda_T T_R + \lambda_t t_R) + \text{h.c.}, \end{aligned} \tag{4.34}$$

where $\tilde{H} = i\sigma^2 H$. The first term of Eq. (4.34), $\lambda_t q_L^\dagger H t_R$, is the usual up-type Yukawa coupling, which becomes the top quark mass term after EWSB, as the Higgs field gets a *vev*. The SM top quarks mass is given with the definition of λ_t and λ_T as

$$\begin{aligned} &M_t = \lambda_t v, \\ &\text{where} \quad \lambda_t = \frac{\lambda_1 \lambda_2}{\sqrt{\lambda_1^2 + \lambda_2^2}}, \qquad \lambda_T = \frac{\lambda_1^2}{\sqrt{\lambda_1^2 + \lambda_2^2}}. \end{aligned} \tag{4.35}$$

Considering the contribution from first and second generation of quarks, there is no need to cancel these contributions to the quadratically divergent terms in the Higgs potential because they are small if the cut-off scale $\Lambda \approx 10\,\text{TeV}$. That is, we do not need to introduce the Collective Symmetry Breaking mechanism to other fermion sector except for the top quark. The Yukawa Lagrangian for the light up-type quarks are similar to the Eq. (4.30) but without the new weak-singlet fields, U_L and U_R. For the down-type and charged leptons, the Lagrangian is also similar but Σ is replaced with the complex conjugate, Σ^*,

$$\mathcal{L}_Y \supset \frac{1}{2} \lambda_d f (\epsilon_{ijk} \epsilon_{xy} \chi_i \Sigma_{jk}^* \Sigma_{ky}^* d_R) + \text{h.c.}, \tag{4.36}$$

where $i = 1, 2$.

4.2.4. Higgs potential; Coleman-Weinberg approach

Since it is a (psuedo-)Nambu Goldstone boson (pNGB), the Higgs field is prevented from generating a potential at tree level. But one-loop and higher order corrections from any particle V coupling to the Higgs boson generate a potential by means of the Coleman-Weinberg mechanism [50]. This can be represented as

$$\begin{aligned} &\frac{\Lambda^2}{16\pi^2} \text{Tr}(M_V^2(\Sigma)) \\ &\quad \sim c f^4 \sum_j (g_j^2 \sum_a \text{Tr} \left[(Q_j^a \Sigma)(Q_j^a \Sigma)^* \right] + c g_j'^2 f^4 \text{Tr} \left[(Y_j \Sigma)(Y_j \Sigma)^* \right]), \end{aligned} \tag{4.37}$$

where $\Lambda \sim 4\pi f$ and M_V is the Higgs-field dependent mass term of V. c is an order-one coefficient that will be determined by the UV completion of the Littlest Higgs theory at the scale Λ.

Expanding Eq. (4.37) in the pNGB fields Σ, we obtain the Higgs potential

$$\begin{aligned} V \quad \supset \quad & c(g_1^2 + g_1'^2) f^2 \left| \Phi_{ij} + \frac{i}{4f}(H_i H_j + H_j H_i) \right|^2 \\ & + c(g_2^2 + g_2'^2) f^2 \left| \Phi_{ij} - \frac{i}{4f}(H_i H_j + H_j H_i) \right|^2 , \end{aligned} \tag{4.38}$$

where $i, j = 1, 2$ and $H_i \equiv \sqrt{2}\Pi_{i3}$, $\phi_{ij} \equiv \Pi_{i,3+j}$ of Eq. (4.25). Couplings related to the coefficients g_1, g_1' leave the $SU(3)_1$ symmetry invariant represented in the lower-right corner of the $SU(5)$ tensor. On the other hand, the coefficients g_2, g_2' are related to the interactions that leave the $SU(3)_2$ symmetry invariant. This is embedded in the upper-left corner of the 5×5 $SU(5)$ representation. The quadratically divergent term of Coleman-Weinberg potential from the top quark loops can be parameterized as the operator

$$-c' \lambda_1^2 \epsilon^{wx} \epsilon_{yz} \epsilon^{ijk} \epsilon_{kmn} \Sigma_{iw} \Sigma_{jx} \Sigma^{*my} \Sigma^{*nz} + \text{h.c.}, \tag{4.39}$$

where ϵ_{ijk} is the permutation tensor, $i, j, k, m, n = 1, 2, 3$, $w, x, j, z = 4, 5$ and λ_1 is the Yukawa coupling constant for the top quark. Expanding the operator in terms of H and Φ, we get parts of the Higgs potential induced by the top loops as

$$V_t \supset -c' \lambda_1^2 f^2 \left| \Phi_{ij} + \frac{i}{4f}(H_i H_j + H_j H_i) \right|^2 . \tag{4.40}$$

We can see the effect of the Collective Symmetry Breaking: the term for the Higgs mass in the Eqs. (4.38) and (4.40) do not exist. As the result of the Collective Symmetry Breaking mechanism, the quadratically divergent contribution to the Higgs mass vanishes. On the other hand, the triplet scalar field Φ gets the contribution from the quadratically divergent one-loop diagrams, which gives the mass term as

$$M_\Phi^2 = \left(a(g_1^2 + g_1'^2 + g_2^2 + g_2'^2) - c' \lambda_1^2 \right) f^2. \tag{4.41}$$

This gives us a constraint for the electroweak symmetry breaking: EWSB can be triggered at the scale $v \sim 246\,\text{GeV}$ only if the triplet scalar Φ has positive mass value. Otherwise, the electroweak symmetry is broken triggered by the vacuum expectation value of Φ proportional to f.

The Higgs field obtains contributions to its mass by logarithmically divergent diagrams. From the loops mediated by the vector bosons, the contribution to the Coleman-Weinberg (CW) potential is given by

$$V_{\text{gauge}} \supset \frac{3}{64\pi^2} \text{tr} M_V^4(\Sigma) \log \frac{M_V^2(\Sigma)}{\Lambda^2}. \tag{4.42}$$

Expanding this with respect to H, we obtain a contribution to the Higgs mass parameter μ

which is given by

$$\mu^2_{\text{gauge}}(H) = \frac{3}{64\pi^2}\left(3g^2 M^2_{W_H}\log\frac{\Lambda^2}{M^2_{W_H}} + g'^2 M^2_{B_H}\log\frac{\Lambda^2}{M^2_{B_H}}\right). \tag{4.43}$$

The contribution to the CW potential by top loop is given by

$$V_t = -\frac{3}{16\pi^2}\text{tr}\left(M_t(\Sigma)M_t^\dagger(\Sigma)\right)^2\log\frac{M_t(\Sigma)M_t^\dagger(\Sigma)}{\Lambda^2}, \tag{4.44}$$

where $M_t(\Sigma)$ is the Σ-dependent top mass squared operator. This gives a negative contribution to the Higgs parameter μ, which is

$$\mu_t^2(H) = -\frac{3\lambda_t^2 M_T^2}{8\pi^2}\log\frac{\Lambda^2}{M_T^2}. \tag{4.45}$$

The scalar sector also contributes to the CW potential, leading to the following effect in the Higgs mass parameter:

$$\mu_s^2(H) = \frac{\lambda}{16\pi^2}M_\Phi^2\log\frac{\Lambda^2}{M_\Phi^2}. \tag{4.46}$$

Thanks to the large Yukawa coupling, the contribution of top quark to the Higgs mass exceeds those of the gauge and scalar couplings. Also, it enables the radiative symmetry breaking [50] at the scale of the Higgs *vev* $\sim 246\,\text{GeV}$.

After EWSB, the Higgs fields can be parameterized as

$$H = \left(\pi^+, \quad \frac{v+h+i\pi^0}{\sqrt{2}}\right)^T \tag{4.47}$$

where $v = 246\,\text{GeV}$ and h is the physical SM-like Higgs field. $\pi^\pm$ and π^0 fields are eaten by the SM gauge bosons, $W^\pm$ and Z. The SM gauge boson mass terms are not proportional to the scale f, but proportional to v and obtain correction terms related to v/f, see Eq. (4.27). These $\mathcal{O}(v/f)$ corrections lead to constraints by the electroweak precision data.

As the Higgs field acquires its *vev*, this form the tadpole for Φ, which cause non-vanishing value for the *vev* for the neutral component of the triplet scalar fields as

$$v' \equiv \langle\Phi_{22}\rangle = -i\frac{v^2 f}{4M_\Phi^2}\left[c\left(g_1^2 + g_1'^2 - g_2^2 - g_2'^2\right) - c'\lambda_1^2\right]. \tag{4.48}$$

The extra contribution of Eq. (4.48) affecting EWSB breaks the custodial $SU(2)$ and gives strong constraints to the electroweak precision data.

Considering all contributions the Higgs potential can be expressed as

$$V = \lambda_{\Phi^2}f^2\text{Tr}(\Phi^\dagger\Phi) + i\lambda_{H\Phi H}f(H\Phi^\dagger H^T - H^*\Phi H^\dagger) - \mu^2 HH^\dagger + \lambda_{H^4}(HH^\dagger)^2, \tag{4.49}$$

ignoring the quartic terms of Φ^4 and $H^2\Phi^2$. The coefficients denoted with λ of Eq. (4.49) can

be found from the radiative corrections to the scalar fields from Ref. [44, 51]

$$\lambda_{\Phi^2} = c\left[\frac{g^2}{s^2c^2} + \frac{g'^2}{s'^2c'^2}\right] + 32c'\lambda_1^2, \tag{4.50}$$

$$\lambda_{H\Phi H} = -\frac{c}{2}\left[g^2\frac{(c^2-s^2)}{s^2c^2} + g'^2\frac{c'^2-s'^2}{s'^2c'^2}\right] + 16c'\lambda_1^2, \tag{4.51}$$

$$\lambda_{H^4} = \frac{c}{4}\left[\frac{g^2}{s^2c^2} + \frac{g'^2}{s'^2c'^2}\right] + 8c'\lambda_1^2 = \frac{1}{4}\lambda_{\Phi^2} \quad . \tag{4.52}$$

4.3. The Littlest Higgs Model with T-Parity

The electroweak precision measurements have constrained the Littlest Higgs model. This originates from the new particles contributions that cancel the quadratic divergence of the Higgs mass. The new Little Higgs particles appear at the TeV scale with around or below TeV mass. In particular, the dimension-six operators such as $|H^\dagger D^\mu H|^2/\Lambda^2$ affect to the electroweak precision observables. To solve this, we introduce another symmetry. It forbids tree level effects without modifying other physics for canceling the quadratically divergent contributions to the Higgs mass by new particles of the Littlest Higgs model. As the simplest way to implement a new symmetry the $\mathbf{Z}_2$ discrete symmetry is introduced, acting on the Little Higgs particles only. This new symmetry is called *T-parity*. Then, the vertex interacting one Little Higgs particle that is T-parity odd with the SM particles which are T-parity even is vanished. Applying this new symmetry, higher dimensional operators can be generated at loop level only.

There are another BSM models with the similar symmetry with the T-parity. A famous example is R-parity of the Minimal Supersymmetric Standard model (MSSM). Under the R-parity, SM particles have positive charge and superpartners have negative one. In the MSSM, the loop induced by superpartners compensates the quadratic divergence of the Higgs mass and because of a number of the model parameters, the electroweak precision measurements of MSSM can be consistent with the experimental data.

Another example is the KK-parity of the Universal Extra Dimensions (UEDs). In the UEDs, the SM particles can propagate to the extra dimensional space. KK-parity behaves similarly; KK (Kaluza-Klein) states are odd and the SM particles are even. At the tree level, KK-parity prevents the lowest KK states from contributing to the higher dimensional operators so that its mass is light as 300 GeV. But in this model, it does not directly lead to the little hierarchy problem.

4.3.1. Implementation of T-parity

The T-parity does not allow one Little Higgs particle with T-parity odd to couple to the SM particles, which mitigates the contributions of the oblique parameters to bounds from the electroweak precision measurements. Processes which violate the custodial $SU(2)$ are removed at tree level and the correction becomes smaller than $16\pi^2$. We discuss how the implementation of the T-parity affect the particle states and interactions in detail.

Gauge and scalar sectors

As the name suggests, the Littlest Higgs model with T-parity shares the global and gauge group structure with the Littlest Higgs model. By the vacuum expectation value $\langle\Sigma\rangle$ the global symmetry $SU(5)$ is broken spontaneously to $SO(5)$ at the scale f and 14 NGBs appear, of which some are eaten by gauge bosons and some are left as the Higgs boson doublet and the scalar triplet Φ. The gauge group structure $(SU(2)\times U(1))^2$ is embedded in $SU(5)$.

Under the T-parity, the generators of $SU(5)$ are transformed as [52] [53]

$$\begin{aligned} T^a &\to T^a \\ X^a &\to -X^a, \end{aligned}$$

where T^a are unbroken generators and X^a are broken generators. In $SU(5)/SO(5)$, a generator τ^a that spans the coset space is transformed like

$$\tau^a \to \langle\Sigma\rangle\,(\tau^a)^T\,\langle\Sigma\rangle. \tag{4.53}$$

Under the T-parity, the non-linear sigma field Σ and the NGB fields π^a are transformed as

$$T:\begin{cases} \Sigma \;\to\; \Sigma' \equiv \langle\Sigma\rangle\Omega\Sigma^\dagger\Omega\langle\Sigma\rangle \\ \Pi \;\to\; -\Omega\Pi\Omega \end{cases} \tag{4.54}$$

where

$$\Pi \equiv \pi^a X_a \tag{4.55}$$

$$\Omega = \mathrm{diag}(1,1,-1,1,1) \tag{4.56}$$

With these transformation rules, the Higgs doublet is even under T-parity and the complex triplet Φ is odd. This forbids the coupling $H\Phi H$ in Eqs. (4.49) and (4.52) because of T-parity conservation.

Also, under T-parity, the gauge bosons of G_1 are transformed to those of G_2 and vice versa.

$$T: \qquad W_{1\mu}^a \overset{T}{\leftrightarrow} W_{2\mu}^a. \qquad B_{1\mu} \overset{T}{\leftrightarrow} B_{2\mu} \tag{4.57}$$

According to the transformation rule Eq. (4.57), the SM gauge bosons are T-parity even and the heavy gauge bosons are T-parity odd by definition in Eq. (4.20).

This feature of T-parity fixes the mixing angle as $\pi/4$, that is,

$$\begin{aligned} s = \frac{g_2}{\sqrt{g_1^2+g_2^2}} = c = \frac{g_1}{\sqrt{g_1^2+g_2^2}} = \frac{1}{\sqrt{2}}, \\ s' = \frac{g_2'}{\sqrt{g_1'^2+g_2'^2}} = c' = \frac{g_1'}{\sqrt{g_1'^2+g_2'^2}} = \frac{1}{\sqrt{2}}, \end{aligned} \tag{4.58}$$

and it fixes also the gauge coupling coefficients as

$$\begin{aligned} g_1 &= g_2 = \sqrt{2}g, \\ g_1' &= g_2' = \sqrt{2}g', \end{aligned} \tag{4.59}$$

where primed coulings are the ones of $U(1)_i$ and unprimed ones are those of $SU(2)_i$. Using Eq. (4.58), the heavy gauge bosons masses in Eq. (4.23) become

$$M_{W_H} = M_{Z_H} = gf, \qquad M_{A_H} = \frac{g'f}{\sqrt{5}}, \tag{4.60}$$

where g is the electroweak gauge constant and g' is the hyper charge coupling of $U(1)$. The more interesting change from fixing the mixing angle as $\pi/4$ is the fact that the custodial symmetry breaking is removed by substituting Eq. (4.27) with Eq. (4.58).

T-parity odd (T-odd) particles do cascade decays similarly to sparticles of Supersymmetry theory. If the T-parity is conserved, T-odd particles decay into lighter T-odd particle than itself and then, the lightest T-odd particle is stable. Thus, as far as T-parity is conserved, the heavy photon A_H becomes a candidate of dark matter.

Fermion sector

For implementing T-parity in the fermion sector, we describe how fermion sectors are transformed under the T-parity and how T-parity odd particles get mass terms.

For the 1st and 2nd generation fermion sectors, with the $SU(5)$ representation, fermion doublets $\psi_1,\ \psi_2$ are embedded into incomplete multiplets as

$$\Psi_1 = \begin{pmatrix} \psi_1 \\ \mathbb{0}_{3\times 1} \end{pmatrix}, \qquad \Psi_2 = \begin{pmatrix} \mathbb{0}_{3\times 1} \\ \psi_2 \end{pmatrix}, \tag{4.61}$$

are embedded into incomplete $SU(5)$ multiplets

$$\Psi_1 \to V^*\Psi_1, \qquad \Psi_2 \to V\Psi_2 \qquad V \in SU(5). \tag{4.62}$$

Not only to give T-odd fermion mass terms, but also to remove potential source of quartic divergence in the Higgs mass [53], the *mirror* fermions $\psi_c,\ \chi_c$ are introduced. They can be represented as complete $SO(5)$ multiplets, Ψ_c,

$$\Psi_c = \begin{pmatrix} \tilde{\psi}_c \\ \chi_c \\ \psi_c \end{pmatrix}. \tag{4.63}$$

Ψ_c is transformed non-linearly under $SU(5)$. To describe its transformation and interactions, a field ξ is also introduced as $\xi = e^{i\Pi/f}$. From the fact that the non-linear sigma field can be

written as $\Sigma = \xi^2\langle\Sigma\rangle$ and that Σ is transformed under the global $SU(5)$ as $\Sigma \to V\Sigma V^T$, ξ can be transformed under the global $SU(5)$ transformation:

$$\xi \to U\xi\langle\Sigma\rangle V^T\langle\Sigma\rangle = V\xi U^\dagger, \tag{4.64}$$

where U is a transformation tensor of $SO(5)$ and for the same U, the mirror fermion multiplet is transformed as $\Psi_c \to U\Psi_c$. T-parity acts on fermion multiplets as

$$\Psi_1 \leftrightarrow \langle\Sigma\rangle\Psi_2, \qquad \Psi_c \to -\Psi_c. \tag{4.65}$$

To be invariant under T-parity, the Yukawa Lagrangian for the down-type quark and charged lepton fields is

$$\mathcal{L}_Y \supset \frac{i\lambda_d f}{2\sqrt{2}}\epsilon_{ij}\epsilon_{xyz}\left(\bar{\Psi}'_x\Sigma_{jy}\Sigma_{jz}X - (\bar{\Psi}\langle\Sigma\rangle)_x\Sigma'_{iy}\Sigma'_{jz}X'\right)d_R. \tag{4.66}$$

where the primed quantities are T-parity images. X which is inserted for gauge invariance is a singlet under $SU(2)_{1,2}$ and has $U(1)_{1,2}$ charges, $(Y_1, Y_2) = (1/10, -1/10)$. X is chosen to be $X = (\Sigma_{33})^{-1/4}$ for *Case A* and $X = (\Sigma_{33})^{1/4}$ for *Case B*, where is the $(3,3)$ component of the non-linear sigma model field Σ. From now on, we limit our discussion to *Case A*. The T-parity invariant Yukawa Lagrangian for up-type quarks is the same with one that is of top quark except for the top partners as Eq. (4.74).

The T-parity invariant Lagrangian to give rise to mass terms for the mirror fermions is

$$\mathcal{L}_\kappa = -\kappa f\left(\bar{\Psi}_2\xi\Psi_c + \bar{\Psi}_2\langle\Sigma\rangle\Omega\xi^\dagger\Omega\Psi_c\right) + \text{h.c.}, \tag{4.67}$$

where $\xi = \exp[i\pi/f]$. This Lagrangian not only adds the T-odd mass terms but also imposes new interactions between the Higgs boson and up-type partners.

$$\mathcal{L}_\kappa \supset -\sqrt{2}\kappa f(\bar{d}_{L-}\tilde{d}_c + \frac{1+c_\xi}{2}\bar{u}_{L-}\tilde{u}_c - \frac{s_\xi}{\sqrt{2}}\bar{u}_{L-}\chi_c - \frac{1-c_\xi}{2}\bar{u}_{L-}u_c) + \text{h.c.} + \cdots \tag{4.68}$$

where $c_\xi = \cos((v+h)/\sqrt{2}f)$, $s_\xi = \sin((v+h)/\sqrt{2}f)$.

We refer to κ as κ_q when it is the coupling coefficient between the Higgs and T-odd quarks and as κ_l for the Higgs and T-odd leptons. The mass spectrum for the T-odd fermions are given at order $\mathcal{O}(v^2/f^2)$ by

$$m_{u-} = \sqrt{2}\kappa_q f(1 - \frac{1}{8}\frac{v^2}{f^2}), \qquad m_{d-} = \sqrt{2}\kappa_q f \tag{4.69}$$

$$m_{\ell_H} = \sqrt{2}\kappa_\ell f. \tag{4.70}$$

The correction term in order $\mathcal{O}(v^2/f^2)$ is a contribution from EWSB since only the up-type quarks have couplings with the Higgs doublet as Eq. (4.68) proportional to c_ξ and s_ξ.

For the top sector, introducing fields or interactions is slightly different from that of other fermions sectors because there is an additional top partner to cancel the quadratical divergent

one-loop contribution to the Higgs mass. To realize the Collective Symmetry Breaking pattern for top quark fields, the interaction states of $SU(3)$ in Eq. (4.31) can be represented in incomplete $SU(5)$ multiplets as

$$\Psi_{t1} = \begin{pmatrix} q_1 \\ T_{1L} \\ \mathbb{0}_{2\times 1} \end{pmatrix}, \qquad \Psi_{t2} = \begin{pmatrix} \mathbb{0}_{2\times 1} \\ T_{2L} \\ q_2 \end{pmatrix}. \tag{4.71}$$

For the quark doublets, we use the following convention

$$q_i = -i\sigma_2 \begin{pmatrix} t_i \\ b_i \end{pmatrix} \tag{4.72}$$

where σ_2 is one of Pauli matrices. T_L is introduced as cancellon field, see Eq. (4.32). The cancellon fields play an important role in the cancellation of the quadratic divergence in the radiative correction of the Higgs mass. Under T-parity, they transform as following:

$$T : \begin{cases} \Psi_{t1} \leftrightarrow -\langle\Sigma\rangle\Psi_{t2} & (q_1 \leftrightarrow -q_2,\ T_{1L} \leftrightarrow -T_{2L}) \\ T_{1R} \leftrightarrow T_{1R} & \\ T_{2R} \leftrightarrow -T_{2R} & \end{cases} \tag{4.73}$$

Including the $SU(5)$ multiplet, the T-parity invariant Yukawa-like Lagrangian is

$$\begin{aligned} \mathcal{L}_Y \supset & \frac{\lambda_1 f}{2\sqrt{2}}\epsilon_{ijk}\epsilon_{xy}\left((\bar{\Psi}_{1t})_i\Sigma_{jx}\Sigma_{ky} - (\bar{\Psi}_{2t}\langle\Sigma\rangle)_i\Sigma'_{jx}\Sigma'_{ky}\right)t_R \\ & + \lambda_2 f(\bar{T}_{1L}T_{1R} + \bar{T}_{2L}T_{2R}) + \text{h.c.} \end{aligned} \tag{4.74}$$

where $\{i,j,k\}$ sum over {1,2,3} and $\{x,y\}$ sum over {4,5}. The SM top and top partner fields form T-parity eigenstates as

$$q_{L\pm} = \frac{(q_1 \mp q_2)}{\sqrt{2}}, \qquad T_{L\pm} = \frac{(T_{1L} \mp T_{2L})}{\sqrt{2}}, \quad \text{and} \quad T_{R\pm} = \frac{(T_{1R} \mp T_{2R})}{\sqrt{2}}, \tag{4.75}$$

where the states with subscripts $+$ are T-parity even states while those with subscript $-$ are T-odd eigenstates. We can express the Lagrangian Eq. (4.74) in terms of the T-parity eigenstates, which is

$$\mathcal{L}_Y \supset \lambda_1 f\left(\frac{s_\Sigma}{\sqrt{2}}\bar{t}_{L+}t_{R+} + \frac{1+c_\Sigma}{2}\bar{T}_{L+}t_{R+}\right) + \lambda_2 f(\bar{T}_{L+}T_{R+} + \bar{T}_{L-}T_{R-}) + \text{h.c.} \tag{4.76}$$

and $s_\Sigma = \sin(\sqrt{2}h/f)$, $c_\Sigma = \cos(\sqrt{2}h/f)$, respectively. We obtain mass terms for T-odd top partner state $T_- \equiv (T_{L-}, T_{R-})$ as

$$M_{T-} = \lambda_2 f. \tag{4.77}$$

For the mass of the T-even combination of the states, one gets

$$\mathcal{L}_Y \supset (\bar{t}_{L+}, \bar{T}_{L+})\mathcal{M}\begin{pmatrix} t_R \\ T_{R+} \end{pmatrix} + \text{h.c.} \quad \text{where} \quad \mathcal{M} = \begin{pmatrix} \frac{\lambda_1 f}{\sqrt{2}} \sin\left(\frac{\sqrt{2}h}{f}\right) & 0 \\ \lambda_1 f \cos^2\left(\frac{h}{\sqrt{2}f}\right) & \lambda_2 f \end{pmatrix}. \tag{4.78}$$

Diagonalizing $\mathcal{M}$ and expanding of Σ at leading order in v/f, one can find the mass spectrum for top quarks,

$$M_{t+} = M_{t_{SM}} = \frac{\lambda_1\lambda_2}{\sqrt{\lambda_1^2+\lambda_2^2}}v, \qquad M_{T+} = f\sqrt{\lambda_1^2+\lambda_2^2}. \tag{4.79}$$

The top partner and SM top quark mass term can be rewrite as functions of R, the ratio between the top Yukawa coupling constants λ_1/λ_2, as

$$M_t = \frac{\lambda_2 R}{\sqrt{1+R^2}}v, \tag{4.80}$$

$$M_{T-} = \frac{M_t}{v}\frac{f\sqrt{1+R^2}}{R}, \tag{4.81}$$

$$M_{T+} = \frac{M_t}{v}\frac{f(1+R^2)}{R} = M_{T-}\sqrt{1+R^2}. \tag{4.82}$$

These expression will be useful when we discuss the phenomenological aspects of this model and its the collider results.

4.3.2. Possible T-parity violation

We discuss the case of the Littlest Higgs model with violated T-parity. This does not imply the complete absence of T-parity. But we assume that T-parity is violated by anomalous term. In fact, T-parity violation can happen by an anomalous Wess-Zumino-Witten term, [54, 55].

As mentioned in Section 4.3.1, A_H is a dark matter candidate with T-parity. By dark matter experiments [56–58], there are strong constraints for the dark matter A_H. To avoid this strong constraints, we study the case that T-parity is violated and the heavy photon A_H decays.

According to Refs. [54] and [59], when it is kinematically allowed, the heavy photon A_H decays into a pair of the electroweak gauge bosons, WW or ZZ, with the partial width

$$\Gamma(A_H \to ZZ) = \frac{1}{2\pi}\left(\frac{Ng'}{40\sqrt{3}\pi^2}\right)^2\frac{m_{A_H}^3 m_Z^2}{f^4}\left(1-\frac{4m_Z^2}{m_{A_H}^2}\right)^{\frac{5}{2}}, \tag{4.83}$$

$$\Gamma(A_H \to W^+W^-) = \frac{1}{\pi}\left(\frac{Ng'}{40\sqrt{3}\pi^2}\right)^2\frac{m_{A_H}^3 m_W^2}{f^4}\left(1-\frac{4m_W^2}{m_{A_H}^2}\right)^{\frac{5}{2}}, \tag{4.84}$$

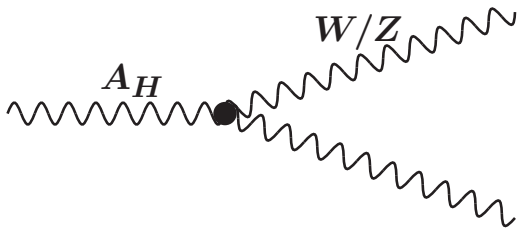

Fig. 4.3.: A_H decay when T-parity is broken

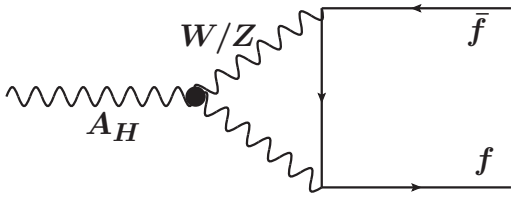

Fig. 4.4.: A_H decay via loop induced by SM gauge bosons

where a integer N is is the number of colors of the $SU(N)$ gauge theory that confines to generate the condensate at scale Λ in order to break the Little Higgs symmetry.

If it is below its kinematical limit, the heavy photon A_H decay via a triangle loop mediated by the electroweak gauge bosons as Fig. 4.4 of which the partial width is

$$\Gamma(A_H \to ff) = \frac{N_{C_f} M_{A_H}}{48\pi}\sqrt{1-\frac{4m_f^2}{M_{A_H}^2}}((c_R-c_L)^2(1-\frac{4m_f^2}{M_{A_H}^2})+(c_R+c_L)^2(1+\frac{2m_f^2}{M_{A_H}^2})) \tag{4.85}$$

where c_L and c_R are the coefficients of the left and right chiral projectors. The fermionic coefficients are shown in Table 4.1.

Based on Eqs. (4.83)-4.85, the heavy photon decays instantaneously around 10^{-17}s when the global symmetry breaking scale f is in the region of $1-10$TeV, N is $\mathcal{O}(1)$ and the total width of A_H is of $0.01-1$eV. Hence, for T-parity violation the heavy photon A_H can no longer be considered as a dark matter candidate.

Particles	c_L^f	c_R^f
$A_H e^+e^-$	$\frac{9\hat{N}}{160\pi^2}\frac{v^2}{f^2}g^4g'(4+(c_w^{-2}-2t_w^2)^2)$	$-\frac{9\hat{N}}{40\pi^2}\frac{v^2}{f^2}g'^5$
$A_H\bar{\nu}\nu$	$\frac{9\hat{N}}{160\pi^2}\frac{v^2}{f^2}g^4g'(4+c_w^{-4})$	0
$A_H\bar{u}_a u_b$	$-\frac{\hat{N}}{160\pi^2}\frac{v^2}{f^2}g^4g'(36+(3c_w^{-2}-4t_w^2)^2)\delta_{ab}$	$-\frac{\hat{N}}{10\pi^2}\frac{v^2}{f^2}g'^5\delta_{ab}$
$A_H\bar{d}_a d_b$	$-\frac{\hat{N}}{160\pi^2}\frac{v^2}{f^2}g^4g'(36+(3c_w^{-2}-2t_w^2)^2)\delta_{ab}$	$-\frac{\hat{N}}{40\pi^2}\frac{v^2}{f^2}g'^5\delta_{ab}$

Table 4.1.: Coefficients for the A_H T-parity violating (TPV) decays

We discuss more in Section 5.4 phenomenological aspects and in Section 5.5.2 about A_H decay.

4.4. The Simplest Little Higgs Model

Simple group Little Higgs models have extended gauge group structure as $SU(N) \times U(1)$. As its name suggests, the Simplest Little Higgs model has the minimum value for N, i.e. this model has $SU(3) \times U(1)_X / SU(2)_L \times U(1)_Y$ as the group structure.

Here, we describe the group structure of the model and how the Collective Symmetry Breaking works in the Simplest Little Higgs model. Other details such as for fermion sectors are in Appendix B.

Gauge and scalar sectors

Global symmetry of the Simplest Little Higgs model is broken as a coset space

$$(SU(3) \times U(1))_1 \times (SU(3) \times U(1))_2 / (SU(2) \times U(1)), \tag{4.86}$$

which gives 10 Nambu-Goldstone bosons. 5 NGBs are eaten by heavy gauge bosons and 4 form the Higgs double H, and 1 is the pseudo-axion η. The vacuum expectation values to trigger the global symmetry breaking are $\langle \Phi_1 \rangle$, $\langle \Phi_2 \rangle$. The scalar fields are parameterized as

$$\Phi_1 = e^{i\Theta f_2/f_1} \begin{pmatrix} 0 \\ 0 \\ f_1 \end{pmatrix}, \qquad \Phi_2 = e^{i\Theta f_1/f_2} \begin{pmatrix} 0 \\ 0 \\ f_2 \end{pmatrix}, \tag{4.87}$$

where

$$\Theta = \frac{1}{f} \begin{bmatrix} \begin{pmatrix} \mathbb{0}_{2\times 2} & H \\ H^\dagger & 0 \end{pmatrix} + \frac{\eta}{\sqrt{2}} \mathbb{1}_{3\times 3} \end{bmatrix}, \qquad H = \begin{pmatrix} h^0 \\ h^- \end{pmatrix}. \tag{4.88}$$

$H^T = (h^0, h^-)$ is a complex scalar doublet corresponding to the SM-like Higgs. f_1, f_2 are the symmetry breaking scales and they can be redefined as $f = \sqrt{f_1^2 + f_2^2}$ and $\tan\beta = f_1/f_2$. Also, we frequently use $c_\beta \equiv \cos\beta = f_1/\sqrt{f_1^2 + f_2^2}$ and $s_\beta \equiv \sin\beta = f_2/\sqrt{f_1^2 + f_2^2}$. Global symmetry as two copies of $SU(3) \times U(1)$, each of them works complementarily in the Collective Symmetry Breaking mechanism.

This model is based two non-linear sigma models, accordingly the kinetic terms of the Lagrangian for the scalar and gauge boson parts are given by

$$\mathcal{L} = |D_\mu \Phi_i|^2 = \left| \left(\partial_\mu + i g A_\mu^a T^a - \frac{i g_x}{3} B_\mu^x \right) \Phi_i \right|^2 \tag{4.89}$$

where we use the covariant derivative given by

$$\mathcal{D}_\mu \;=\; (\partial_\mu + igA^a_\mu T^a - \frac{i}{3} g_x B^x_\mu). \tag{4.90}$$

Here, B^x_μ is the gauge field of $U(1)_X$, A^a_μ is that of $SU(3)$ and T^a are the generators of $SU(3)$. $A_\mu T^a$ can be expressed as

$$A^a_\mu T^a = \frac{A^3}{2}\begin{pmatrix} 1 & & \\ & -1 & \\ & & 0 \end{pmatrix} + \frac{A^8}{2\sqrt{3}}\begin{pmatrix} 1 & & \\ & 1 & \\ & & -2 \end{pmatrix} + \frac{1}{\sqrt{2}}\begin{pmatrix} & W^+ & Y^0 \\ W^- & & X^- \\ \bar{Y}^0 & X^+ & \end{pmatrix} \tag{4.91}$$

where $X^\pm$, Y^0, $\bar{Y}^0$ are massive gauge fields and the linear combination of A^8 with B_μ gives heavy neutral gauge fields. g is the same constant as the SM $SU(2)$ gauge coupling constant and g_x is the gauge coupling constant of $U(1)_X$ and can be fixed by g and the weak mixing angle $t_W (= \tan\theta_W)$ as

$$g_x = \frac{g\, t_W}{\sqrt{1 - t_W^2/3}}. \tag{4.92}$$

The gauge fields X and Y get their masses from symmetry breaking at the scale f and so does Z_H, the linear combination of A^8 and B_μ. Their masses are

$$M_{X^\mp} = M_{Y^0} = M_{\bar{Y}^0} = \frac{gf}{\sqrt{2}}, \qquad M_{Z_H} = gf\sqrt{\frac{2}{2 - t_W}}. \tag{4.93}$$

Before electroweak symmetry breaking (EWSB), the gauge bosons of $SU(2)_W \times U(1)_Y$ are still massless. There is already mixing.

After spontaneous symmetry breaking triggered by Φ_1, Φ_2 there are mixing for the neutral massive gauge field Z_H and B, the hyper gauge boson, parameterized as

$$Z_H = \frac{\sqrt{3}gA^8 + g_x B^x}{\sqrt{3g^2 + g_x^2}} = \frac{1}{\sqrt{3}}(\sqrt{3 - \tan^2\theta_w}A^8 + \tan\theta_w B^x), \tag{4.94}$$

$$B = \frac{-g_x A^8 + \sqrt{3}gB^x}{\sqrt{3g^2 + g_x^2}} = \frac{1}{\sqrt{3}}(-\tan\theta_w A^8 + \sqrt{3 - \tan^2\theta_w}B^x). \tag{4.95}$$

Hypercharge is defined via

$$Y = -\frac{1}{\sqrt{3}}T^8 + Q_X$$

with the eigenvalue of 8th generator of $SU(3)$,

$$T^8 = \frac{1}{2\sqrt{3}}\mathrm{diag}(1, 1, -2).$$

Y is the hypercharge of $U(1)_Y$ and Q_X is the charge of of $U(1)_X$.

After EWSB, the heavy gauge boson fields yield additional corrections of $\mathcal{O}(v^2/f^2)$, in particular Z_H, which is a combined state of a gauge field of $SU(3)$ and that of $U(1)$ seen in Eq. (4.94), which affects the mass terms for gauge bosons. The mass terms of the SM gauge bosons become [47]

$$M_Z = \frac{g\ v}{2c_W}\left(1 + \frac{v^2}{f^2}\frac{(1-t_W^2)^2}{16} + \mathcal{O}\left(\frac{v^2}{f^2}\right)\right), \tag{4.96}$$

$$M_W = \frac{g\ v}{2}\left(1 - \frac{1}{12}\frac{v^2}{f^2}\frac{t_\beta^4 - t_\beta^2 + 1}{t_\beta} + \mathcal{O}\left(\frac{v^2}{f^2}\right)\right). \tag{4.97}$$

Comparing the mass of the SM gauge bosons $M_W^{SM} = gv_{SM}/2$ with Eq. (4.97), we can see the correction term for *vev* as well,

$$v = v_{SM}\left(1 + \frac{1}{12}\frac{v_{SM}^2}{f^2}\frac{t_\beta^4 - t_\beta^2 + 1}{t_\beta}\right). \tag{4.98}$$

We can consider the Higgs potential as in the SM

$$V = m^2 H^\dagger H + \lambda (H^\dagger H)^2, \tag{4.99}$$

where m is required to be negative for Electroweak symmetry breaking. Similarly to the other Little Higgs models, in the SLH model the potential for the Higgs is generated by the Coleman-Weinberg mechanism. As it is shown in Ref. [46,60], a nontrivial result for the pseudo-Goldstone boson is obtained only by $\left|\Phi_1^\dagger \Phi_2\right|^2$ term in the CW potential up to dimension-4 operators. It is interesting that the term $\left|\Phi_1^\dagger \Phi_2\right|^2$ does not have any η-dependence,

$$\Phi_1^\dagger \Phi_2 = f^2 s_\beta c_\beta \exp\left[-i\left(t_\beta + \frac{1}{t_\beta}\frac{\eta}{\sqrt{2}f}\right)\right]\cos\left(\frac{h}{f c_\beta s_\beta}\right). \tag{4.100}$$

To give rise to a mass term for η, we introduce a new term by hand,

$$-\mu^2\left(\Phi_1^\dagger \Phi_2 + \text{h.c.}\right). \tag{4.101}$$

This term explicitly breaks the $SU(3)$ global symmetry and ruins the CSB mechanism since it generates the 1-loop quadratically divergent corrections to the Higgs mass. But, this correction has numerically insignificant effects. So, we adopt this extension as Ref. [46]. Expanding this potential with the scalar fields Φ_1, Φ_2 by substituting Eq. (4.87) gives

$$\begin{aligned} V &= \mu^2 \Phi_1^\dagger \Phi_2 + \text{h.c.} \\ &= 2 s_\beta c_\beta \mu^2 \cos\left(\frac{\eta}{\sqrt{2} s_\beta c_\beta}\right)\left[1 - \frac{1}{2 s_\beta^2 c_\beta^2}(h^\dagger h) + \frac{f (h^\dagger h)^2}{24 s_\beta^3 c_\beta^3} + ...\right]. \end{aligned} \tag{4.102}$$

Adding radiative corrections to the Higgs fields in order to form the mass terms by the

Coleman-Weinberg mechanism, which generates one-loop corrections to the Higgs mass δm^2.

$$\delta m^2 = -\frac{3}{8\pi^2}\left[\lambda_t^2 M_T^2 \log\left(\frac{\Lambda^2}{M_T^2}\right) - \frac{g^2}{4} M_X^2 \log\left(\frac{\Lambda^2}{M_X^2}\right) - \frac{g^2}{8}(1+\tan^2\theta_w) M_{Z_H}^2 \log\left(\frac{\Lambda^2}{M_{Z_H}^2}\right)\right] \tag{4.103}$$

Considering all terms for scalar fields as in Ref. [61, 62], the potential becomes

$$\begin{aligned} V = &\left(\delta m^2 + \frac{\mu^2}{s_\beta c_\beta}\right) H^\dagger H + \frac{\mu^2}{s_\beta c_\beta}\frac{\eta^2}{2} - \left(\frac{\mu^2}{12(s_\beta c_\beta f)^2} - \delta\lambda\right)(H^\dagger H)^2 \\ &- \frac{\mu^2}{12(s_\beta c_\beta f)^2}\left(\frac{\eta^4}{4} + \frac{3(H^\dagger H)\eta}{2}\right) + ... \end{aligned} \tag{4.104}$$

Clearly, there are the Higgs and the η mass terms,

$$M_\eta^2 = \frac{\mu^2}{s_\beta c_\beta}, \tag{4.105}$$

$$M_H^2 = -2(\delta m^2 + m_\eta^2). \tag{4.106}$$

Since we know the mass of the Higgs and all the coefficients of the CW corrections to the Higgs mass Eq. (4.103), M_η is a dependent quantity with respect to the model parameters $(f, \tan\beta)$.

4.5. Electroweak precision tests

As aforementioned, the Littlest Higgs model has constrained by electroweak precision observables. We discuss how electroweak precision observables are parameterized with regard to the Littlest Higgs model using S, T, and U parameterization, Section 2.4.

In the Littlest Higgs with T-parity

As we mentioned in the previous section, the Littlest Higgs model is strictly constrained from EWPO in its parameter space and T-parity is introduced to mitigate the constraints by minimizing the contributions to the oblique parameters from Little Higgs model particles.

In Refs. [45], [64], [65], and [63], electroweak precision observables in the LHT model are scrutinized in detail.

We list the most important points here. In the LHT model, there is no contribution of LHT particles at tree level. The effects of LHT on EWPO appear only via the process including loop diagrams which are induced by the T-parity even top partner T^+, T-odd heavy fermions, and heavy gauge bosons.

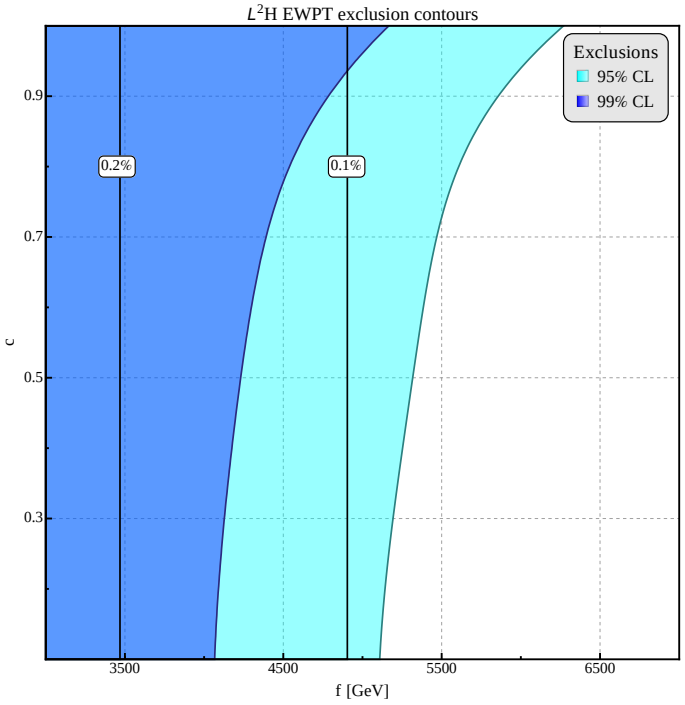

Fig. 4.5.: Excluded regions in Littlest Higgs model parameter space at 95% and 99%, [63]

The T-even top partner T^+ contributions to oblique parameters can be expressed as

$$S_{T^+} = \frac{s_\beta^2}{2\pi}\left[\left(\frac{1}{3}-c_\beta^2\right)\log x_t + c_\beta^2\frac{1+x_t^2}{1-x_t^2} + \frac{2c_\beta^2 x_t^2(3-x_t)\log x_t}{(1-x_t)^3} - \frac{8c_\beta^2}{3}\right], \tag{4.107}$$

$$T_{T^+} = \frac{3s_\beta^2 M_t^2}{16\pi s_W^2 c_W^2 M_Z^2}\left[\frac{s_\beta^2}{x_t} - 1 - c_\beta^2 - \frac{2c_\beta^2}{1-x_t}\log x_t\right], \tag{4.108}$$

$$U_{T^+} = -\frac{s_\beta^2}{2\pi}\left[s_\beta^2\log x_t + c_\beta^2\frac{1+x_t^2}{1-x_t^2} + \frac{2c_\beta^2 x_t^2(3-x_t)\log x_t}{(1-x_t)^3} - \frac{8c_\beta^2}{3}\right], \tag{4.109}$$

where $x_t = M_t^2/M_{T^+}^2$ and s_β is the sine of t-T^+ mixing angle $\sin\beta = (\lambda_1^2)/(\lambda_1^2+\lambda_2^2)(v/f)$. Even though we assume the T^+ mass to be minimal, it is much larger than the SM top mass. With the condition $x_t \ll 1$, the oblique parameters become much simpler. For $x_t \ll 1$ Eq. (4.108), for example, becomes

$$T_{T^+} = \frac{3}{8\pi s_W^2 c_W^2}\frac{M_t^4}{M_Z^2}\frac{R^2}{M_{T^+}^2}\left[\log\left(\frac{M_{T^+}^2}{M_t^2}\right) - 1 + \frac{R^2}{2}\right]. \tag{4.110}$$

Interestingly, when $R = 1$, i.e. the ratio of λ_1 and λ_2 is 1, the mass of T^+ has its minimum and corrections to EWPO mostly cancel. So, exclusion limits by EWPO get weakened around $R \approx 1$. The region $f < 405\,\text{GeV}$ is excluded for $R \approx 1$ and $f < 1.3\,\text{TeV}$ is excluded for $R \approx 3$. [63]

For our study, we concentrate on a 4-fermion box diagram with mirror fermions, of which

the effective operator is

$$\mathcal{O}_{\text{4-f}} = -\frac{\kappa_i^2}{128\pi^2 f^2}\bar{\psi}_L\gamma^\mu\psi_L\bar{\psi}'_L\gamma^\mu\psi'_L, \tag{4.111}$$

where ψ refer to SM fermions. κ_i refer to the Yukawa coupling constants, κ_q or κ_ℓ, of T-odd mirror fermions and we use κ_q for T-odd quarks and κ_ℓ for T-odd leptons. 2-loop diagrams contains SM- and mirror fermion loops into the W-/Z self energies. The constraint from the 4-fermion operator Eq. (4.111) comes from searches for contact interactions, i.e. from LEP $ee \to jj$ processes for the $(\ell\ell)(ee)$ operator $(\kappa_q\kappa_\ell)$ and from LHC dijet searches from the $(qq)(qq)$ operator (κ_q^2).

For what corrections EWPO this operator induces a contribution to the T parameter in the form

$$T_{q_H,\ell_H} = -\frac{\kappa_i^2}{192\pi^2\alpha}\left(\frac{v}{f}\right)^2. \tag{4.112}$$

T_{q_H,ℓ_H} depends on κ_i as well as f, but not on R. If f is fixed, T_{q_H,ℓ_H} will increase with the mirror fermion masses. Sometimes we set κ_q different from κ_l and sometimes set them equal. We will not apply such assumptions, but we distinguish the Yukawa coupling of T-odd quarks and that of T-odd leptons only. We will investigate how the operator of contact interactions in Eq. (4.112) constrains the LHT model parameter space in comparison to LHC Run2 data in Section 6.1.5.

4.6. Naturalness

To be considered for a model or parameter space as natural, radiative corrections to the scalar potential should be in a *natural* order, which is usually in the small order as the scalar mass term from the mechanism that created that mass term. The fact that how much a Higgs is fine-tuned in the model can be measured as the ratio of the bare mass term of the Higgs and its radiative correction term.

With regard to Little Higgs models, the largest contribution of a radiative correction to the Higgs mass is coming from the cancellon top partner. The cancellon for the top quark loop contribution to the Higgs quadratic divergence is the top partner, $T^\pm$.

There is no universal definition for the degree of fine-tuning, we use the definition of Ref. [43].

The quadratic divergence of SM-like Higgs can be canceled by new particleswith similar quantum numbers as the SM particles that induce the quadratic divergence.

By constraining this mass gap, we can avoid fine-tuning as well as give upper bounds how heavy the new particles can be. For the Littlest Higgs model the cancellon for the Higgs divergence is the top partner, $T^\pm$, and the dominant log-divergent contribution is caused by

$T^{\pm}$, thus it is taken account into:

$$\begin{aligned} \mu^2_{exp} &= \frac{m_h^2}{2} \\ \delta\mu^2 &= -\frac{3\lambda_t m_T^2}{8\pi^2}\log\frac{\Lambda^2}{m_T^2} \end{aligned} \tag{4.113}$$

where $\Lambda = 4\pi f$, λ_t is the SM top Yukawa coupling. We can quantify the fine-tuning through the parameter:

$$\Delta = \frac{\mu^2_{exp}}{|\delta\mu^2|} \tag{4.114}$$

We will use this parameter Δ and compare it with the exclusions from contact interactions. and LHC Run2 data in Section 6.1.5. We not only compare it with the exclusions from LHC run 2 data and contact interactions, but also study how much higher/more severe the fine tuning becomes by taking the constraints from the new data into account.

Chapter 5.

Phenomenology of LHT at the LHC

This chapter details the phenomenology the Littles Higgs model with T-parity (LHT) to the LHC experiments. All possible pair productions of new particles and their topologies including decays are studied for the LHT model. As signatures of the model depend on several model parameters, we distinguish cases depending on the LHT spectrum; the Fermion Universality *model, the* Heavy q_H*-model and the* Light ℓ_H *model. Each benchmark scenario represent the result for that parameters. In addition, we study the case where T-parity is broken and the consequences of this breaking for the model phenomenology. We present the toolchain for the simulation of the LHT processes at the LHC and to recast LHC SUSY searches for the LHT model.*

5.1. Considered production processes

As discussed in the previous chapter, the LHT provide extra classes of particles according to the group structure and the Collective Symmetry Breaking. From production channels of the additional particles we expect to see distinguishable effects at the LHC experiments. We consider 6 process classes, which are of relevance for the hadron collider phenomenology of the Littlest Higgs model with T-parity (LHT), namely:

$$1.\ pp \to q_H q_H, q_H \bar{q}_H, \bar{q}_H \bar{q}_H, \tag{5.1a}$$
$$2.\ pp \to q_H V_H, \tag{5.1b}$$
$$3.\ pp \to \ell_H \bar{\ell}_H, \tag{5.1c}$$
$$4.\ pp \to V_H V_H, \tag{5.1d}$$
$$5.\ pp \to T_+ T_+, T_- T_-, \tag{5.1e}$$
$$6.\ pp \to T_+ \bar{q}, \bar{T}_+ q, T_+ W^\pm, \bar{T}_+ W^\pm. \tag{5.1f}$$

These are regarded as the major production channels of LHT particles at the LHC.

Here, we will refer to T-parity odd quarks, $\{u_H,\ d_H,\ c_H,\ s_H,\ b_H,\ t_H\}$, as q_H, heavy gauge bosons, $\{A_H, Z_H, W_H\}$, as V_H, and T-parity odd leptons, $\{e_H, \nu_H, \tau_H, \mu_H\}$ as ℓ_H. After being produced, they decay into a plethora of possible final states discussed below. To analyze the multidimensional parameter space of the general LHT model, we define benchmark scenarios with several assumptions about the masses of the T-odd particles.

For unbroken T-parity, all of the T-parity odd particles are produced in pairs. Among LHT particles, only T_+ introduced as a cancellon for the Higgs-top loop divergence can be produced in association with SM particles because T_+ is T-parity even like the SM particles.

Their production cross sections are decreasing functions with increasing f because all of the particle masses are proportional to f.

T-odd quarks q_H decay into a heavy gauge boson V_H and a SM quark, if the process is kinematically allowed. Although the heavy gauge bosons V_H have several decay channels, if kinematically allowed, the dominant decays are $W_H \to A_H W$, $Z_H \to A_H H$. As A_H does not decay as the lightest T-parity odd particle, the major final state of q_H decay would be SM gauge boson and jets with missing transverse momentum.

The heavy gauge bosons V_H can also decay to q_H and a SM quark if $M_{V_H} > M_{q_H}$ and it is followed by the decay $q_H \to A_H q$. The major final state of that decay would be jets and missing transverse momentum. We will go into details about the features of production channels for LHT particles and decays in the following Section 5.5.

Various signatures allow to test the LHT. The dominant search elements depend on the mass spectrum of the LHT particles. Thus,we have investigated the parameter space of the LHT model in terms of the following parameters at the center of mass energy $\sqrt{s} = 13\,\text{TeV}$: the symmetry breaking scale f, the Yukawa coupling parameters of the extended LHT group κ_q, κ_ℓ and the top Yukawa coupling ratio R.

5.2. Benchmark scenarios

We distinguish three cases with respect to the relative and absolute size of the model parameters κ_q, and κ_ℓ; κ_q refers to the Yukawa coupling parameter of T-parity odd quarks q_H and κ_ℓ is the Yukawa coupling parameter of the T-odd leptons ℓ_H. These are the parameters giving rise to mass terms of the fermionic LHT particles q_H and ℓ_H. Furthermore, we separate cases with two mass scales for the particles $T^\pm$ whose mass is set by the model parameter R. For each of the benchmark scenarios, we also consider the corresponding case with T-parity violation.

In this section, we detail each benchmark scenario. They are summarized in Table 5.1.

5.2.1. Fermion Universality model

Firstly, the *Fermion Universality* model makes the assumption that the κ_q and κ_ℓ are equal, i.e. we always scan $f-\kappa$ where $\kappa := \kappa_q = \kappa_\ell$. Even if the T-odd quark and lepton partners have the same mass spectrum, the production cross section related to the color-charged fermions q_H is much larger than that of the color-neutral fermions. When scanning the $f-\kappa$ plane, the variation of f changes the mass of all LHT particles, while that of κ only affects the T-odd fermion mass. As we can see in the comparison of Eqs. (4.60) and (4.69), if κ is less than 0.4, then $M_{V_H} > M_{q_H}$, W_H decays into $q_H q$ or $\ell_H \nu$ and Z_H decays into $q_H q$ or $\ell_H \ell$. Otherwise, M_{q_H} is always heavier than M_{V_H}, so that all q_H decay into V_H.

5.2.2. Heavy q_H model

Second, the *Heavy* q_H model assumes the T-parity odd quarks q_H to be decoupled from the detectable spectrum, i.e. to be much as heavier than the T-parity odd leptons ℓ_H. Again, as

Sector	Model	Constraint	Phenomenology	Considered Topology
f_H	*Fermion Universality*	$\kappa_l = \kappa_q$	• mass degeneracy of q_H, ℓ_H • ℓ_H production negligible	Exclude process 3
	Heavy q_H	$\kappa_q = 4.0$	• q_H decoupled • ℓ_H production relevant	Exclude processes 1, 2
	Light ℓ_H	$\kappa_l = 0.2$	• ℓ_H very light • V_H branching ratios change	Exclude process 3
$T^\pm$	*Light* $T^\pm$	$R = 1.0$	• $T^\pm$ are light/accessible	Include process 4, 5
	Heavy $T^\pm$	$R = 0.2$	• $T^\pm$ are heavy/inaccessible	Exclude process 4, 5
A_H	*TPC*	No TPV	• A_H is stable and invisible	A_H stable
	TPV	With TPV	• A_H is unstable	$A_H \to VV$ decays

Table 5.1.: Definitions of the considered benchmark models of this study. In this work we consider all $3 \times 2 \times 2$ combinations of the options given in this table. The process numbers refer to the list in Eq. (5.1).

we can see in Eqs. (4.69) and (4.70), T-parity odd fermions mass terms are proportional to $\kappa_q,\ \kappa_\ell$.

$$M_{u_H} = \sqrt{2}\kappa_q f(1 - \frac{1}{8}\frac{v^2}{f^2}), \qquad M_{d_H} = \sqrt{2}\kappa_q f$$
$$M_{\ell_H} = \sqrt{2}\kappa_\ell f \tag{5.2}$$

By raising the κ_q value, we make q_H much heavier than in the other benchmarks. When M_{q_H} reach to the multi-TeV-scale, q_H is too heavy to be produced at the LHC. Thus, we hardly can see interactions originated by the q_H production. Then, what we can expect is to observe other interactions that used to be covered with signatures of q_H. For example, final states related to ℓ_H would become distinguishable than before. Therefore, we expect to have insight into the LHC bounds that are derived from the color-neutral LHT T-odd particles.

5.2.3. Light ℓ_H model

Finally, for the *Light* ℓ_H model, we fix $\kappa_\ell = 0.2$, which makes ℓ_H very light. This permits for more particles to decay into leptonic states. Especially, heavy gauge bosons V_H are expected to decay into ℓ_H with $\sim 100\%$ probability and the purpose of this scenario to observe how the bounds change compared to the *Fermion Universality* model.

Summary

We categorize benchmark scenarios of some extreme cases to observe effects of the model parameters. In the *Heavy* q_H model, more T-odd leptons contributions are expected to con-

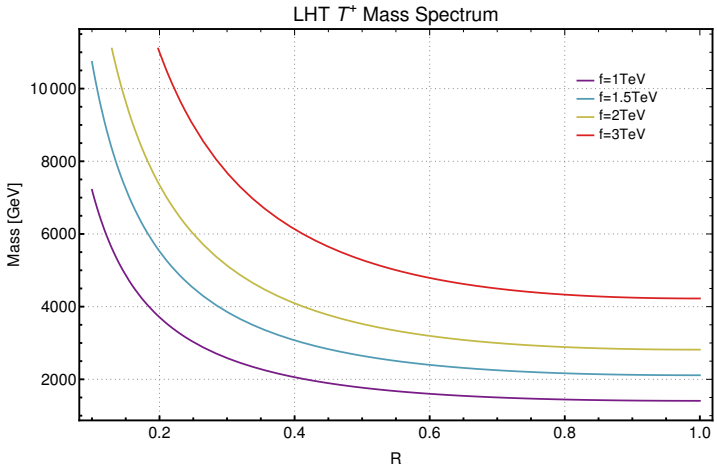

Fig. 5.1.: Mass spectrum of top partner T^+ with respect to R. The T^- mass distribution as a function of R is very similar.

tribute to the result compared to the *Fermion Universality* model, because T-odd quarks are already decoupled in the given center-of-mass energy. This is why production process 1 and 2 of Eq. (5.1) are not considered for the result analyses. Thus, $\ell_H\ell_H$ production, 3 of Eq. (5.1), is considered in the *Heavy* q_H model. On the other hand, in the *Fermion Universality* and the *Light* ℓ_H model, process 3 of Eq. (5.1) is not considered. If masses of T-odd fermions are degenerate, the amount of ℓ_H production is unimportant compared to that of q_H because of the strong production at the proton-proton collision.

5.3. R-dependence of $T^\pm$

The phenomenology of the LHT model also depend on the mass of the top partners $T^\pm$ and hence on the parameter R. The $T^\pm$'s mass terms, see Eq. (**??**), depend on f and R, where R is the ratio of the Yukawa coupling parameters λ_1/λ_2. We do not scan R but consider two cases: $R = 1$ and $R = 0.2$ where $T^\pm$ is either light with masses comparable to the V_H masses, or heavy so that the $T^\pm$ are experimentally decoupled, respectively. Fig. 5.1 shows the R-dependence of the $T^\pm$ mass term.

5.4. T-parity violation

Until now, we only discussed the case that A_H does not decay because it is the lightest T-odd particle and stable thanks to T-parity conservation. As we discussed in Section 4.3.2, it is possible to introduce decays of A_H by the Wess-Zummino-Witten (WZW) anomaly terms.

According to the Eqs. (4.83) and (4.84), A_H may decay into WW and ZZ. Also, taking 2-loop diagrams into account as in Eq. (4.85), fermionic decays into ff, $\ell\ell$ may appear.

Although it seems as if no more invisible particle would be predicted, Supersymmetry motivated searches still are expected to be useful for analyzing this scenario. This is because there may be still a notable amount of missing transverse momentum thanks to the leptonic decays

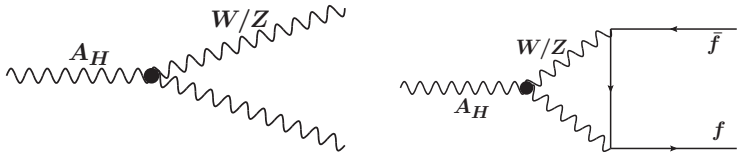

Fig. 5.2.: A_H decays

of the W boson into $\ell\nu$ and the invisible decay of the Z boson into $\nu\nu$. For testing the LHT, we distinguish cases with conserved T-parity and with broken T-parity.

5.5. Topologies

To allow for a more comprehensive view on the results later, we first discuss the expected final state topologies resulting from LHT particle production and decays.

5.5.1. Production cross sections

We show the production cross sections of the processes in Eq. (5.1) as a function of f and κ in Figs. 5.3 and 5.4 for a center-of-mass energy of $\sqrt{s} = 13\,\text{TeV}$ at the LHC. Since color neutral fermions ℓ_H do not affect the production cross sections of the other particles of the LHC, changing κ_ℓ to 0.2 does not affect the cross sections and, thus, the production cross sections of the *Fermion Universality* model with $\kappa = \kappa_q = \kappa_\ell$ and that of the *Light* ℓ_H model are identical. Regarding the top partners $T^\pm$, if $T^\pm$ are heavy and in the decoupling limits, their cross section is almost vanishing. So, we only show the figures for the *Light* $T^\pm$ case for which the cross sections are experimentally accessible. Also, the case where T-parity is violated (TPV) has no effects on the production cross sections, our discussion refers to both the case where T-parity is conserved (TPC) and TPV scenarios.

All masses of the LHT particles are proportional to f which causes the cross sections of all processes to decrease as f increases due to kinematics. Production channels involving q_H happen through QCD interactions, which depend on the mass of q_H and the strong coupling constant α_s. And because only their masses depend on κ, see Eqs. (4.69) and (4.70), the production cross section depends on κ. Note that $T^\pm$ have a dependence on R, but as we scanned our benchmark scenarios with fixed R values, we only observe an f dependence for $T^\pm$.

Interestingly, even though mass terms of V_H depend only on f, we can find a small κ-dependence from $V_H V_H$ channel of the *Fermion Universality* model in the lower panel of Fig. 5.3. This is an effect caused by q_H in t-channel production which destructively interferes with electroweak s-channel diagrams. This effect is observed for $\kappa \approx 0.5$ regardless of f, and results in the fact that the production cross section of the V_H pair for $\kappa \approx 0.5$ is nearly 5 times smaller in comparison to $\kappa_q \cong \kappa_\ell$ i.e. when there is no effect by t-channel quarks q_H since they are decoupled. Note that by the same reason, in the *Heavy* q_H model shown in Fig. 5.4 this effect disappears since q_H are decoupled by construction. The production cross section values can exceed 10^3 fb and thus we expect that the LHC can probe the parameter space sensitively

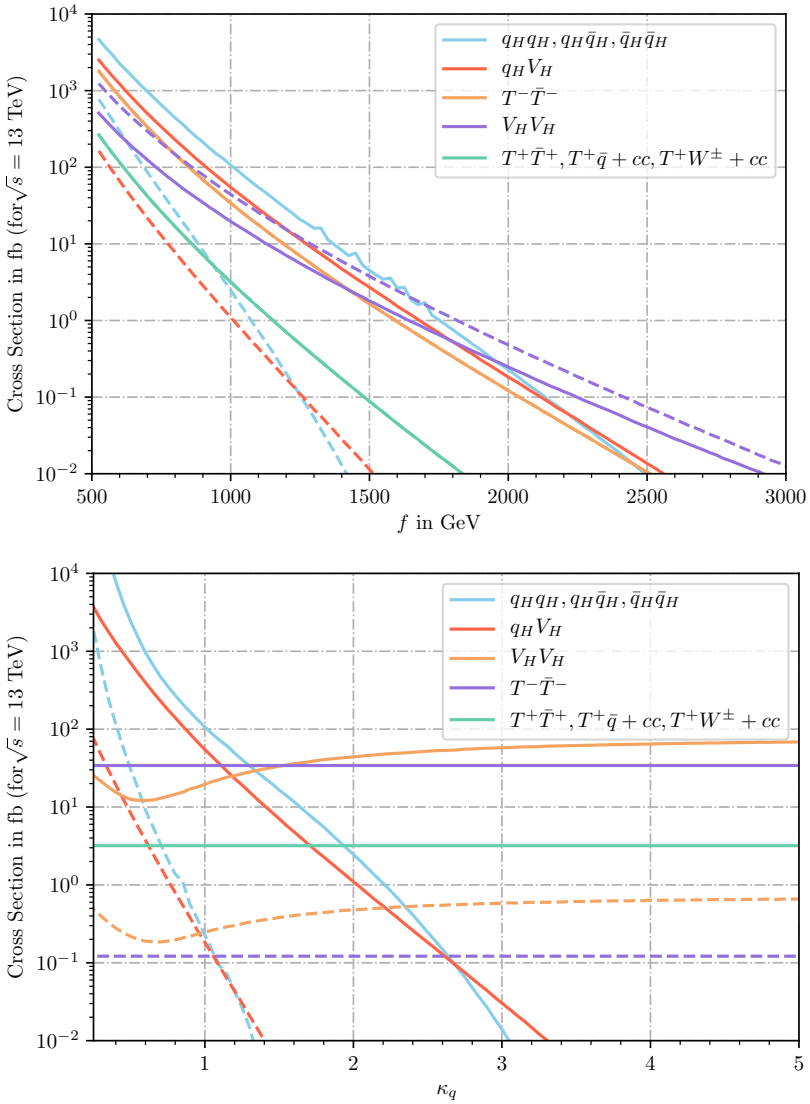

Fig. 5.3.: LHC production cross sections ($\sqrt{s} = 13\,\text{TeV}$) for benchmark models *Fermion Universality/Light* ℓ_H + *Light* $T^\pm$. Upper panel: Dependence on f for fixed $\kappa = 1.0$ (solid), $\kappa = 2.0$ (dashed). Lower panel: Dependence on κ for fixed $f = 1\,\text{TeV}$ (solid), $f = 2\,\text{TeV}$ (dashed). Labels in the legend appear in decreasing order of the respective maximum value of the solid lines.

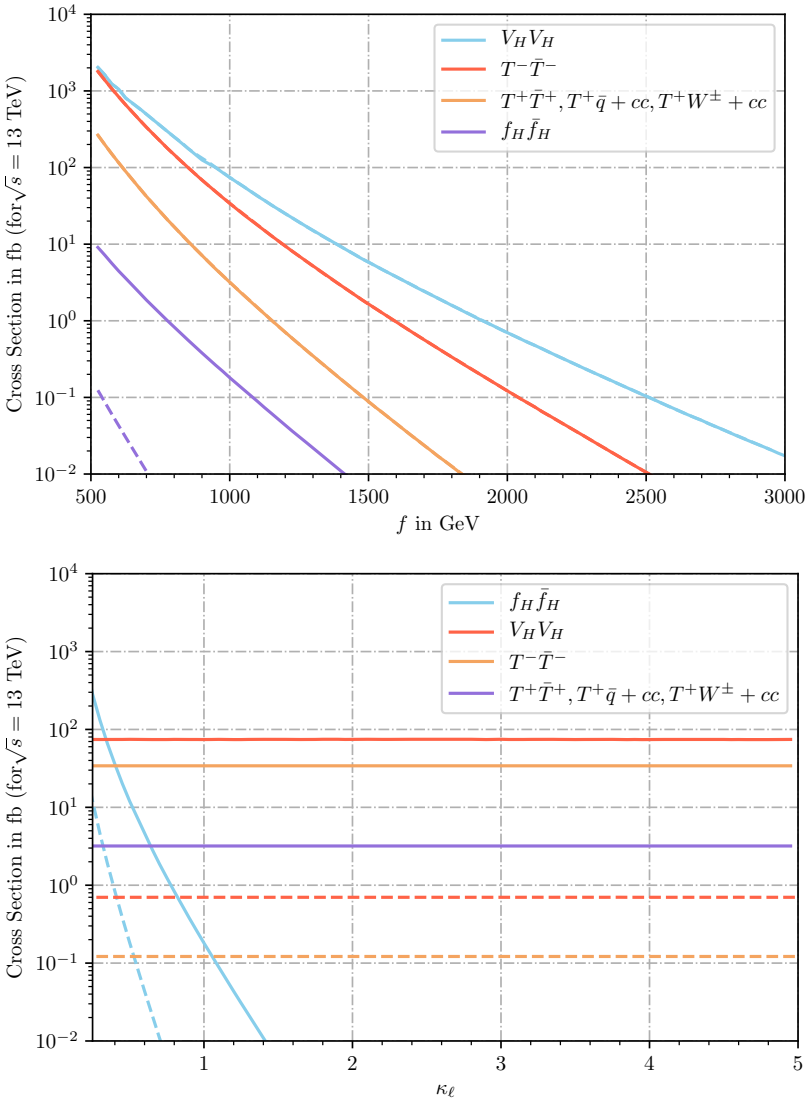

Fig. 5.4.: Same as Fig. 5.3 for benchmark model *Heavy* q_H + *Light* $T^\pm$.

at $\sqrt{s} = 13\,\text{TeV}$. Furthermore, the cross section is order 10^{-1} fb when $f \sim 3\,\text{TeV}$ and therefore we also expect detectable event rates at scales which were not accessible during LHC Run 1, Ref. [63].

From Figs. 5.3 and 5.4 it is clear that none of the cross sections for one process is systemically higher than for the others. Depending on the position in the $f - \kappa - R$ parameter space, we expect different final states to be dominant.

When the κ_q and κ_ℓ are small such that q_H and ℓ_H are light, T-parity odd fermions are expected to be produced more. Thanks to the strong production, the production rate of q_H is 2-3 orders of magnitude higher than that of ℓ_H. Thus, ℓ_H production becomes relevant only when f and κ are small such as $f \lesssim 1\,\text{TeV}$ and $\kappa \lesssim 0.5$

On the other hand, when κ is large, the production of heavy vector bosons becomes important because their mass is independent of κ, which is different from that of T-odd fermions q_H and ℓ_H whose mass gets larger, such that they get less produced. If $T^\pm$ are light, they are also experimentally accessible and they will be produced nearly as abundantly as V_H. The T-parity even vectorlike top T^+ appears to be negligible as it is always heavier than the T-odd vectorlike top T^-, see Eqs. (4.77) and (4.79). Note that $T^\pm$ cross sections are only of the same size as the V_H cross sections in our special case $R = 1$.

5.5.2. Branching Ratios

In order to determine the exclusive final states, in this section we discuss the branching ratios of the heavy particles. We considered only two-body decays and in the following we only discuss final states with a branching ratio large than 1%. We shall consider all decays, including those with $\texttt{BR} < 1\%$, in our collider analysis later. We only discuss the *Fermion Universality* model and the *Light* ℓ_H model because the *Heavy* q_H model has nearly identical decay patterns as the *Fermion Universality* model. So, the branching ratio figures for the *Heavy* q_H model are the same as those for the *Fermion Universality* model. *TPV* affects the branching ratio of A_H which we obtain at the end. The decays of the other particles are affected very little. Thus, we consider A_H decays only.

Decays of T-parity odd fermions

For the T-odd quark q_H branching ratio, the *Fermion Universality* model and the *Light* ℓ_H model have the same dependence in parameter space as we see in Figs. 5.5 and 5.6 . Their masses depend on both f and κ, as do their branching ratios. Up- and down-type T-odd quarks decay dominantly into $W_H\ q$ with a branching ratio 60% in the kinematically allowed region. The second most decay is to $Z_H\ q$ with a branching ratio 30% and the last is the decay to $A_H\ q$ with 10%. In the right panels of Figs. 5.5 and 5.6, a small dependence on f appears because of the factor v/f of each coupling constant. The dependence is different with respect to the kind of up- and down-type particles, and thus, the branching ratio dependences on f are different for $u_H,\ d_H$.

Because the *Fermion Universality* model assumes that $\kappa_q = \kappa_\ell$, the particles related with κ_q and κ_ℓ, i.e. T-odd qua have the same masses by construction. The interesting thing is that

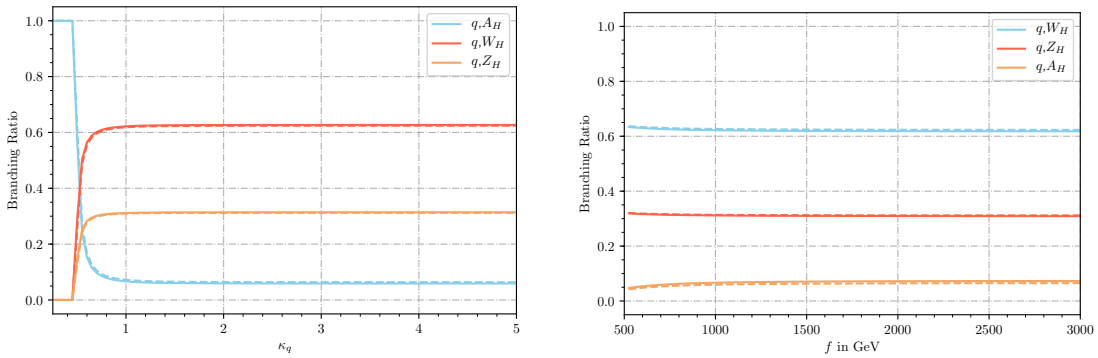

Fig. 5.5.: Branching Ratios of d_H in the *Fermion Universality/Light* ℓ_H model. Items in legend appear in decreasing order of the maximum value of the respective curve. Left: Fixed $f = 1\,\text{TeV}$ (solid), $f = 2\,\text{TeV}$ (dashed). Right: Fixed $\kappa = 1$ (solid), $\kappa = 2$ (dashed).

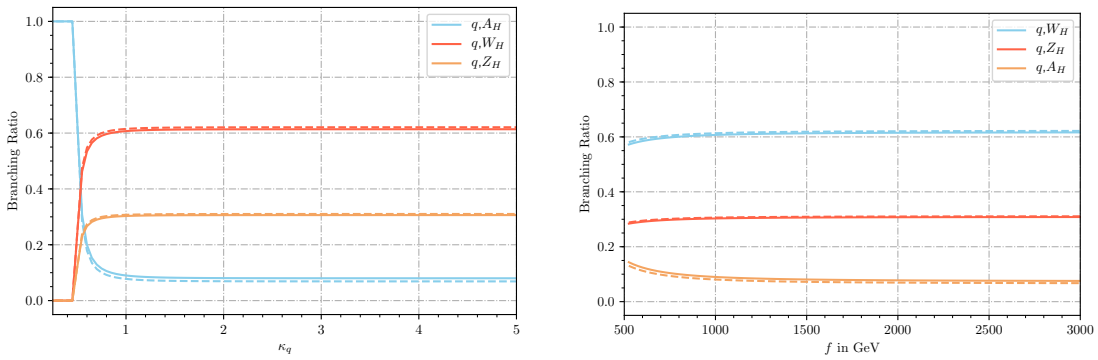

Fig. 5.6.: Branching Ratios of u_H in the *Fermion Universality/Light* ℓ_H model. Parameters as in Fig. 5.5.

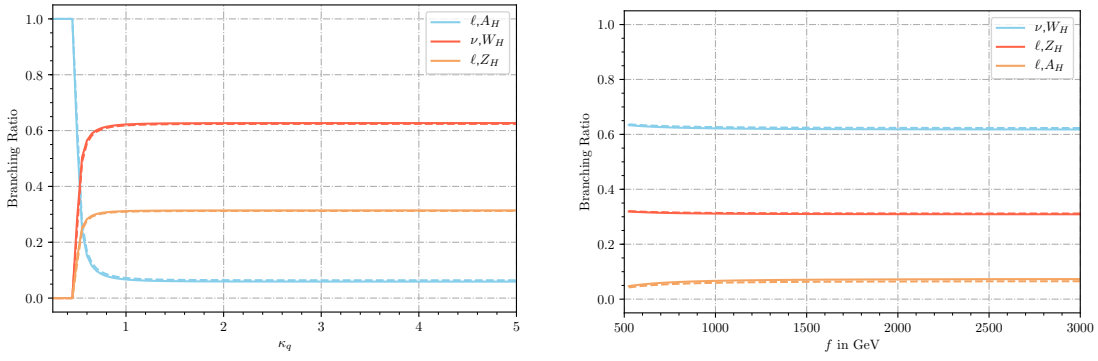

Fig. 5.7.: Branching Ratios of e_H in the *Fermion Universality* model

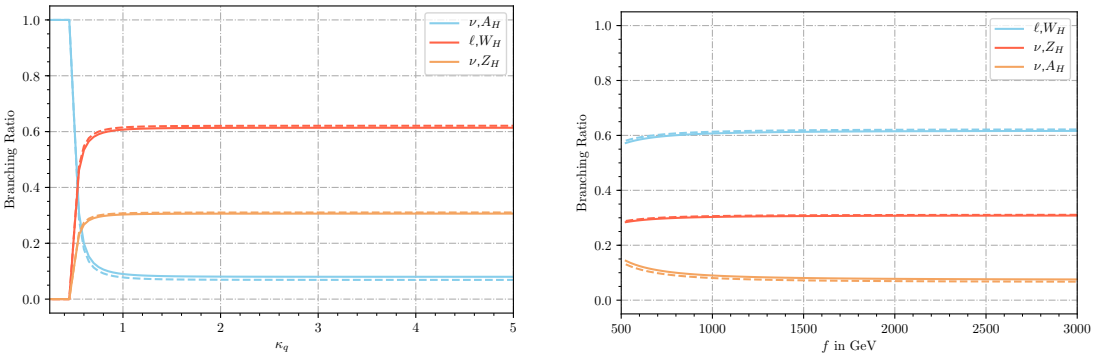

Fig. 5.8.: Branching Ratios of $\nu_{e,H}$ in the *Fermion Universality* model

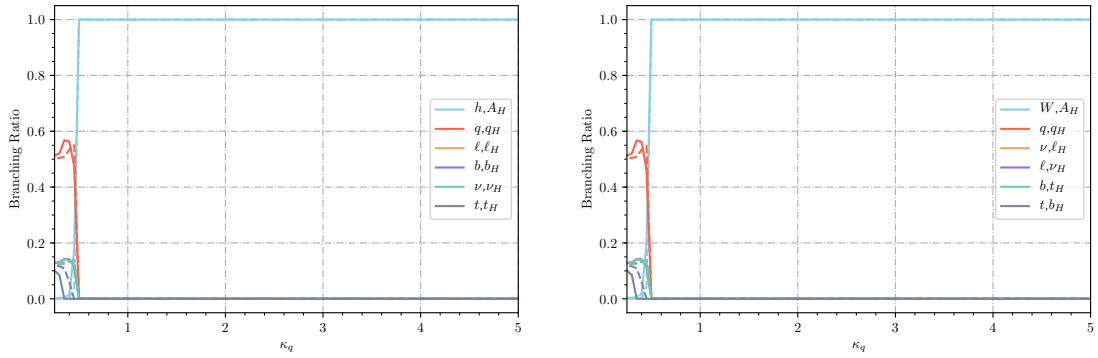

Fig. 5.9.: Branching Ratios of Z_H (left) and W_H (right) in the *Fermion Universality* (*Heavy* q_H is very similar, see text). Parameters as in Fig. 5.5. In both plots, curves corresponding to decays with ν, ℓ or b are nearly identical.

the decay patterns for particles in the same component of $SU(2)$ doublets are identical. For example, the branching ratio for $\nu_H \to W_H\ e$ is the same as that for $u_H \to W_H\ d$.

Decays of V_H

The figure for the branching ratios of W_H, Z_H in the *Fermion Universality* model is Fig. 5.9 and that of the *Light* ℓ_H model is Fig. 5.10. We show the figures for the branching ratio only as a function of κ because there is no dependence on f. For the *Fermion Universality* model, the possible decays of W_H are into $W\ A_H$, $q\ q_H$, $\nu\ \ell_H$, $\ell\ \nu_H$, $b\ t_H$ and $t\ b_H$. A kinematical threshold is visible around $\kappa \approx 0.4$. While $W\ A_H$ is the only allowed decay channel in the region $\kappa > 0.4$, decays into fermions are possible and $W\ A_H$ becomes subdominant for $\kappa < 0.4$. Similarly, Z_H decays mainly into $h\ A_H$ for $\kappa > 0.4$ whereas it becomes subdominant and other decay channels appear in the region of $\kappa < 0.4$.

When it comes to the *Light* ℓ_H model, the picture is different. As ℓ_H are by construction light particles, the heavy gauge bosons W_H and Z_H decay into states that consist of ℓ, ℓ_H, ν and ν_H. Those are $W_H \to \nu\ \ell_H$, $W_H \to \ell\ \nu_H$ with 50% each and $Z_H \to \nu\ \nu_H$, $Z_H \to \ell\ \ell_H$ also with 50% each. In case of $\kappa_q < 0.4$, decays into $q\ q_H$ are also allowed and become dominant.

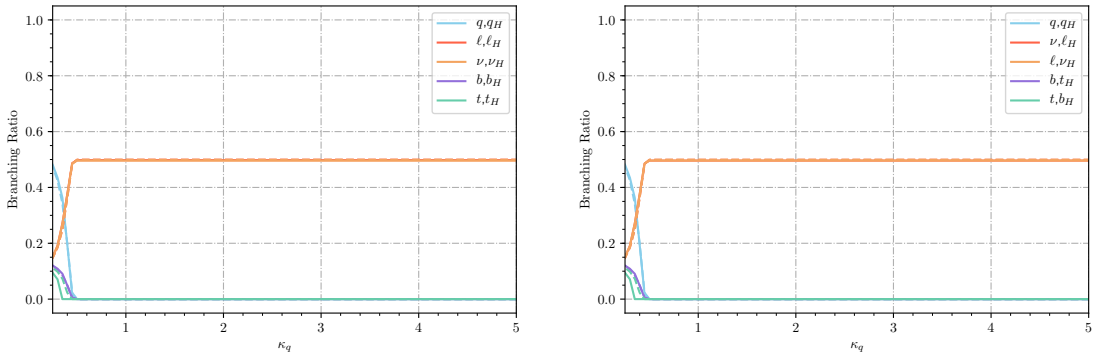

Fig. 5.10.: Branching Ratios of Z_H (left) and W_H (right) in the *Light* ℓ_H model. f is chosen as in Fig. 5.5, left. In both plots, the curves corresponding to decays with ν or ℓ are nearly identical.

Note that for the *Heavy* q_H model, the branching ratios are similar to the *Fermion Universality* model except that for $\kappa < 0.4$, no decays $V_H \to q_H\ q$ are allowed and the branching ratios from $V_H \to \ell^+\ \ell^-$ scale up accordingly.

Decays of $T^{\pm}$

$T^{\pm}$ masses depend both on f and R. The T-odd vectorlike top partner T^- decays only into $A_H\ t$ with a branching ratio of 100%. Fig. 5.11 shows the branching ratios of T^+ and since T^+ is a T-parity even particle, it has to decay into a pair of T-odd particles or a pair of SM particles. There are 4 possible decays: the decay into $b\ W$ is the prominent channel with a branching ratio of 45%. It is followed by $t\ Z$ and $t\ H$ with 20% each, which is because of $SU(2)$ properties of the couplings. The decays of a vector-like top quark partner i.e. $SU(2)$ singlet should be 50% for Wb, and 25% each for Zt and Ht, which is here only modified by the decay to the doubly T-odd final state T^-A_H.

The decays into a pair of T-odd particles, $T^-\ A_H$, is also possible although its branching ratio is only around 10%. These branching ratios do not depend on κ and they depend only a little on f because for the case shown in Fig. 5.11 we fix $R = 1$ to make $T^{\pm}$ light. Of course, changing R triggers variations of its branching ratios as well.

Decays of A_H

For the decay width we follow the calculation of Ref. [59]. In Fig. 5.12, the branching ratio of A_H is given in dependence of f. The branching ratios drastically depends on the kinematical condition $M_{A_H} > 2M_W,\ 2M_Z$. As a function of f, the mass of A_H is greater than $2M_W$ and $2M_Z$ ($\sim 180\,\text{GeV}$) if $f \gtrsim 1200\,\text{GeV}$. Thus, in the region of $f \gtrsim 1200\,\text{GeV}$ A_H decays mainly into a pair of SM gauge bosons.

When f is in the range where $M_{A_H} \lesssim 180\,\text{GeV}$, decays to a pair of SM gauge bosons become suppressed and 2-loop leptonic decays become equally important. For f smaller than 900 GeV, decays into pairs of SM fermions become dominant.

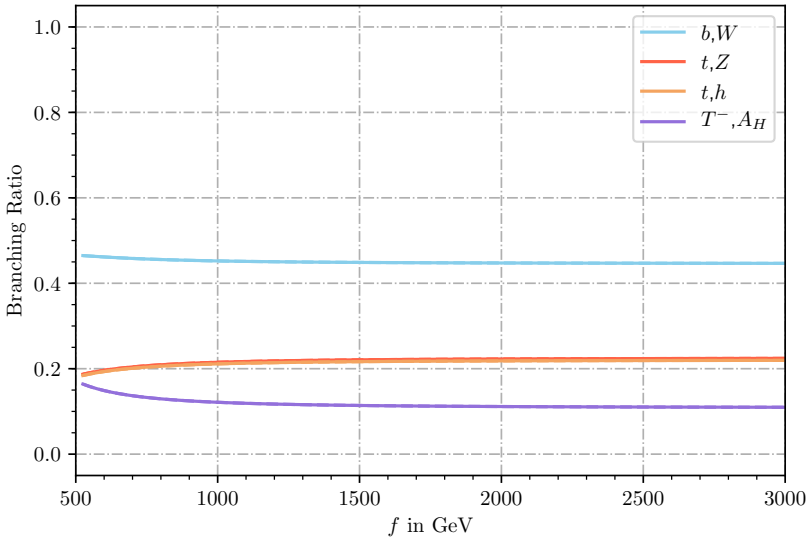

Fig. 5.11.: Branching Ratios of T^+ in the *Light* $T^{\pm}$ scenario.

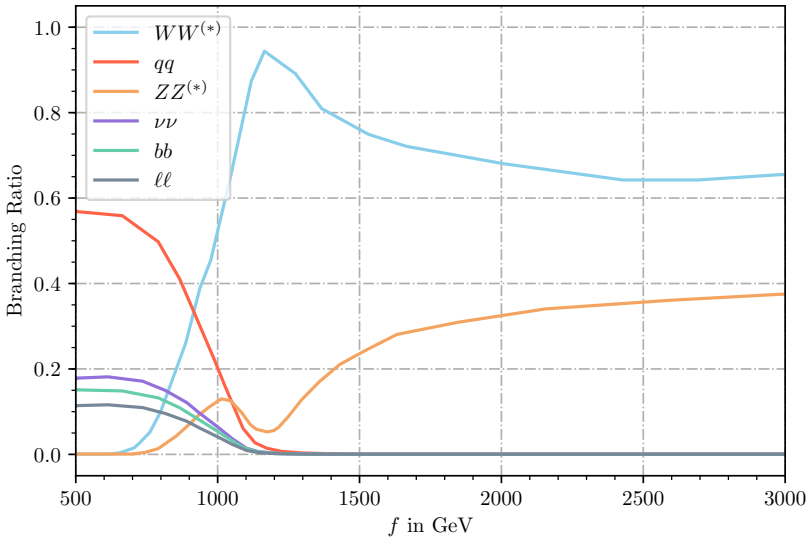

Fig. 5.12.: Branching Ratios of A_H in the *TPV* scenario.

5.5.3. Expected final state topologies

As we discussed in Section 4.3.1, there is the invisible lightest T-odd particle A_H and thanks to the T-parity the relevant processes are expected to generate similar signatures as in searches for Supersymmetry. Thus, we combine the features from the different production processes with the decay processes and recast the experimental searches for supersymmetric signatures.

- With conserved T-parity, all T-parity odd particle decays have A_H at the end of the decay chain, which is invisible in the detector but generates a missing transverse energy $\not{E}_T$. This is similar to the properties of the neutralino in the Supersymmetry model if R-parity is conserved. SUSY searches are looking for $\not{E}_T$. Thus, the search required $\not{E}_T$ in the events are expected to be sensitive to the LHT model.

- The heavy gauge bosons of the LHT model have various final states depending on the decay patterns i.e. they have different final states depending on the benchmark scenarios.

  In the *Fermion Universality* model, W_H decays into states including W and W decays itself may generate jets from hadronic decay or hard lepton from leptonic decay. Z_H decays into states with a Higgs H which is followed by a decay dominantly into b-jets. This is similar to supersymmetric electroweakino production $\tilde{\chi}_1^{\pm}\tilde{\chi}_2^0 + \tilde{\chi}_1^{\pm}\tilde{\chi}_1^{\pm} + \tilde{\chi}_2^0\tilde{\chi}_2^0$ with a Wino-like chargino and a Higgsino-like neutralino.

  In the *Light* ℓ_H model, heavy gauge bosons mostly decay into a SM lepton ℓ and a corresponding heavy lepton partner ℓ_H, which decays into SM lepton and A_H. This signature corresponds to the search for an electroweakino with light scalar leptons in supersymmetric models.

- T-odd quarks q_H decay into q A_H and they result in the signature involving jets and missing transverse momentum. q_H also decays into the state including heavy gauge bosons, then the signature includes more leptons with b-jets or light jets in the events. This is similar to the topologies of supersymmetric scalar quark production that decay into the states with the lightest supersymmetric particle or have charginos or neutralinos at the end.

- The T-odd top partner T^- has a signature involving the SM top quark and $\not{E}_T$, which is the same very typical signature of a natural Supersymmetry model with a light scalar top.

- The T-even top partner T^+ decays mostly into b W^+ like a top quark with not necessarily missing transverse momentum. It is expected to have an impact on the SM top measurement, Higgs or gauge boson relevant final states. However, the production process including T^+ has a reduced cross section and we mostly focus on SUSY-like final states, and therefore the effects from T^+ related production channels are expected to be almost negligible.

- When T-parity is broken, there are much more possible final states. Productions and decays of LHT particles are similar as in the T-parity conserving case. For example, final

states would consist of a pair of A_H and the same hard final state objects we mentioned before. However, since A_H can decay into a pair of SM particles, even more final states appear. Especially, for $f > 1.2\,\text{TeV}$, four SM gauge bosons are expected in the final state. Each of them decay hadronically or leptonically, which results in many final states including additional jets and leptons. These can be covered with a search designed for very large final state multiplicities in case that the SM background is small. Furthermore, the signatures of processes may have missing transverse momentum since both Z and W decay into neutrinos. Thus, the mentioned analysis strategies that can cover the case of conserved T-parity may still be applicable.

In summary, we expect several similar final states with that of supersymmetric models. Also, the LHC searches designed for supersymmetric particles can be applied to this model very well. However, although aspects of the final states of the LHT model are theoretically akin to that of Supersymmetry, it is not guaranteed to produce large enough number of events for testing it. Furthermore, it is not a priori obvious to tell clearly which topologies are the most sensitive.

In our recast procedure, we take the dedicated SUSY analyses to set bounds to the model according to our benchmark scenarios.

5.6. Software Chain and Validation

In this section, we describe our tool chain for getting the Feynman rules from the model definition, generating collider events to recast LHC analyses to set limits on the parameter space.

With the FeynRules implementation of the LHT model as in Ref. [63–65], we slightly extended the model definition such that the heavy fermion Yukawa couplings κ are transformed into independent coupling constants κ_ℓ and κ_q. We then exported the LHT model to the event generators `MadGraph` [66] and `WHIZARD` [30–33] via the UFO file format.

For numerical simulations of our LHT benchmark models and comparisons to LHC data, the automated tool CheckMATE is used. Fig. 5.13 provides an intuitive view describing how CheckMATE is working. CheckMATE is an automatized program for testing given BSM models.

By using `MadGraph`, `Pythia 8` , `Delphes` and etc., CheckMATE calculates relevant quantities analytically and numerically and tests given BSM models. These segment of calculations are steered via a `C++` based program, `Fritz`. It connects all program modules and triggers runs on them. While it proceeds, not all the results are stored because of the large size of intermediate result files. If all data of results are saved, the information produced from the Monte Carlo program can easily exceed one GiB per process. Usually the programs scan processes on whole grid of the parameter space, which results in producing data of several dozens of Terabyte. Furthermore, the reading from a hard drive and writing on it takes non-negligible time. Thus, only selected information will be kept for the final result.

Once CheckMATE starts running, software chains to test a model are automatically followed. If users enter processes within a input file with mandatory or optional parameters,

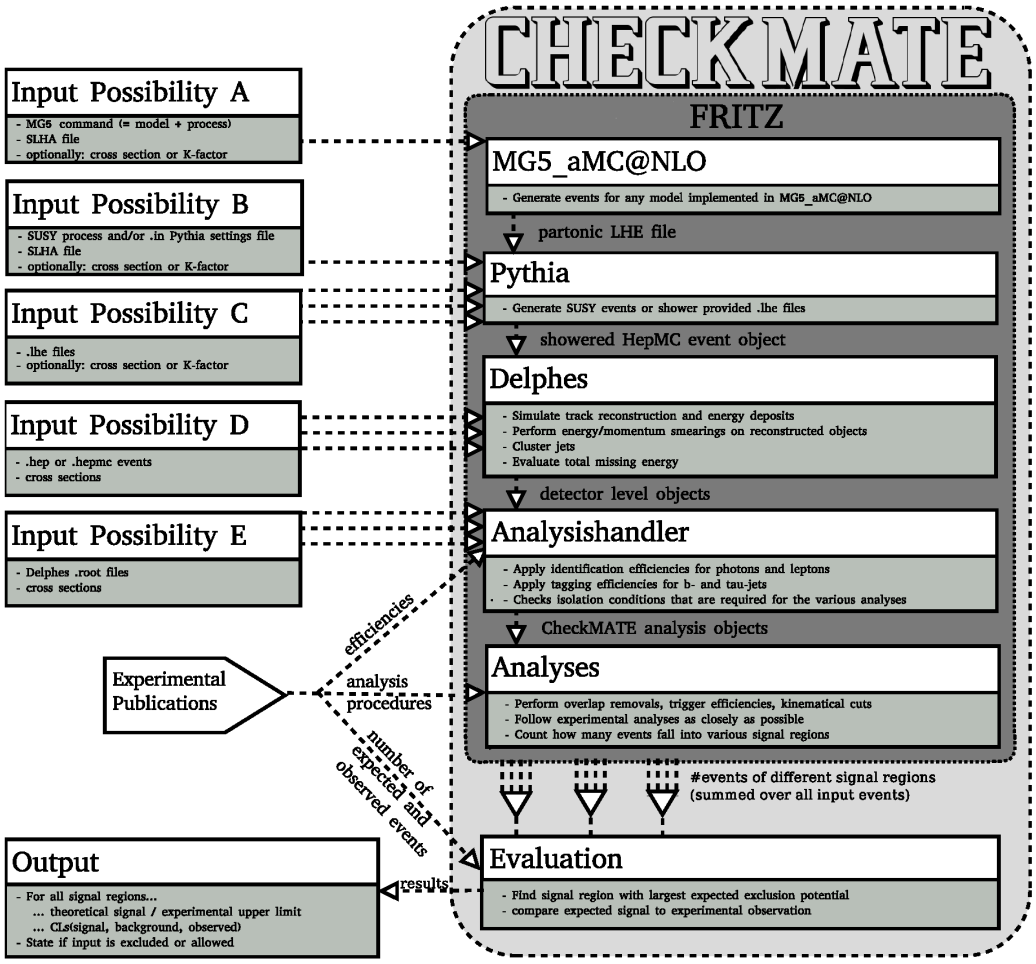

Fig. 5.13.: Flow chart to show how CheckMATE works, Ref. [67]

CheckMATE calls `MadGraph` to generate partonic events for the processes based on UFO model file created by model-building tools, `FeynRules` or `SARAH`. Then, `Pythia 8` is called for parton showering and hadronization, to mimic the hadronic Monte Carlo events as in the LHC. The information is delivered to the fast detector simulation program `Delphes` that filter events using kinematic and efficiency cuts. The output of the simulation is analyzed by internal modules of CheckMATE. It checks the consistency of the prediction derived from the input file comparing to the experimental observable data of published results. Finally, CheckMATE concludes whether the events are `excluded` or `allowed` at 95% confidence level in the given BSM.

Chapter 6.

Results for 13TeV data at the LHC

This chapter details the comparison with 13TeV data at the LHC for the Littlest Higgs model with T-parity according to the benchmark scenarios mentioned in the previous chapter. Analyses implemented in CheckMATE are used. The benchmark scenarios are chosen to understand how the result change depending on the parameters. We represent the results for 13TeV data at the LHC. LHC Run 2 true analyses recasts are compared to recasts for projections done by the two ATLAS and CMS experiments. Finally, we combine the results for the LHC data and for the electroweak precision observables, i.e. for the contact interactions.

6.1. Collider Results

Based on the aforementioned discussion in the last chapter 5, let us now discuss the results from our CheckMATE analyses. Figs. 6.1 - 6.12 show the results for all our benchmark scenarios.

Plots show the respective exclusion limits and were drawn by two guiding principles. One is to show which regions of the parameter space can be excluded using results from 8 TeV and 13 TeV. The region excluded by 8 TeV can be compared with results from earlier studies in Ref. [63]. Our results agree very well and show the validity of our CheckMATE analyses. Results from $\sqrt{s} = 13\,\text{TeV}$ extend the exclusion limits thanks to the higher center of mass energy and integrated luminosities, i.e. more data. Also, these plots contain the mass contours of the relevant particles, which helps to translate parameter bounds into limits on the masses of LHT particles.

The other guiding principle is to tell which analyses in particular exclude a given point shown in the plots. They contain the LHC analyses information in the legend of the plot, so that we can see which point is excluded by which analysis. Some points are excluded by one, some by several analyses. We only show the minimal set of analyses sufficient to cover all excluded points. Especially regions with small f and small κ are excluded by far more analyses than those shown in the plots.

The full list of analyses implemented in CheckMATE are shown in Appendix C. The analyses in Table 6.1 are the ones contributing to our exclusion limits among the full list in Appendix C.

6.1.1. *Fermion Universality* model

For the *Fermion Universality* model, our discussion is based on the assumption that the Yukawa coupling constants, κ_q and κ_ℓ, are equal. That is, the mass spectrum of T-odd fermions q_H and ℓ_H is degenerate.

CM identifier	Final State	Designed for	Ref.
atlas_conf_2016_096	$\not{E}_T$ + 2-3 ℓ	$\tilde{\chi}^{\pm}, \tilde{\chi}^0, \tilde{\ell}$	[68]
atlas_conf_2016_054	$\not{E}_T$ + 1 ℓ + (b)-j	$\tilde{q}, \tilde{g}$	[69]
atlas_conf_2017_022	$\not{E}_T$ + 0 ℓ + 2-6 j	$\tilde{q}, \tilde{g}$	[70]
atlas_conf_2017_039	$\not{E}_T$ + 2-3 ℓ	$\tilde{\chi}^{\pm}, \tilde{\chi}^0, \tilde{\ell}$	[71]

Table 6.1.: Small summary of all $\sqrt{s} = 13\,\text{TeV}$ analyses which appear in the discussion of our results. More details, also on other tested analyses, are given in Tab. **??** in the appendix.

Heavy $T^{\pm}$ case, T-parity conserved

First, we look at the T-parity conserved case with heavy $T^{\pm}$. The plot Fig. 6.1 shows the result with $R = 0.2$ which makes $T^{\pm}$ too heavy to be detected. We can understand the results by discussing two parameter regions.

For $f \gtrsim 1\,\text{TeV}$, the shape of exclusion limits is nearly parallel to the mass contour of q_H. The most sensitive analysis for this result is 'atlas_conf_2017_022', the search for more than 2 jets plus missing transverse momentum. The decay topology that is the most relevant one is the decay chain of two T-odd quarks. T-odd quark q_H decays into SM quarks and T-odd photon induced by QCD interactions, which can trigger additional particles X in the process that $q_H q_H$ decay into $qqA_H A_H + X$. Since the A_H does not decay it produces a large amount of missing transverse momentum if T-parity is conserved and A_H is stable. As q_H production mainly depends on M_{q_H}, the bounds follow the mass contour of q_H which is roughly $f \times \kappa$ where $\kappa = \kappa_q = \kappa_\ell$. The excluded area is $f \times \kappa < f \times \kappa_{max}$ with $f \times \kappa_{max} \approx 1.5\,\text{TeV}$ for $\sqrt{s} = 8\,\text{TeV}$ and $f \times \kappa_{max} \approx 2\,\text{TeV}$ for $\sqrt{s} = 13\,\text{TeV}$. However, the limit drops a bit faster than the q_H mass contour. This is because the heavy vector bosons V_H to $q_H q_H$ production is slightly affected by κ change. Thus, the bound runs along $M_{q_H} > 3\,\text{TeV}$ for $f \approx 1\,\text{TeV}$ while it does along $M_{q_H} > 2\,\text{TeV}$ for $f \approx 3\,\text{TeV}$.

In case of $f \lesssim 1\,\text{TeV}$, most of the area in Fig. 6.1 is excluded and we do not observe obvious dependence on κ nor f especially in the region $f \lesssim 800\,\text{GeV}$. This is because T-odd quarks are not produced abundantly enough when κ is large compared to f, and V_H pair production becomes more relevant, as the V_H mass only depends on f not κ. However, the bound depends slightly on κ in the region of f between (800, 900)GeV. The reason is, as it is mentioned in Section 5.5.1, that T-odd quarks interfere destructively in the production of the heavy vector bosons via t-channel diagrams. Compared to the region for $f \gtrsim 1\,\text{TeV}$, the main contributing process to the exclusion changed from $q_H q_H$ to $q_H V_H$, but the most sensitive analysis does not change, which is still the search for multijets plus missing transverse momentum. Here, this final state topology comes from the hadronic decays of W in $W_H \to W\ A_H$ and from b-jets in the H decay $Z_H \to H\ A_H$.

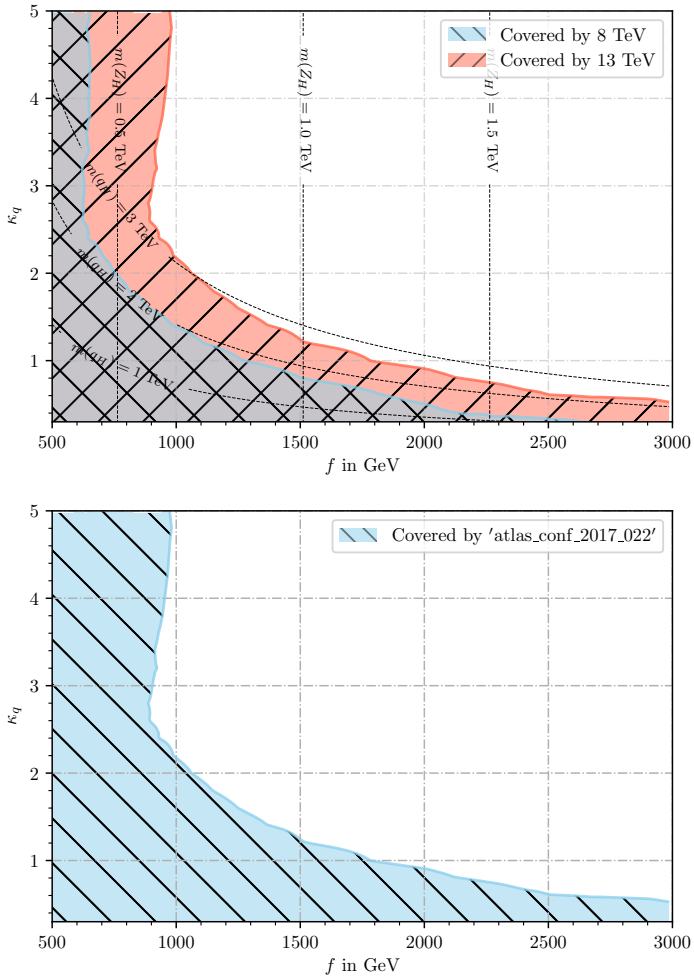

Fig. 6.1.: Results for scenario (*Fermion Universality*)×(*Heavy* $T^{\pm}$)×(*TPC*), Upper panel shows the center-of-mass energies covering exclusion regions and mass contours of LHT particles. Lower one shows the analysis covering exclusion regions. x-axis is the symmetry breaking scale f and y-axis is the Yukawa coupling constant κ. For the *Fermion Universality* model, $\kappa_q = \kappa_\ell = \kappa$.

Light $T^{\pm}$case, T-parity conserved

To see the sensitivity to the cancellon $T^{\pm}$, we choose $R = 1.0$ and show the results in Fig. 6.2 . Different from the previous benchmark case, the $T^{\pm}$ are experimentally accessible with the mass of $T^{\pm}$ affected only by f since R is fixed. As a result, in the large f region, the production of $T^{\pm}$ gets decreased, thus, the bound becomes just the same with the result of the previous heavy $T^{\pm}$ case. $T^{\pm}$ can be produced for $f \lesssim 1.5$TeV and has notable effects on the bound. Not only the κ-dependence has disappeared in the region of $f \subset (800,\ 900)$GeV, but also the vertical exclusion limit is extended up to $f \sim 1.3\,$TeV. In other words, the $V_H V_H$-induced bound with κ-dependence is fully covered by $T^{\pm}$ production, at least for the special case $R = 1.0$. The most sensitive analysis for this is also `'atlas_conf_2017_022'`, the search for multijets with $\not{E}_T$.

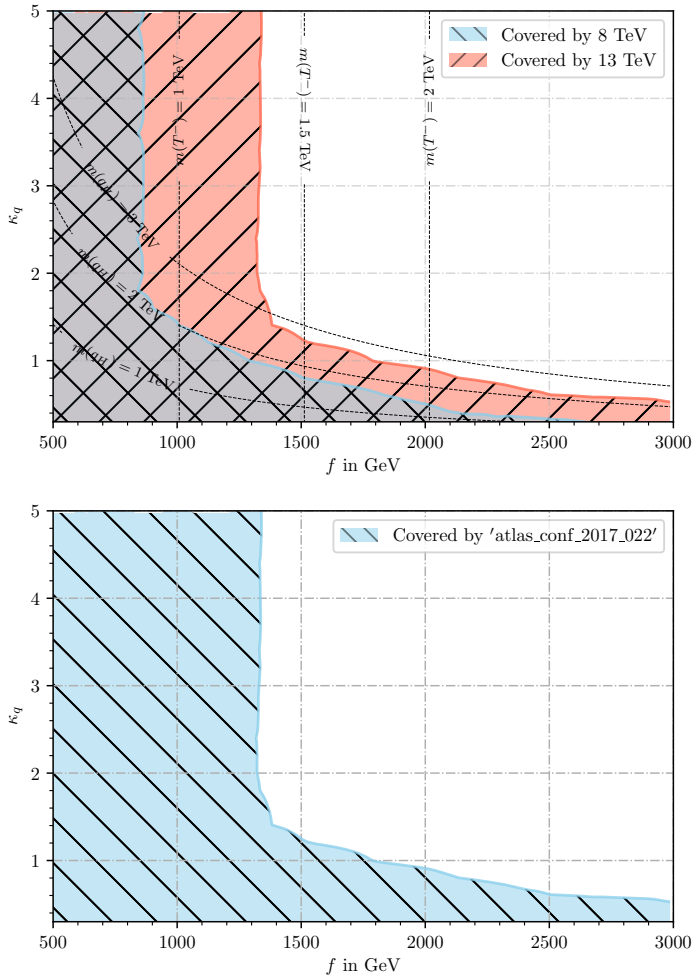

Fig. 6.2.: Results for scenario (*Fermion Universality*)×(*Light* $T^{\pm}$)×(*TPC*)

T-parity violated case

Plots Figs. 6.3 and 6.4 show the results of the *Fermion Universality* model with violated T-parity(TPV). Fig. 6.3 is without top partners $T^{\pm}$ (*Heavy* $T^{\pm}$) and Fig. 6.4 includes the effects of (*Light* $T^{\pm}$). Again, the results seem to be separable into two area: $f \gtrsim 1\,\text{TeV}$ and $f \lesssim 1\,\text{TeV}$.

When $f \gtrsim 1\,\text{TeV}$**,** the bound still has a large dependence on κ and runs along with the contour of the q_H mass. The area with $M_{u_H} \lesssim 2.5\,\text{TeV}$ for $f \approx 1\,\text{TeV}$ and $M_{u_H} \lesssim 1.5\,\text{TeV}$ for $f \approx 3\,\text{TeV}$ is excluded. As T-parity is violated, more final state topologies appear and thus more analyses contribute to the result. Especially, the two analyses, `'atlas_conf_2016_054'` and `'atlas_conf_2017_022'` are almost equally sensitive to the exclusion area. The former one is the search for 1 lepton, multijets and $\not{E}_T$ and the latter one is for no lepton, multijets and $\not{E}_T$. The fact that they are equally sensitive to the result is understandable if we take into account the final state of SM gauge boson decays in $A_H \to VV$. From the decays of SM gauge bosons, final states that did not exist in the previous benchmark scenarios appear produced via

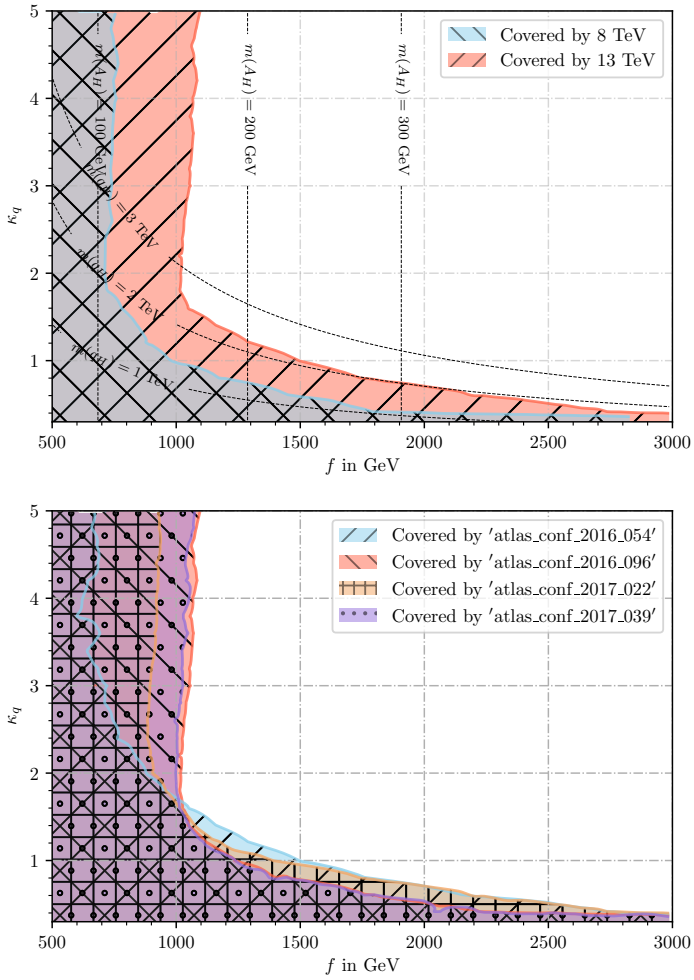

Fig. 6.3.: Results for scenario (*Fermion Universality*)×(*Heavy* $T^{\pm}$)×(*TPV*)

leptonic and hadronic decays of the many additional W and Z bosons. As the two mentioned analyses only differ by their expected lepton multiplicity and as gauge bosons decay roughly equally into hadrons and leptons, we expect similar event rates and similar sensitivities. To be more precise, A_H decays preferably into WW than into ZZ, especially when f is smaller, see Fig. 6.3. Since the decay of W produces more charged leptons than that of Z, we can expect slightly more leptonic final states in the region with smaller f. This makes the analysis with one lepton in the final state, `'atlas_conf_2016_054'`, slightly more sensitive in κ and we observe this in Fig. 6.3 in the region $f \subset [1,\ 1.5]$TeV.

It is interesting to observe that the exclusion area does not change dramatically if the ℓ_H decays into SM particles with invisible signal. This is because of the role of neutrinos in the final states. From the processes that we are observing, a pair of heavy photons A_H is produced from $q_H q_H$ or $V_H V_H$ and these decay each into WW or ZZ for broken T-parity. If W and Z decay leptonically, missing transverse momentum is produced from neutrinos. As 25 % of all SM gauge bosons decay into $\nu + X$ on average and we expect 4 gauge bosons from a pair of heavy photons, approximately 70 % of decays of all TPV case still produce missing

transverse momentum. The visible final states are the same as in the previous *TPC* case, plus additional boosted particles from the ℓ_H decay, which may help the event to pass cuts for high multiplicity signal regions with nearly no SM background. This is why the bound does not change significantly compared to the previous case.

Next, for $f \lesssim 1\,\text{TeV}$, let us discuss the κ independent limit. Compared with the *Fermion Universality* model with conserved T-parity, the limit on f is extended. The LHT-TPV model is excluded when $f \lesssim 1\,\text{TeV}$ with $\kappa \lesssim 1.5\,\text{TeV}$ and $f \lesssim 1.1\,\text{TeV}$ with $\kappa \lesssim 4.0\,\text{TeV}$. To understand the reason behind the exclusion, we again scrutinize the analyses of the LHC from the right plot of Fig. 6.3. The multijet search `'atlas_conf_2017_022'` that had a crucial impact on the bound for the previous cases is not the most important one any more. For this result, the electroweakino searches `'atlas_conf_2016_096'` and `'atlas_conf_2017_039'` play more important roles. Specifically, the signal region `SR-slep-e` generates the exclusion bound. This analysis looks for three high-p_T charged leptons not coming from a pair of W or Z and a large amount of $\not{E}_T$. It was not possible to pass this cut for the case with conserved T-parity because the decay chain without A_H decays, for example, $W_H W_H \to qqWWA_HA_H$ has only two leptons.

As a decaying A_H for broken T-parity produces additional SM leptons, a third charged lepton may appear. Furthermore, there is no constraint about jet multiplicity for the final states, which may bring about a large number of events expected via this analysis regardless of how the other SM gauge bosons decay.

We now discuss the TPV scenario if the top partner $T^\pm$ is light and kinematically accessible. This extends the exclusion limit by 100 GeV, as we can see from Fig. 6.4. So the additional events generated by light $T^\pm$ are not so many, which is different from the case of *TPC*. Still, the electroweakino search is the most important analysis. For the $T^\pm$ search, the final topologies produced from $pp \to T^-\bar{T}^- \to b\,W\,b\,W\,WWVV$ play a crucial role. Since the mass term of $T^\pm$ depends on R and f, the limits generated by $T^\pm$ very much depend on the value of R. To see dependence on f well, we set the value for $R = 1$. Here, we just look at the single case R = 1 to compare to the *TPC* case.

The multijet analysis `'atlas_conf_2017_022'`, does not play crucial role by considering the $T^\pm$ to be experimentally accessible. To explain its reason, we detail the multijet analysis. This analysis covers various hierarchies and topologies of Supersymmetric particles $\tilde{g},\ \tilde{q}$. To detect different jet multiplicities, it defines various signal regions and uses cuts as the amount of missing energy momentum and p_T^{jet}. In particular, the analysis uses a cut requiring the minimum of the ratio $\not{E}_T / \sum p_T^{\text{jet}}$. This works in Supersymmetry because jet multiplicity, total hadronic energy, and $\not{E}_T$ increases at the same time in Supersymmetric model. Heavier particles have longer decay chain as offering more momentum to visible jets and to invisible neutralinos. Thus, $\not{E}_T / \sum p_T^{\text{jet}}$ gets a good signal acceptance rate. But, in TPV case of the *Fermion Universality* model this cut is not so helpful, in particular for the decay $T^+ \to tA_H$. Since A_H decay into the SM gauge bosons for the broken T-parity, it is expected that notably more amount of jets and hadronic energy is produced. This lessens the amount of $\not{E}_T$ and results in lowering the signal acceptance. Therefore, the bound is not improved.

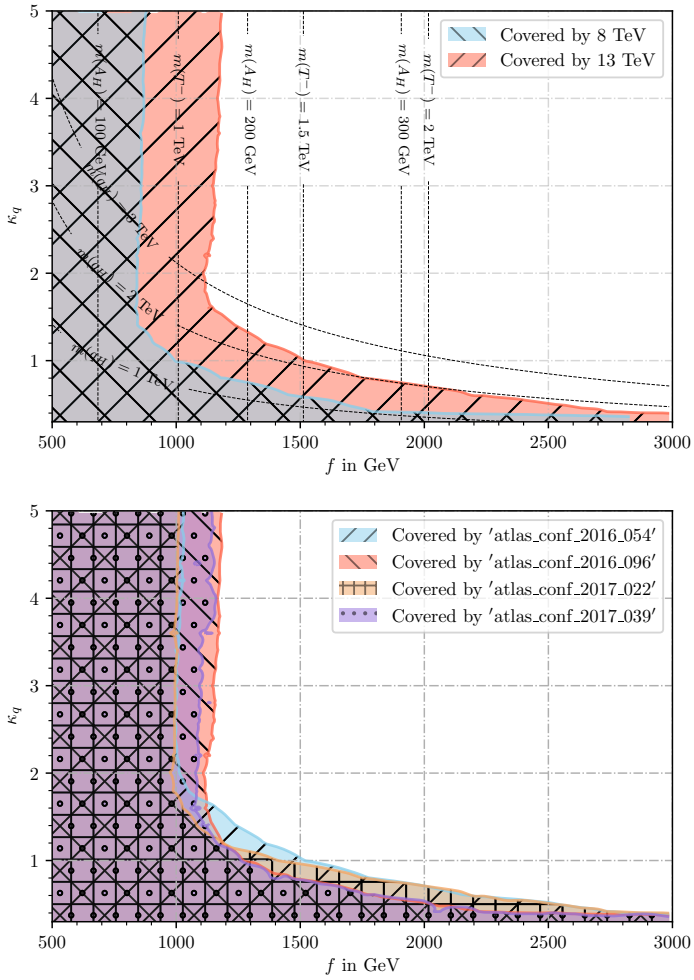

Fig. 6.4.: Results for scenario (*Fermion Universality*)×(*Light* $T^{\pm}$)×(*TPV*)

6.1.2. *Heavy* q_H model

We now discuss the results for the *Heavy* q_H model i.e. κ_q is fixed to a value of 4.0. The result plots are shown in Figs. 6.5 - 6.8. The fixed large value of κ_q causes the q_H to be decoupled at the energy scale of the LHC. Therefore the production channels associated with q_H become irrelevant and ℓ_H production turns to be considered instead. For this reason, we now show ℓ_H mass contours instead of those for q_H on the plots.

Since the q_H are decoupled within the *Heavy* q_H model, the topology that mainly contributes to the results for small κ_ℓ is ℓ_H decaying into ℓ V_H instead of $q_H \rightarrow q$ V_H. That is, the dominant final state topologies change from multijets states to multilepton states. At the LHC, the production event rate for $\ell_H\ell_H$ is about 2 to 3 orders of magnitude smaller than that for q_Hq_H, hence it is expected that the parameter region where q_Hq_H production set bounds in the previous benchmarks will crucially get weaker i.e. for large f and small κ.

Besides, while the V_HV_H production is affected by κ_q factor of t-channel diagrams involving q_H, κ_ℓ does not have any effect on the V_HV_H production. Thus, the exclusion area formed

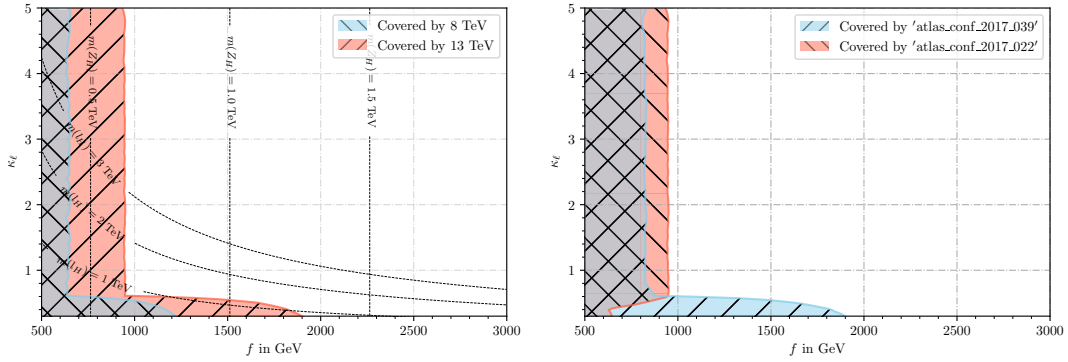

Fig. 6.5.: Results for scenario $(Heavy\ q_H)\times(Heavy\ T^{\pm})\times(TPC)$, Upper panel shows the center-of-mass energies covering exclusion regions and mass contours of LHT particles. Lower one shows the name of the analyses covering exclusion regions.

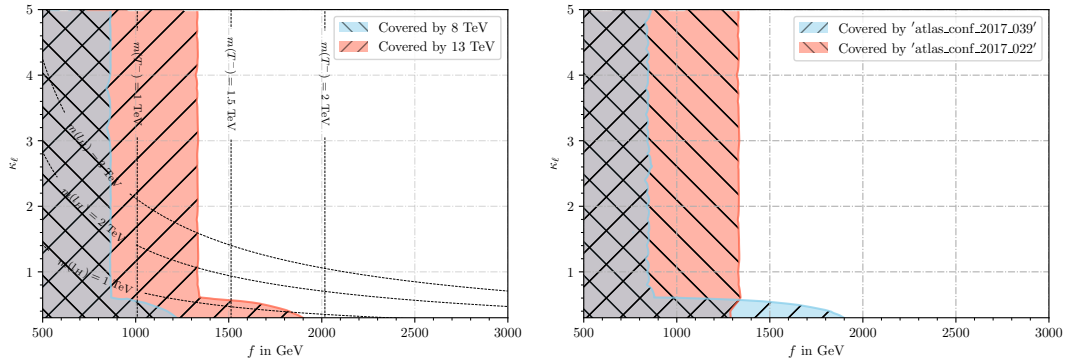

Fig. 6.6.: Results for scenario $(Heavy\ q_H)\times(Light\ T^{\pm})\times(TPC)$

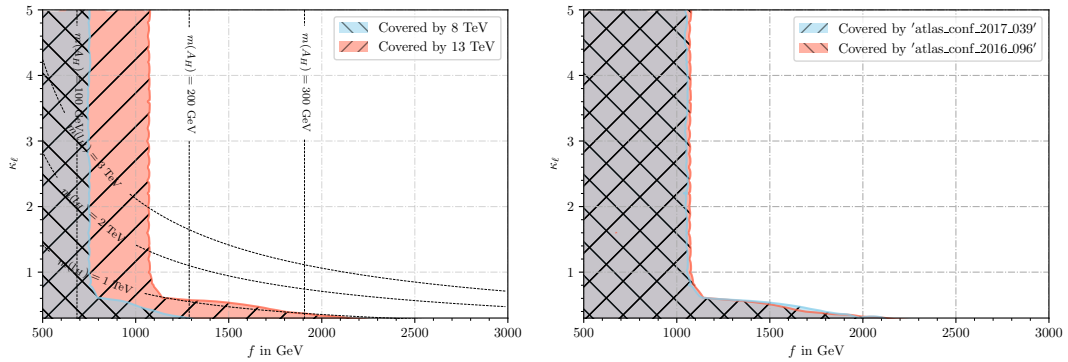

Fig. 6.7.: Results for scenario $(Heavy\ q_H)\times(Heavy\ T^{\pm})\times(TPV)$

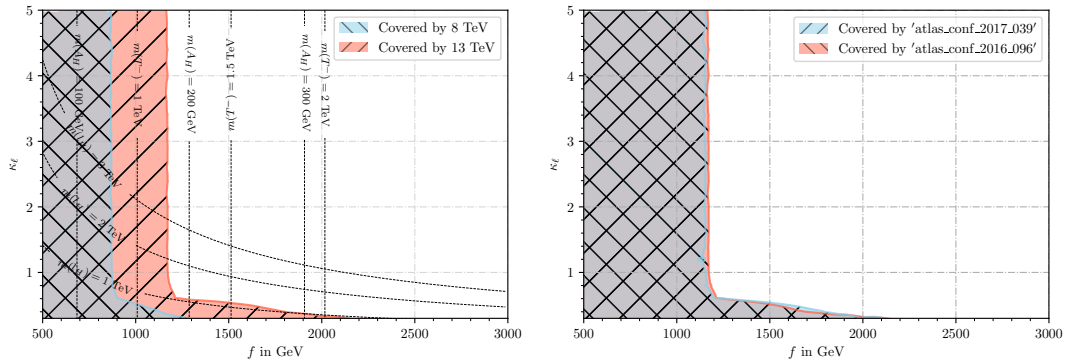

Fig. 6.8.: Results for scenario $(Heavy\ q_H)\times(Light\ T^{\pm})\times(TPV)$

	$T^{\pm}$ is heavy	$T^{\pm}$ is light
T-parity is conserved(TPC)	$f \lesssim 950\,\text{GeV}$	$f \lesssim 1350\,\text{GeV}$
T-parity is broken(TPV)	$f \lesssim 1100\,\text{GeV}$	$f \lesssim 1200\,\text{GeV}$

Table 6.2.: Excluded regions for the *Heavy* q_H model

by the contribution of the $V_H V_H$ production channel is predicted to have the same result for $\kappa = 4.0$ of the *Fermion Universality* model.

Similarly to the previous benchmarks, the results are divided into two areas, as follows:

For f of order 1 TeV and large κ_ℓ, the most sensitive processes are again heavy vector boson or cancellon production. Both are independent of κ_ℓ, thus the exclusion limit becomes a vertical line.

Table 6.2 shows the allowed area with respect to the different benchmark cases and they are in agreement with the results of the *Fermion Universality* model for $\kappa = 4.0$, which tells us that the effect of κ_ℓ is tiny. Also, the most influential topologies are still multijet final states for the T-parity conserved case and multilepton final states for the T-parity violated case.

If κ_ℓ is less than 0.5, the mass hierarchy between heavy vector V_H and T-odd lepton ℓ_H is changed, see the discussion in Section 5.5.2. Boosted leptonic states are produced by this decay which would be observed by the multilepton analysis `'atlas_conf_2017_022'` and are excluded f up to 1.9 TeV. These decays depends on κ_ℓ, as does the bound.

The bound for $f \times \kappa_{max}$ has vanished as the q_H are decoupled from the detectable energy scale by the choice $\kappa_q = 4.0$. Furthermore, in case of TPC, $\ell_H \ell_H$ has too small a production event rate to yield any exclusion limit, even for $\sqrt{s} = 13\,\text{TeV}$. However, in case of TPV, we observe a weak exclusion bound along with the mass contour of ℓ_H. Again, this is thanks to the increased number of hard final state particles from the gauge bosons produced in $A_H \to VV$.

Comparing the results for the *Heavy* q_H benchmark with those from the previous *Fermion Universality* benchmark, we find that the details of the heavy fermion sector have a crucial impact on the exclusion limits in the region $\kappa \lesssim 1.5$ at the LHC. However, the exclusion limits caused by heavy gauge bosons are nearly κ-independent and thus very stable against details of the T-odd fermion sectors.

6.1.3. *Light* ℓ_H model

For the *Light* ℓ_H model, we fix κ_ℓ to 0.2 such that T-parity odd leptons become even lighter and the mass gap between T-odd quarks and leptons increases. A distinct feature of the *Light* ℓ_H model are decays of the heavy gauge bosons W_H, Z_H, which are $Z_H \to \ell\ell_H$ and $W_H \to \ell_H \nu(\nu_H \ell)$ followed by $\ell_H \to \ell A_H$ or $\nu_H \to \nu A_H$ while in *Fermion Universality* model,

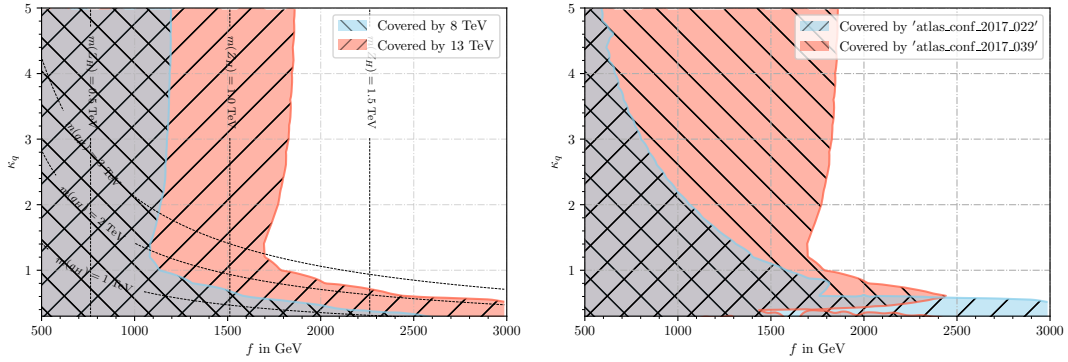

Fig. 6.9.: Results for scenario $(Light\ \ell_H)\times(Heavy\ T^{\pm})\times(TPC)$

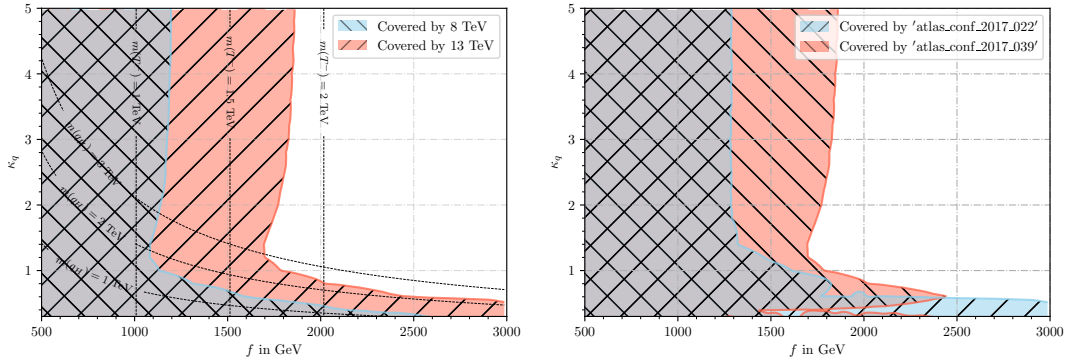

Fig. 6.10.: Results for scenario $(Light\ \ell_H)\times(Light\ T^{\pm})\times(TPC)$

their dominant decays are $Z_H \to hZ_H$ and $W_H \to WA_H$. The results for the *Light* ℓ_H model are shown in Figs. 6.9 - 6.12.

As for the previous benchmarks, the excluded region can be divided into two areas as follows:

For smaller κ_q**,** the bound follows the q_H mass contour. For $\kappa_q \gtrsim 0.5$, we can check that it is covered by *the multilepton analysis*, see Fig. 6.9 right, which originates from a $q_H q_H \to qqW_H W_H$ decay topology followed by $W_H \to \ell\nu A_H$. The leptons are boosted thanks to the mass gap between M_{q_H} and M_{W_H}. For $\kappa_q \lesssim 0.5$, it is covered by *the multijet analysis* `'atlas_conf_2017_022'` as in the *Fermion Universality* model because the q_H are light enough for decays $V_H \to q_H q$ to happen.

For larger value of κ_q**,** again, the exclusion limit becomes nearly κ-independent and is produced by the heavy gauge bosons V_H whose mass only depends on f not on κ_q. However, as mentioned earlier, the production of heavy gauge bosons inherits a small dependence on κ_q from t-channel q_H exchange.

By comparison to the result of the *Fermion Universality* model, we observe that the exclusion area is extended considerably, i.e. $f \lesssim 1.6\,\text{TeV}$ for $\kappa_q \lesssim 1.5$ and $f \lesssim 2\,\text{TeV}$ for $\kappa_q < 5.0$. The reason why the bound is significantly improved is thanks to the clean signal of boosted leptons, i.e. $V_H \to \ell_H \ell_H$, $\ell_H \to \ell\ell_H$. As the analyses coverage map shows, this topology is

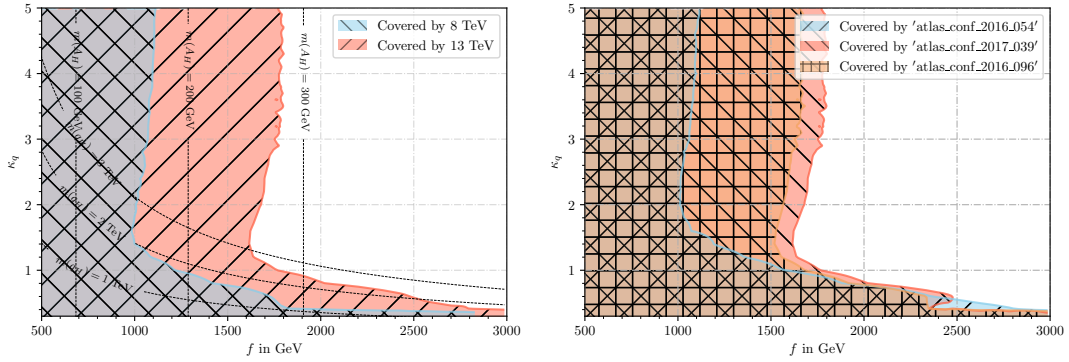

Fig. 6.11.: Results for scenario $(Light\ \ell_H)\times(Heavy\ T^{\pm})\times(TPV)$

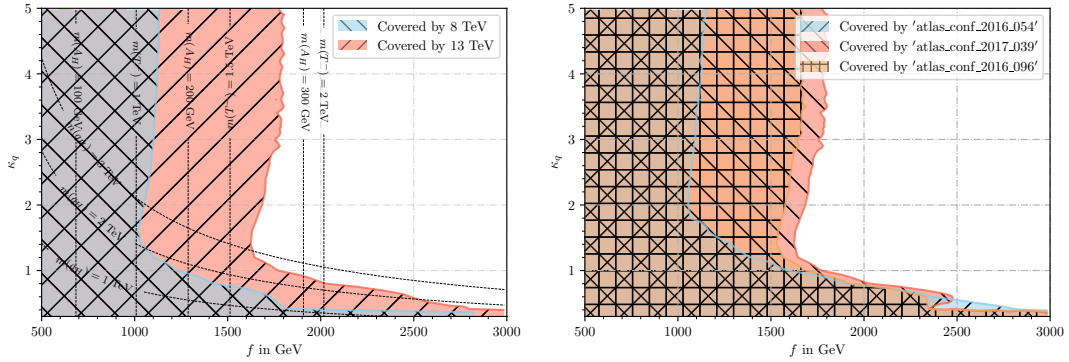

Fig. 6.12.: Results for scenario $(Light\ \ell_H)\times(Light\ T^{\pm})\times(TPV)$

covered by the multilepton analysis `'atlas_conf_2017_039'` that detect boosted leptons not from SM gauge bosons decays. Therefore, the signal produced by the $V_H V_H$ process is clean and strongly distinguishable from SM background.

The heavy top partner $T^{\pm}$ does not generate any noticeable change in the plots because the bound by the processes related to V_H is already strong enough. As before, the production of $T^{\pm}$ affects only the region $f \lesssim 1.35\,\text{TeV}$ which however is already covered by V_H processes. Also, the final states of $T^{\pm}$ decay do not match the topology of the multilepton analysis `'atlas_conf_2017_039'`.

For the T-parity broken case, the result plots are Figs. 6.11 and 6.12. There is no extension of the exclusion area compared to the result when A_H does not decay, as A_H decays only to WW or ZZ which results in a small loss of $\not{E}_T$ cut efficiency, see discussion Section 6.1.1

With κ_ℓ below a certain value, the heavy gauge boson V_H decays into $\ell_H \ell$ with nearly 100% probability. Since its decay width depends on the mass of ℓ_H, the heavier the ℓ_H mass is chosen, the less V_H will decay into ℓ_H. Therefore, in a scenario with heavier ℓ_H, the result plots of the *Light* ℓ_H model will gradually come closer to that of the *Fermion Universality* model.

The highly boosted leptons generated from $V_H \to \ell\ell' A_H$ decay mainly contribute to the multilepton analysis. The decay is mediated by on-shell ℓ_H, thus, a different κ_ℓ value changes

the ℓ_H mass and affects also the energy distribution of the final state. As a result, it would change the signal acceptance of the multilepton analysis. However, as the mass gap between M_{V_H} and M_{A_H} is around 750 GeV for $f \approx 1.5$ TeV, we always expect high-energetic leptons that will pass cuts of the analysis, regardless of the mass of the ℓ_H.

6.1.4. Prospects for $\sqrt{s} = 14$ TeV

Comparing the $\sqrt{s} = 8$ TeV and $\sqrt{s} = 13$ TeV results of the previous discussion, we see that it can extend the exclusion limits considerably to increase the center of mass energy and the integrated luminosity. Now, we discuss how the result may further improve when the center of mass energy is increased to $\sqrt{s} = 14$ TeV. For this, we use CheckMATE at $\sqrt{s} = 14$ TeV and $\int \mathcal{L} = 3000\,\text{fb}^{-1}$.

We do not discuss all the previously discussed benchmarks because the available 14 TeV analyses do not cover all the multiparticle topologies that we discussed above. The results that we discuss now are for the case of *Heavy* $T^{\pm}$ and T-parity conservation (*TPC*), for all three cases *Fermion Universality*, *Heavy* q_H and *Light* ℓ_H. Actually, as we have seen above, that the *TPV* case does not generate a big difference compared to *TPC* and neither does *Heavy* $T^{\pm}$ from *Light* $T^{\pm}$. Thus, it is sufficient for us to give a rough overview of the overall tendency for the case with conserved T-parity in $\sqrt{s} = 14$ TeV

The results are in Figs. 6.13 - 6.15. We show the results for values of f up to 4 TeV while before were only drawn up to $f \approx 3$ TeV. Plots are shown twice for the same benchmark; one tells us how much area is excluded more compared with $\sqrt{s} = 13$ TeV data as well as the relevant particles' mass contours and the other plot as before includes the information which analyses exclude the marked area. Note that there is fluctuation from Monte Carlo statistical uncertainty, still the qualitative excluded limit is not affected from it. As the results of the previous sections, the exclusion regions are divided into two areas: a nearly vertical bound with rather large κ and small f plus a nearly horizontal area following the q_H mass contour for small κ and large f.

Fermion Universality model

Fig. 6.13 shows the *Fermion Universality* model that assumes T-odd quarks have the same mass with T-odd leptons. Comparing Fig. 6.13 to Fig. 6.1 we observe the data from $\sqrt{s} = 14$ TeV extends the exclusion area significantly. For the bound running along the q_H mass contour, the bound on f improves by 1-1.5 TeV more of f for the same value of κ. It would exclude $M_{q_H} \lesssim 4$ TeV for $f \approx 2$ TeV and $M_{q_H} \lesssim 3$ TeV for $f \approx 4$ TeV. The main contributing analysis is again the one sensitive to a multijet final state with missing transverse momentum, defined to target squarks $\tilde{q}$ and gluinos $\tilde{g}$ in Supersymmetry.

The nearly vertical bound with large κ excludes up to $M_{V_H} \approx 1$ TeV for $f \approx 1.5$ TeV. Here, the most sensitive analysis is a multilepton search `'atlas phys 2014 010 sq hl'` with $\not{E}_T$. For the multijet analysis with higher luminosity, the scalar sum of p_T for all the reconstructed objects should pass 3 TeV, however, in this area, the dominant process is $V_H \to A_H V$ follwed by $V \to$ hadrons, which is not able to pass this constraint because high p_T ISR lowers the expected event rate for the boosted final state.

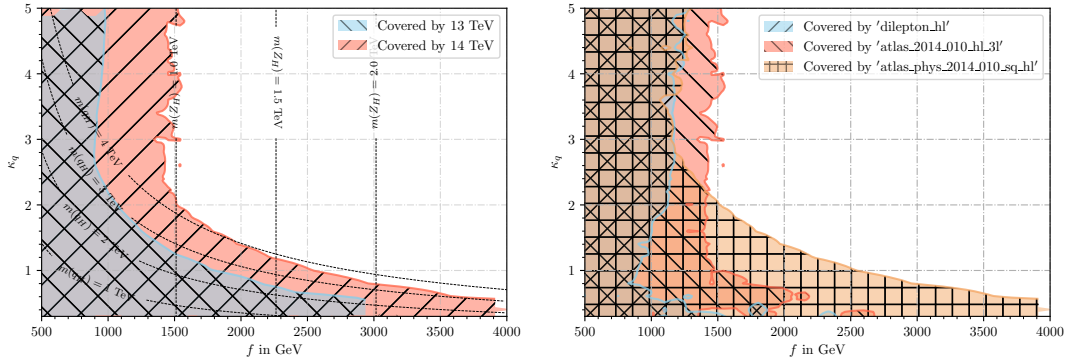

Fig. 6.13.: Expected results at $\sqrt{s} = 14\,\text{TeV}, \int \mathcal{L} = 3000\,\text{fb}^{-1}$ for scenario (*Fermion Universality*)×(*Heavy* $T^{\pm}$)×(*TPC*).

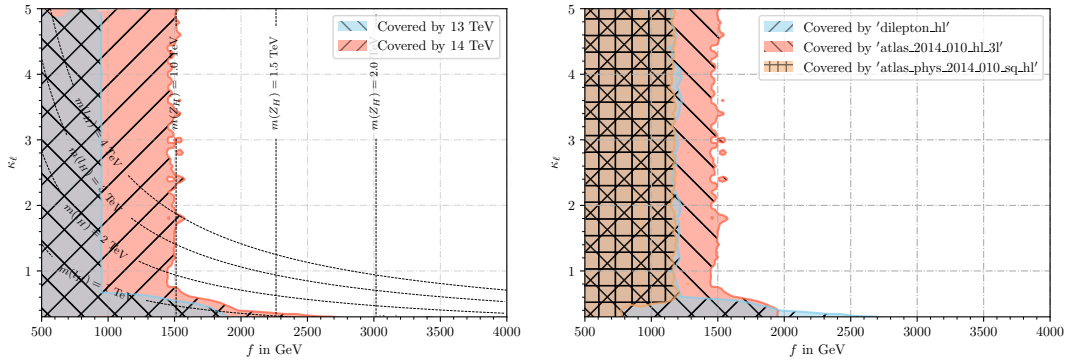

Fig. 6.14.: Expected results at $\sqrt{s} = 14\,\text{TeV}, \int \mathcal{L} = 3000\,\text{fb}^{-1}$ for scenario (*Heavy* q_H)×(*Heavy* $T^{\pm}$)×(*TPC*).

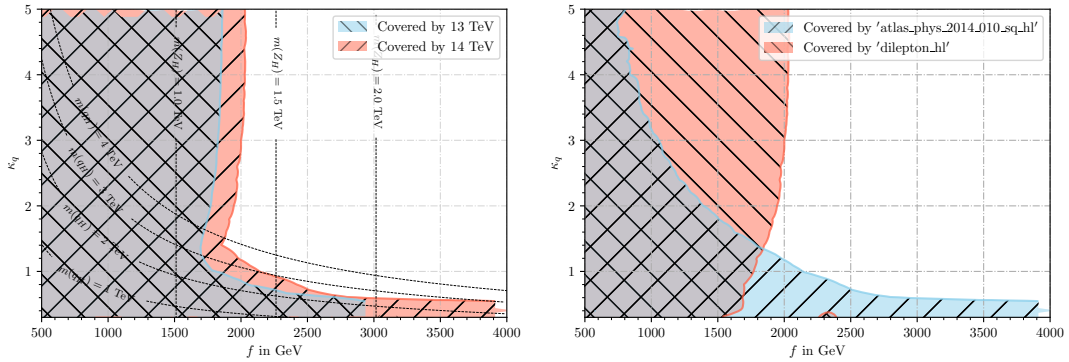

Fig. 6.15.: Expected results at $\sqrt{s} = 14\,\text{TeV}, \int \mathcal{L} = 3000\,\text{fb}^{-1}$ for scenario (*Light* ℓ_H)×(*Heavy* $T^{\pm}$)×(*TPC*).

Heavy q_H model

For the *Heavy* q_H model with $\kappa_q \approx 4.0$, we expect the bound along the l_H mass contour instead of the q_H mass when κ_ℓ is small. As one can see from Fig. 6.14, the exclusion area is not so much extended with respect to the one that of the 13 TeV result. The study for the dilepton state which was relevant at $\sqrt{s} = 13\,\text{TeV}$ is not implemented at $\sqrt{s} = 14\,\text{TeV}$ in CheckMATE yet. For the exclusion limit along the M_{V_H} mass, it is very similar with that of the *Fermion Universality* model.

Light ℓ_H model

The exclusion limit is improved only a little compared to 13 TeV data from the LHC Run2. For the bound along the q_H mass contour, the main contributing analysis looks for a multijet final state with one lepton that is not contaminated by SM background.

For the κ-independent exclusion limit, the mass bound on Z_H is improved roughly 100 GeV thanks to the analysis with 2 leptons in the final state, motivated by Supersymmetric processes $\tilde{\ell}\tilde{\ell} \to \ell\ell\tilde{\chi}\tilde{\chi}$ or $\tilde{\chi}^+\tilde{\chi}^- \to WW\tilde{\chi}\chi$. But, their final states do not overlap with those of our topologies.

6.1.5. Comparison of LHC limits with Bounds from Electroweak Precision Observables

In Figs. 6.16 - 6.21, the results from the LHC Run1 and Run2 are overlaid with the bounds from electroweak precision observables. Also, the fine tuning ratio for the Higgs sector is there. The theoretical background was given in previous sections 4.5 and 4.6.

We discuss the results for some generic scenarios: Three scenarios with different values for κ_q and κ_ℓ with heavy or light top partners $T^\pm$ depending on R. We do not take into account the case of violated T-parity (TPV) in this section because electroweak precision observables (EWPO) are not affected by whether T-parity is violated and the collider results for TPC are similar to those for TPV. Fine tuning depends on the ratio of Yukawa coupling constants R as well as the symmetry breaking scale f. The limits from collider results and EWPO bounds are complementary in their coverage of the parameter space.

Fermion Universality model

Figs. 6.16 and 6.17 show the results for the case that the Yukawa coupling constants for mirror fermions are the same for quarks and leptons, $\kappa_q = \kappa_\ell = \kappa$, and T-parity is conserved. Fig. 6.16 is the result with heavy top partners $T^\pm$, which become very heavy by setting $R = 0.2$. Fine tuning is weaker than in Fig. 6.17, where $T^\pm$ is light.

In the case of heavy $T^\pm$, the fine tuning level required for the "naturalness" of the model is below 0.5 % for $f > 1.3\,\text{TeV}$ and independent of κ. We observe that the bounds from EWPO become weaker when $T^\pm$ gets lighter. At the same time, the exclusion limits from collider results are getting stronger, which results in the general lower bound $f \gtrsim 1.3\,\text{TeV}$.

More specifically, we can conclude that $f < 1\,\text{TeV}$ is not allowed any more for the range $R \in [0.2,\ 1.0]$ in the benchmark scenarios of Figs. 6.16 and 6.17.

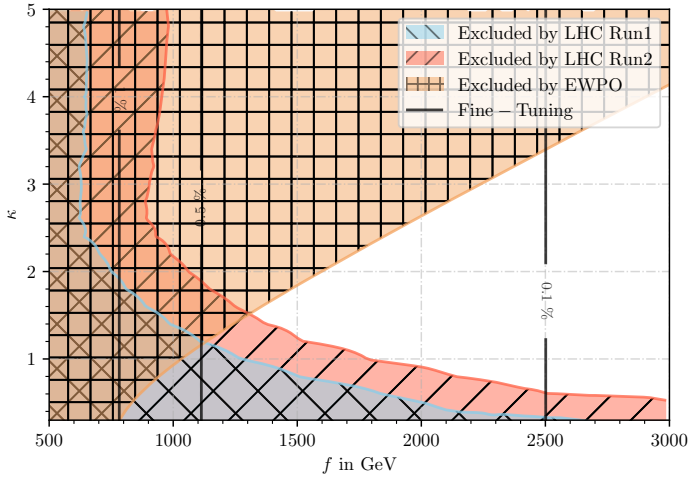

Fig. 6.16.: Combined results for scenario $(Fermion\ Universality)\times(TPC)\times(Heavy\ T^{\pm})$

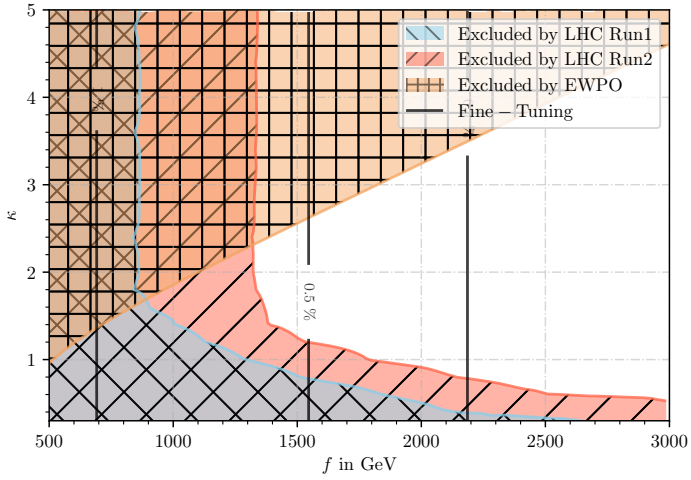

Fig. 6.17.: Combined results for scenario $(Fermion\ Universality)\times(TPC)\times(Light\ T^{\pm})$

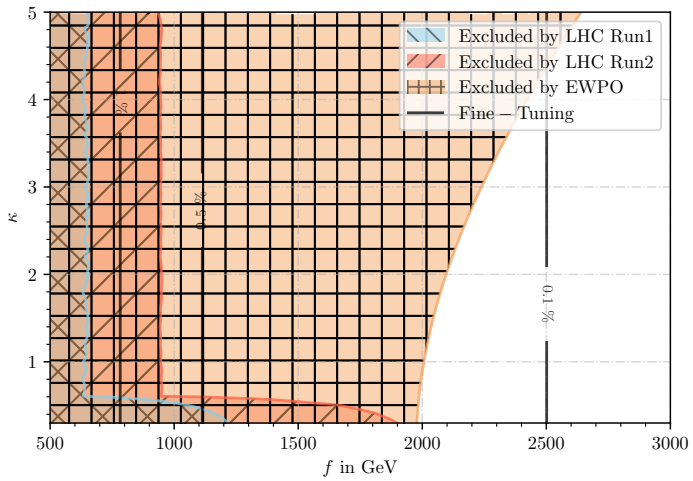

Fig. 6.18.: Combined results for scenario (*Heavy* q_H)×(*TPC*)×(*Heavy* $T^{\pm}$), κ in y-axis refers to the Yukawa coupling constants of T-odd mirror leptons ℓ_H.

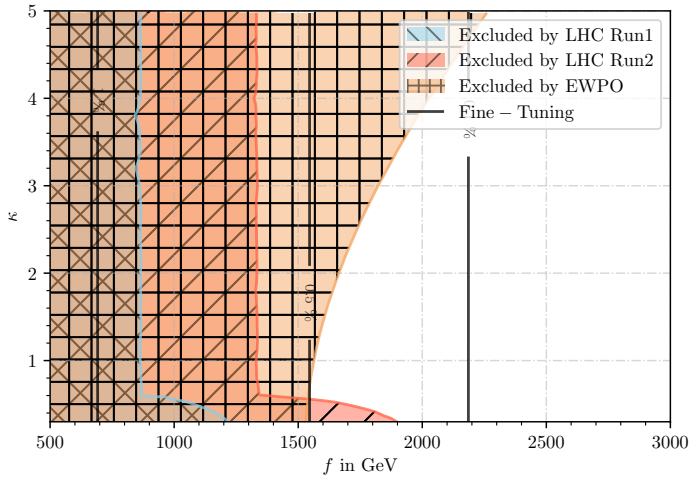

Fig. 6.19.: Combined results for scenario (*Heavy* q_H)×(*TPC*)×(*Light* $T^{\pm}$), κ in y-axis refers to the Yukawa coupling constants of T-odd mirror leptons ℓ_H.

Heavy q_H model

Figs. 6.18 and 6.19 show the results when we fix the Yukawa coupling constant of mirror fermions to $\kappa_q = 4.0$. As previously, T-parity is conserved.

The bounds from EWPO and from collider results are similar to the previous case. In this *Heavy* q_H benchmark scenario, T-odd quarks are decoupled from the experimentally accessible energy range, which results in a big reduction of the exclusion area from the collider results. But, thanks to the κ-dependence as in Eq. (4.112), the exclusion area from EWPO extends when we fix $\kappa_q = 3.0$.

When the top partner $T^\pm$ is light, i.e. R is fixed as $R = 1.0$, $f < 1.5\,\text{TeV}$ is excluded. When $T^\pm$ is heavy, i.e. $R = 0.2$, $f < 2\,\text{TeV}$ is excluded.

In case of heavy $T^\pm$, the region excluded by 4-fermion operators fully covers the bounds from the LHC Run results and the fine tuning level is below 0.25%. This is to first approximation also true for the case with light $T^\pm$ except for very small κ, where $V_H \to \ell_H \ell$ pushes the bounds by several hundreds GeV.

Light ℓ_H model

For Figs. 6.20 and 6.21, we assume the T-odd leptons to be very light by $\kappa_\ell = 0.2$, which makes the bounds from EWPO slightly weaker than those of the *Fermion Universality* model in Figs. 6.16 and 6.17, while the bounds from the result of the LHC Run improve significantly since the final states of relevant processes in this scenario are distinctively producing hard leptons, see Section 6.1.3. The region $f < 1.7\,\text{TeV}$ is excluded independent of the choice of top partner sector $T^\pm$.

We observe that the bounds derived by EWPO are more relevant when $f > 1.8\,\text{TeV}$ with $\kappa_q > 2.5$. For the scenario with heavy $T^\pm$, around 0.35% of fine tuning is allowed and for the scenario with light $T^\pm$, it is around 0.4%.

Conclusions

Considering only EWPO excludes up to 1% fine-tuning level for light q_H and $T^\pm$. This area of parameter space is testable by collider experiments and the results from the LHC data are cutting this area already substantially. Specific constraints are depending on the symmetry breaking scale f, the Yukawa coupling constants κ fixing the masses of heavy fermions, the mass of heavy top partners $T^\pm$, and the violation (or conservation) of T-parity. In summary, the region $f < 1.3\,\text{TeV}$ and around 0.5% level of fine tuning is excluded throughout all the benchmark scenarios that we considered. The exclusions by EWPO appeared as complementary area that by LHC data.

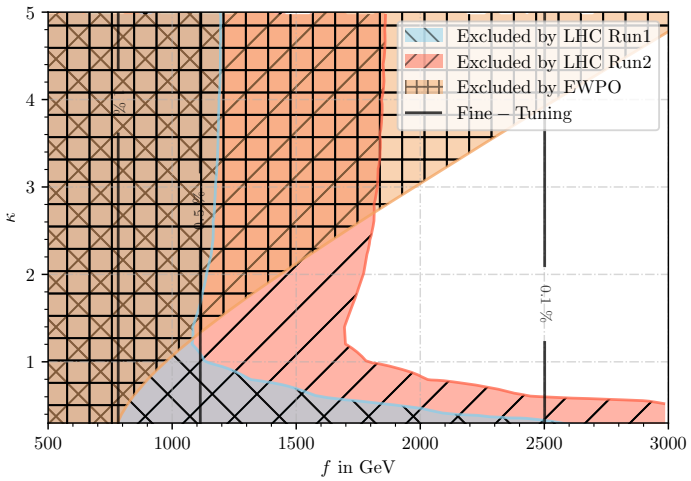

Fig. 6.20.: Combined results for scenario $(Light\ \ell_H)\times(TPC)\times(Heavy\ T^{\pm})$, κ in y-axis refers to the Yukawa coupling constants of T-odd mirror quarks q_H.

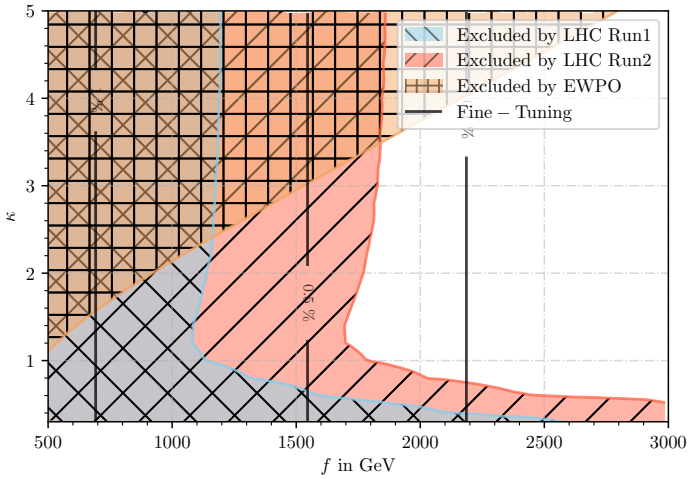

Fig. 6.21.: Combined results for scenario $(Light\ \ell_H)\times(TPC)\times(Light\ T^{\pm})$, κ in y-axis refers to the Yukawa coupling constants of T-odd mirror quarks q_H.

Chapter 7.

Conclusions and Overlook

Physic beyond the Standard Model provides lots of solutions to the hierarchy problem, one of them being the Little Higgs paradigm. Little Higgs models have an extended global symmetry group that is broken spontaneously at a scale $f \sim \mathcal{O}$TeV. Little Higgs models consider the Higgs as a pseudo-Nambu-Goldstone boson and stabilize the Higgs mass against radiative corrections the Collective Symmetry Breaking mechanism, thereby pushing quadratically divergent contributions to the Higgs mass from the one-loop level to the two-loop level. We reviewed the Little Higgs models and analyzed the compatibility of the Littlest Higgs model with T-parity that is a discrete $\mathbf{Z}_2$ symmetry with the recent data collected in collider experiments.

We compared the productions from the Littlest Higgs model with T-parity to available Run 2 data at $\sqrt{s} = 13\,\text{TeV}$ of the LHC and studied the dependence of the exclusion regions on the model parameters. The relevant parameters are the scale f, the quark and lepton partner mass parameters κ_q and κ_ℓ as well as the ratio of top sector Yukawa-like couplings R. The dependence is investigated in terms of several different benchmark spectra. In the region of $f > 1\,\text{TeV}$ where T-odd quark partners are produced abundantly, the bounds are dependent on the parameters f and the quark-mass parameter κ_q. The bounds go along with the iso-mass contour of T-odd quarks. Roughly speaking, the excluded area is where the mass of T-odd quarks is below 2 TeV.

In the region of $f < 1\,\text{TeV}$, the exclusion limit is derived by other production processes, especially of heavy gauge bosons provides the bound. As heavy vector production only depends on their mass, the exclusion bounds here only depend on f. If top partners are allowed to be produced kinematically, the bounds then also have a dependence on the ratio of top Yukawa couplings R. Generically, the full area $f < 1\,\text{TeV}$ is excluded. Altogether, we obtained at 95% confidence level exclusion bounds on the scale $f < 1\,\text{TeV}$ and the heavy quark partner mass of $M_{q_H} < 2\,\text{TeV}$.

We showed results with regard to electroweak precision observables. The exclusion bounds are proportional to κ^2 for contact interactions, so complementarily for large κ, while the iso-contours prefer exclusions for small κ where f is light and quarks are accessible. All in all, the area $f < 1.3\,\text{TeV}$ and the fine-tuning level above 0.5% are excluded for the Littlest Higgs model with T-parity.

As a second project, we investigated six-dimensional operators in the Effective Field Theory formalism. A full set of bosonic $\mathcal{CP}$-even dimension-six operators has been implemented in the event generator `WHIZARD`. This has been documented as a contribution to the CERN Yellow Report Vol. 4.

From the development of ILC, it will reach to the level that can test physics regarding the Higgs precision tests and contact interactions in the LHT model. As a future project, I want to compare this reach in precise Higgs physics to the dijet search from LHC.

Although in this thesis we focused on the Littlest Higgs model with T-parity, we expect to also notably constrain the Simplest Little Higgs model when employing the recent data of the LHC. The Simplest Little Higgs model is expected to appear with different signatures from the LHT model: Vector-like quarks, heavy gauge bosons Z', W' have decay channels without cascades. Also, a light pseudo-scalar particle η of the SLH model has diphoton and $b\bar{b}$ as final states.

Appendix A.

Dimension-6 operators in WHIZARD

A.1. How to implement new vertices into WHIZARD

In this secton, the parts which have to be adapted to implement new vertices in WHIZARD are discussed in the following. Especially, to implement six-dimensional operators into WHIZARD seven files are needed to be modified. Paths in the following list are relative to the top level of WHIZARD. We describe files with regard to the SM with additional vertices. If one wants to modify a different model, then the "SM" or "SM_ac" in the file name can be replaced with another model name. The descriptions for the files are following:

- In /trunk/omega/src directory
  - omegalib.nw contains the O'Mega library written in FORTRAN. It includes Lorentz structures for vertices. If there is any new vertex, that should be added to the corresponding model file. If there is any new vertex that did not exist in the file, then one needs to define a new kind of vertex or function with the help of the LSZ reduction theorem.
  - targets.ml is written in O'Caml. It provides particles' Lorentz index numbers and corresponds the functions to the Lorentz structures' name in modellib_SM.ml.
  - modellib_SM.ml defines vertex types, particle contents, Lorentz structures, and coupling coefficients in O'Caml code.
  - coupling.mli constitutes the O'Caml interface, which lists all vertices and propagator types for all models in O'Mega.
  - colorize.mli is same as above, but for color flow objects.
- In the /trunk/share/models/ directory,
  - SM_ac.ml defines parameters such as Wilson coefficients in O'Caml interface.
- In /trunk/src/models/ directory,
  - parameters.SM_ac.f90 is written in FORTRAN, which initializes model parameters and reads numerical values such as coupling coefficients with respect to the given equations.

Steps to include a new vertex for WHIZARD

Based on the list above, we can specify what to do for the implementation of new vertices:

1. /trunk/omega/src/omegalib.nw : Define new vertices.

2. /trunk/omega/src/targets.ml : Define the new Lorentz structures for using in modellib_SM file provide dummies for the OVM module.

3. /trunk/omega/src/coupling.mli : Provide LaTeX documentation for new vertices.

4. /trunk/omega/src/colorize.ml : Give informations for *(coupling coefficient)* (color factor)*

5. /trunk/omega/src/modellib_SM.ml : Define vertices with coupling coefficients and the type of Lorentz structure.

6. /trunk/share/models/SM_ac.ml : add the Wilson coefficients as new free parameter to the model.

7. /trunk/src/models/parameters.SM_ac.f90 : Specify the coupling coefficients.

After the steps in the list above, to compile is the last steps by typing *$ make* and *$ make install*.

A.2. How to use the dimension-6 operators in WHIZARD

Here is an example SINDARIN code for using 6 dimensional operators. Model is for specifying the model for running WHIZARD. The words starting with c6 refer to the Wilson coefficients, which are turned off with set as zero. Their values are zero by default. lamdac6 is the cut-off scale of dimension-six operators in GeV. Other commands for simulating WHIZARD can be looked up in WHIZARD [30–33].

```
Model: SM_6dim

c6pb = 1
c6dw = 1
c6db = 1
c6dpw = 1
c6dpb = 1
lambdac6 = 1000

###################################
# Processes                       #
###################################
process eeahz = e1, E1 => Z, H { $restrictions = "1+2 ~ A" }

compile

$description = "test running"
$x_label = "$\sqrt{s}$/GeV"
$y_label = "$\sigma(s)$/pb"

# Allocate one plot
$title = "The cross section in $e^+e^-\to \gamma \to Z+H$"
plot lineshape_eeahz { x_min = 300 GeV  x_max = 1000 GeV }

scan sqrts = ((300 GeV => 400 GeV /+ 5 GeV)   ,
              (410 GeV => 500 GeV /+ 10 GeV),
              (550 GeV => 1000 GeV /+ 50 GeV))
{  beams = e1, E1
  integrate (eeahz) { iterations = 2:1000:"gw", 1:2000 }
  record lineshape_eeahz (sqrts, integral (eeahz) / 1000)}

compile_analysis { $out_file = "SMdim6_AHZ.dat" }
```

Appendix B.

The Simplest Little Higgs model

Fermion sectors

We have to find a proper to reconcile the fermion sector with the peculiar group structure of the Simplest Little Higgs. Since the Simplest Little Higgs model has enlarged gauge symmetry $SU(3) \times U(1)$, incomplete multiplets are not applicable. There are two ways for this: *universal embedding* and *anomaly-free embedding*. *Universal embedding* is an embedding that is the same for all quantities, howevers, it generates a Wess-Zumino-Witten anomaly for the global symmetries. This can be avoided by *anomaly-free embedding*.

The leptons can be expressed with the left-handed triplets of $SU(3)$ and two right-handed singlets,

$$L_m^T = (\nu_L, \ell_L, iN_L)_m, \qquad \ell^c_{R\ m}, N_{R\ m} \qquad m \in \{1,2,3\}, \tag{B.1}$$

where m is the generation index and N_m is a new heavy particle, namely a neutrino partner. The third generation of quarks are similarly represented like the lepton sector, whereas the first and second generation quarks should contain an $SU(3)$ left-handed conjugate triplet;

$$\begin{aligned} Q_1^T &= (d_L, -u_L, iD_L), & d^c_R, u^c_R, D^c_R \\ Q_2^T &= (s_L, -c_L, iS_L), & s^c_R, c^c_R, S^c_R \\ Q_3^T &= (t_L, b_L, iT_L), & t^c_R, b^c_R, T^c_R \end{aligned} \tag{B.2}$$

which have quantum numers like in Table B.1.

Lepton Yukawa couplings

The mass terms for leptons are generated from the Yukawa Lagrangian

$$\mathcal{L} \supset i\lambda_{N_m} N^c_m \Phi_2^\dagger L_m + \frac{i\lambda_e^{mn}}{\Lambda} e^c_m \epsilon_{ijk} \Phi_1^i \Phi_2^j L_n^k + \text{h.c.}, \tag{B.3}$$

where $n,\ m$ are the generation indices for generations of leptons. The heavy neutrino partners N_m have the mass

$$M_{N_m} \ = \ \lambda_{N_m} s_\beta f$$

from the first term of the Lagrangian. The second term is dimension-5, which is normalised by the cutoff scale Λ. This operator gives rise to the mass terms of charged leptons via the mixing matrix V^ℓ_{im}, which describes the mixing between e_i and N_m similar to the CKM mixing. This can happen in association with the gauge boson X^- in the $X^- \bar{e}_i N_m$ coupling, which can be

fermion	$Q_{1,2}$	Q_3	$u^c_m,\ T^c$	$d^c_m,\ D^c,\ S^c$	L_m	N^c_m	e^c_m
Q_x charge	0	1/3	-2/3	1/3	-1/3	0	1
$SU(3)$ rep.	$\bar{\mathbf{3}}$	**3**	**1**	**1**	**3**	**1**	**1**

Table B.1.: Anomaly-free enbedding

found in the Lagrangian as

$$\mathcal{L} \supset -\frac{g}{\sqrt{2}} V^{\ell}_{im} X^-_{\mu} \bar{e}_i \gamma^{\mu} P_L N_m \quad . \tag{B.4}$$

But, the mixing is suppressed by GIM mechanism [72] and vanishes, when V^{ℓ}_{im} is diagonalized.

After EWSB, mixing between neutrinos ν_{m0} and the heavy neutrino partners N_{m0} appears at order v/f,

$$N_{m0} = N_m + \delta_\nu V^{\ell\dagger}_{mi} \nu_i, \qquad \nu_{i0} = (1 - \frac{1}{2}\delta^2_\nu)\nu_i - \delta_\nu V^{\ell}_{im} N_m. \tag{B.5}$$

Quark Yukawa couplings

The quark Yukawa interaction Lagrangian is given by

$$\mathcal{L}_Y \supset i(\bar{d}^1_R,\ \bar{d}^2_R) Q^T_1 \begin{pmatrix} \lambda^d_1 \Phi_1 \\ \lambda^d_2 \Phi_2 \end{pmatrix} + i(\bar{s}^1_R,\ \bar{s}^2_R) Q^T_2 \begin{pmatrix} \lambda^s_1 \Phi_1 \\ \lambda^s_2 \Phi_2 \end{pmatrix} \tag{B.6}$$

$$+ i(\bar{t}^1_R,\ \bar{t}^2_R) \begin{pmatrix} \lambda^d_1 \Phi_1 \\ \lambda^d_2 \Phi_2 \end{pmatrix} Q_3 + \sum_m \frac{\lambda^m_b}{\Lambda} \bar{d}_{R\ m} \epsilon_{ijk} \Phi^i_1 \Phi^j_2 Q^k_3 \tag{B.7}$$

$$+ \sum_{m,n} \frac{\lambda^{mn}_u}{\Lambda} \bar{u}_{R\ m} \epsilon_{ijk} \Phi^{i*}_1 \Phi^{j*}_2 Q^k_n. \tag{B.8}$$

Because third generation quarks have a different expression than the other two generations for *anomaly-free embedding*, the Lagrangian of the Yukawa interaction for quarks have different expressions as follows,

$$\begin{aligned} \mathcal{L}_3 &= \lambda^t_1 i t^c_1 \Phi^\dagger_1 Q_3 + \lambda^t_2 i t^c_2 \Phi^\dagger_2 Q_3 + \frac{\lambda^m_b}{\Lambda} i d^c_m \epsilon_{ijk} \Phi^i_1 \Phi^j_2 Q^k_3 + \text{h.c.}, \\ \mathcal{L}_{1,2} &= \lambda^{dn}_1 i d^{nc}_i Q^T_n \Phi_1 + \lambda^{dn}_2 i d^{nc}_2 Q^T_n \Phi_2 + \frac{\lambda^{mn}_u}{\Lambda} i u^c_m \epsilon_{ijk} \Phi^{*i}_1 \Phi^{*j}_2 Q^k_n + \text{h.c.}, \end{aligned} \tag{B.9}$$

where $n = 1, 2$ and $m = 1, 2, 3$ refer to the generation indices; and $i, j, k = 1, 2, 3$ are $SU(3)_L$ indices. The linear combinations of $t^c_{1,2}$ form the states for the heavy top partner T^c and the SM top t^c, and similarly $d^{nc}_{1,2}$ form those of $D^c,\ d^c$ for $n = 1$ and $S^c,\ s^c$ for $n = 2$.

The heavy quark T^c state is orthogonal to t^c states as

$$T^c = \frac{\lambda_1^t c_\beta u_1^c + \lambda_2^t s_\beta u_2^c}{\sqrt{\lambda_1^{t2} c_\beta^2 + \lambda_2^{t2} s_\beta^2}}, \qquad t^c = \frac{-\lambda_2^t s_\beta u_1^c + \lambda_1^t c_\beta u_2^c}{\sqrt{\lambda_1^{t2} c_\beta^2 + \lambda_2^{t2} s_\beta^2}}, \tag{B.10}$$

where the β is $\arctan(f_1/f_2)$ and $\lambda_{1,2}^t$ is the Yukawa coupling constant for top belonging to the group $SU_{1,2}(3)$, respectively. The coupling of T^c to T gives rise to its mass leaving t^c massless,

$$M_T = f\sqrt{\lambda_1^{t2} c_\beta^2 + \lambda_2^{t2} s_\beta^2} \quad . \tag{B.11}$$

Also, $D^c,\ d^c$ consist of $d_{1,2}^{1c}(d_{1,2}^c)$ and $S^c,\ s^c$ consist of $d_{1,2}^{2c}(s_{1,2}^c)$ which are expressed as

$$\begin{aligned} D^c &= \frac{\lambda_1^d c_\beta d_1^c + \lambda_2^d s_\beta d_2^c}{\sqrt{\lambda_1^{d2} c_\beta^2 + \lambda_2^{d2} s_\beta^2}}, & d^c &= \frac{-\lambda_1^d s_\beta d_1^c + \lambda_1^d c_\beta d_2^c}{\sqrt{\lambda_1^{d2} c_\beta^2 + \lambda_2^{d2} s_\beta^2}}, \\ S^c &= \frac{\lambda_1^s c_\beta s_1^c + \lambda_2^s s_\beta s_2^c}{\sqrt{\lambda_1^{s2} c_\beta^2 + \lambda_2^{s2} s_\beta^2}}, & s^c &= \frac{-\lambda_1^s s_\beta s_1^c + \lambda_1^s c_\beta s_2^c}{\sqrt{\lambda_1^{s2} c_\beta^2 + \lambda_2^{s2} s_\beta^2}}. \end{aligned} \tag{B.12}$$

Each D^c and S^c couple to D and S, which give them masses as

$$M_D = f\sqrt{\lambda_1^{d2} c_\beta^2 + \lambda_2^{d2} s_\beta^2}, \quad M_S = f\sqrt{\lambda_1^{s2} c_\beta^2 + \lambda_2^{s2} s_\beta^2}, \tag{B.13}$$

leaving d^c and s^c massless.

After EWSB, the Lagrangians containing the quark mass terms are

$$\begin{aligned} \mathcal{L}_{\text{up mass}} &= -M_T T^c T + \frac{v}{\sqrt{2}} \frac{s_\beta c_\beta (\lambda_1^{t2} - \lambda_2^{t2})}{\sqrt{\lambda_1^{t2} c_\beta^2 + \lambda_2^{t2} s_\beta^2}} T^c t - \frac{v}{\sqrt{2}} \frac{\lambda_1^t \lambda_2^t}{\sqrt{\lambda_1^{t2} c_\beta^2 + \lambda_2^{t2} s_\beta^2}} t^c t, \\ &\quad + \frac{v}{\sqrt{2}} \frac{f}{\Lambda} \lambda_u^{mn} u_m^c u_n + \text{h.c.} \end{aligned} \tag{B.14}$$

$$\begin{aligned} \mathcal{L}_{\text{down mass}} &= -M_D D^c D - \frac{v}{\sqrt{2}} \frac{s_\beta c_\beta (\lambda_1^{d2} - \lambda_2^{d2})}{\sqrt{\lambda_1^{d2} c_\beta^2 + \lambda_2^{d2} s_\beta^2}} D^c d + \frac{v}{\sqrt{2}} \frac{\lambda_1^d \lambda_2^d}{\sqrt{\lambda_1^{d2} c_\beta^2 + \lambda_2^{d2} s_\beta^2}} d^c d \\ &\quad - M_S S^c S - \frac{v}{\sqrt{2}} \frac{s_\beta c_\beta (\lambda_1^{s2} - \lambda_2^{s2})}{\sqrt{\lambda_1^{s2} c_\beta^2 + \lambda_2^{s2} s_\beta^2}} S^c s + \frac{v}{\sqrt{2}} \frac{\lambda_1^s \lambda_2^s}{\sqrt{\lambda_1^{s2} c_\beta^2 + \lambda_2^{s2} s_\beta^2}} s^c s \\ &\quad + \frac{v}{\sqrt{2}} \frac{f}{\Lambda} \lambda_b^m d_m^c b + \text{h.c.}, \end{aligned} \tag{B.15}$$

where u_n=u,c; $u_m^c = u^c, c^c, t^c, T^c$; and $d_m^c = d^c, s^c, b^c, D^c, S^c$. The terms with coefficients λ_u^{mn} and λ_b^m cause the mixing between different generation quarks in up and down sectors leading to the CKM matrix. To convert the flavour basis of quarks to the mass basis, we need the

CKM matrix;

$$V^u \begin{pmatrix} u' \\ c' \\ t' \end{pmatrix} = \begin{pmatrix} u \\ c \\ t \end{pmatrix}, \qquad V^d \begin{pmatrix} d' \\ s' \\ b' \end{pmatrix} = \begin{pmatrix} d \\ s \\ b \end{pmatrix} \tag{B.16}$$

where primed fields refer to the flavour bases and unprimed ones are the mass bases. V^u and V^d form the CKM matrix:

$$V^{\mathrm{CKM}} = V^u V^{d\dagger} \tag{B.17}$$

To avoid confusion with the mixing matrices for quarks, one must keep in mind that there are two mixing matrices. One is the CKM matrix V^{CKM} discussed above, which includes mixing information among the flavour and mass bases. The other one results from the mixing between the light SM quark fields and their heavy Little Higgs quark partners after EWSB.

The mixing of up quark sector is induced also by EWSB as mentioned. Because of the breaking of the $SU(3)$ symmetry as well as the $SU(2)_L \times U(1)_Y$ symmetry afterwards, the light SM quarks and heavy quark partners mix Eq. (B.14). We now take a detailed look at the mass bases of quarks. Before EWSB, the $SU(3)$ state T_0 can be expressed in terms of the mass eigenstate T with mixing terms induced by EWSB as $T_0 = T + \delta_{u_i} u_i'$ with $i = 1, 2, 3$, of which δ_{u_i} are given by

$$\delta_u = \frac{v}{\sqrt{2}\Lambda} \frac{\lambda_u^{T^c u}}{\sqrt{\lambda_1^{t2} c_\beta^2 + \lambda_2^{t2} s_\beta^2}}, \quad \delta_c = \frac{v}{\sqrt{2}\Lambda} \frac{\lambda_u^{T^c c}}{\sqrt{\lambda_1^{t2} c_\beta^2 + \lambda_2^{t2} s_\beta^2}}, \quad \delta_t = \frac{v}{\sqrt{2}f} \frac{s_\beta c_\beta (\lambda_1^{t2} - \lambda_2^{t2})}{\sqrt{\lambda_1^{t2} c_\beta^2 + \lambda_2^{t2} s_\beta^2}}. \tag{B.18}$$

To suppress the mixing terms of T to u and c, we make the couplings $\lambda_u^{T^c u}$ and $\lambda_u^{T^c c}$ small enough to neglect these mixing terms. Consequently, the relation between the mass and the interaction eigenstates becomes

$$T_0 = T + \Delta_{u_i} u_i, \qquad \Delta_{u_i} = V_{ij}^{u*} \delta_{u_j} \simeq V_{i3}^{u*} \delta_t. \tag{B.19}$$

The up quarks can be expressed as

$$u_{i0} = (1 - \frac{1}{2}|\Delta_{u_i}|^2) u_i - \Delta_{u_i} T, \tag{B.20}$$

where we expect Δ_{u_i} correction might be constrained from quark charged current couplings to the W boson.

Mixing in the down quark sector is similar. The $SU(3)$ state D_0 and S_0 which are the state before EWSB can be written in terms of the mass eigenstates D, S and the SM fermions

in the interacion basis as

$$D_0 = D + \delta_{Dd_i} d'_i, \qquad S_0 = S + \delta_{Sd_i} d'_i, \tag{B.21}$$

where $i = 1,\ 2,\ 3$ and

$$\delta_{Dd} = \frac{-v}{\sqrt{2}f} \frac{s_\beta c_\beta (\lambda_1^{d2} - \lambda_2^{d2})}{\sqrt{\lambda_1^{d2} c_\beta^2 + \lambda_2^{d2} s_\beta^2}}, \qquad \delta_{Ds} = 0, \qquad \delta_{Db} = \frac{v}{\sqrt{2}\Lambda} \frac{\lambda_b^{D^c}}{\sqrt{\lambda_1^{d2} c_\beta^2 + \lambda_2^{d2} s_\beta^2}}, \tag{B.22}$$

$$\delta_{Sd} = 0, \qquad \delta_{Ss} = \frac{-v}{\sqrt{2}f} \frac{s_\beta c_\beta (\lambda_1^{s2} - \lambda_2^{s2})}{\sqrt{\lambda_1^{s2} c_\beta^2 + \lambda_2^{s2} s_\beta^2}}, \qquad \delta_{Sb} = \frac{v}{\sqrt{2}\Lambda} \frac{\lambda_b^{S^c}}{\sqrt{\lambda_1^{s2} c_\beta^2 + \lambda_2^{s2} s_\beta^2}}. \tag{B.23}$$

Thanks to the Collective Symmetry Breaking mechanism, the mixing between $D - s$ and $S - d$ became zero. To suppress the mixing of D, S with b quark, we assume $\lambda_b^{D^c}$ and $\lambda_b^{S^c}$ to be small. Also, to be consistent with the SM, one of $\lambda_{1,2}^d$ and $\lambda_{1,2}^s$ is expected to be small from Eq. (B.15), which can result in tiny mixing effects in the down quark sector much like the mixing effects in the neutrino sector. Then,

$$\delta_{Dd} \simeq \delta_{Ss} \simeq \frac{v}{\sqrt{2} t_\beta f} = -\delta_\nu. \tag{B.24}$$

The D and S states become

$$\begin{aligned} D_0 &= D + \Delta_{Dd_i} d_i, \qquad \Delta_{Dd_i} = V_{ij}^{d*} \delta_{Dd_j} \simeq -V_{i1}^{d*} \delta_\nu, \\ S_0 &= S + \Delta_{Sd_i} d_i, \qquad \Delta_{Sd_i} = V_{ij}^{d*} \delta_{Sd_j} \simeq -V_{i2}^{d*} \delta_\nu, \end{aligned} \tag{B.25}$$

Considering the mixings, the down quarks in the mass basis become

$$d_{i0} = (1 - \frac{1}{2}|\Delta_{Dd_i}|^2 - \frac{1}{2}|\Delta_{Sd_i}|^2) d_i - \Delta_{Dd_i} D - \Delta_{Sd_i} S, \tag{B.26}$$

where $|\Delta_{Dd_i}|^2$ and $|\Delta_{Sd_i}|^2$ terms are left of order v^2/f^2.

Appendix C.

Full List of CheckMATE Analyses

CheckMATE identifier	Search designed for	#SR	L_{int} Ref.
	$\sqrt{s} = 8\,\text{TeV}$		
atlas_1308_1841	New phenomena in final states with large jet multiplicities and $\not{E}_T$	13	20.3 [73]
atlas_1308_2631	Direct $\tilde{t}/\tilde{b}$ pair production in final states with $\not{E}_T$ and two b-jets	6	20.1 [74]
atlas_1402_7029	Direct production of $\tilde{\chi}^{\pm}/\tilde{\chi}^0$ in events with 3 ℓ and $\not{E}_T$	20	20.3 [75]
atlas_1403_4853	Direct $\tilde{t}$ pair production in final states with 2ℓ	12	20.3 [76]
atlas_1403_5222	Direct $\tilde{t}$ pair production in events with a Z, b-jets and $\not{E}_T$	5	20.3 [77]
atlas_1404_2500	Supersymmetry in final states with jets and 2 SS ℓ or 3ℓ	5	20.3 [78]
atlas_1405_7875	Search for $\tilde{q}$ and $\tilde{g}$ in final states with jets and $\not{E}_T$	15	20.3 [79]
atlas_1407_0583	$\tilde{t}$ pair production in final states with 1 isol. ℓ, jets and $\not{E}_T$	27	20.3 [80]
atlas_1407_0608	Pair produced 3rd gen. squarks decaying via c or compressed scenarios	3	20.3 [81]
atlas_1411_1559	New phenomena in events with a photon and $\not{E}_T$	1	20.3 [82]
atlas_1501_07110	Direct production of $\tilde{\chi}^{\pm}/\tilde{\chi}^0$ decaying into a Higgs boson	12	20.3 [83]
atlas_1502_01518	New phenena in final states with an energetic jet and large $\not{E}_T$	9	20.3 [84]
atlas_1503_03290	Supersymmetry in events with an SFOS ℓ pair, jets and large $\not{E}_T$	1	20.3 [85]
atlas_1506_08616	Direct Pair production third generation squarks	12	20.0 [86]
atlas_conf_2012_104	Supersymmetry in final states with jets, 1 isolated lepton and $\not{E}_T$	2	5.8 [87]
atlas_conf_2013_024	Directo $\tilde{t}$ pair production in the all-hadronic $t\bar{t} + \not{E}_T$ final state	3	20.5 [88]
atlas_conf_2013_049	Direct $\tilde{\ell}/\tilde{\chi}^{\pm}$ production in final states with 2 OS ℓ, no jets and $\not{E}_T$	9	20.3 [89]
atlas_conf_2013_061	Strongly produced Supersymmetric particles with ≥ 3 b-jets and $\not{E}_T$	9	20.1 [90]
atlas_conf_2013_089	Strongly produced Supersymmetric particles decaying into 2 leptons	12	20.3 [91]
atlas_conf_2015_004	Invisibly decaying Higgs bosons produced in vector boson fusion	1	20.3 [92]
atlas_conf_2012_147	New phenomena in monojets plus $\not{E}_T$	4	10.0 [93]
atlas_conf_2013_035	Direct production of $\tilde{\chi}^{\pm}/\tilde{\chi}^0$ in events with 3 leptons and $\not{E}_T$	6	20.7 [94]
atlas_conf_2013_037	Direct $\tilde{t}$ pair production in final states with 1 isolated ℓ, jets and $\not{E}_T$	6	20.7 [95]
atlas_conf_2013_047	$\tilde{q}$ and $\tilde{g}$ in final states with jets and $\not{E}_T$	10	20.3 [96]
cms_1303_2985	Supersymmetry in hadronic final states with b-jets and $\not{E}_T$ using α_T	59	11.7 [97]
cms_1408_3583	Dark Matter, Extra Dimensions and Unparticles in monojet events	7	19.7 [98]
cms_1502_06031	New Physics in events with 2ℓ, jets and $\not{E}_T$	6	19.4 [99]
cms_1504_03198	Dark Matter produced in association with $t\bar{t}$ in final states with 1ℓ	1	19.7 [100]
cms_sus_13_016	Supersymmetry in events with 2 OS ℓ, many jets, b-jets and large $\not{E}_T$	1	19.5 [101]
cms_exo_14_014	Heavy Majorana neutrinos in events with SS dileptons and jets	16	19.7 [102]

Table C.1.: Full list of all CheckMATE analyses for 8 TeV of the center-of-mass-energy used for this study. The column labelled #SR yields the number of signal regions. Entries for the integrated luminosities L_{int} are given in fb^{-1}.

CheckMATE identifier	Search designed for	#SR	L_{int}	Ref.
	$\sqrt{s} = 13\,\text{TeV}$			
atlas_1602_09058	Supersymmetry in final states with jets and two SS leptons or 3 leptons	4	3.2	[103]
atlas_1604_01306	New phenomena in events with a photon and $\not{E}_T$	1	3.2	[104]
atlas_1604_07773	New phenomena in final states with an energetic jet and large $\not{E}_T$	13	3.2	[105]
atlas_1605_03814	$\tilde{q}$ and $\tilde{g}$ in final states with jets and $\not{E}_T$	7	3.2	[106]
atlas_1605_04285	Gluinos in events with an isolated lepton, jets and $\not{E}_T$	7	3.3	[107]
atlas_1605_09318	Pair production of $\tilde{g}$ decaying via $\tilde{t}$ or $\tilde{b}$ in events with b-jets and $\not{E}_T$	8	3.3	[108]
atlas_1606_03903	$\tilde{t}$ in final states with one isolated lepton, jets and $\not{E}_T$	3	3.2	[109]
atlas_1609_01599	Measurement of ttV cross sections in multilepton final states	9	3.2	[110]
atlas_conf_2015_082	Supersymmety in events with leptonically decaying Z, jets and $\not{E}_T$	1	3.2	[111]
atlas_conf_2016_013	Vector-like t pairs or 4 t in final states with leptons and jets	10	3.2	[112]
atlas_conf_2016_050	$\tilde{t}$ in final states with one isolated lepton, jets and $\not{E}_T$	5	13.3	[113]
atlas_conf_2016_054	$\tilde{q}$, $\tilde{g}$ in events with an isolated lepton, jets and $\not{E}_T$	10	14.8	[69]
atlas_conf_2016_076	Direct $\tilde{t}$ pair production and DM production in final states with 2ℓ	6	13.3	[114]
atlas_conf_2016_078	Further searches for $\tilde{q}$ and $\tilde{g}$ in final states with jets and $\not{E}_T$	13	13.3	[115]
atlas_conf_2016_096	Supersymmetry in events with 2ℓ or 3ℓ and $\not{E}_T$	8	13.3	[68]
atlas_conf_2017_022	$\tilde{q}$, $\tilde{g}$ in final states with jets and $\not{E}_T$	24	36.1	[70]
atlas_conf_2017_039	Electroweakino production in final states with 2 or 3 leptons	37	36.1	[71]
atlas_conf_2017_040	Dark Matter or invisibly decaying h, produced in associated with a Z	2	36.1	[116]
cms_pas_sus_15_011	New physics in final states with an OSSF lepton pair, jets and $\not{E}_T$	47	2.2	[117]
	$\sqrt{s} = 14\,\text{TeV}$			
atlas_phys_pub_2013_011	Search for Supersymmetry at the high luminosity LHC ($\tilde{t}$ sector)	4	3000	[118]
atlas_2014_010_hl_3l	Search for Supersymmetry at the high luminosity LHC ($\tilde{\chi}^{\pm}/\tilde{\chi}^{0}$ sector)	1	3000	[119]
atlas_phys_2014_010_sq_hl	Search for Supersymmetry at the high luminosity LHC ($\tilde{q}/\tilde{g}$ sector)	10	3000	[119]
dilepton_hl*	Custom Search for $\tilde{\ell}/\tilde{\chi}^{\pm}$ in final states with 2 leptons and $\not{E}_T$	9	3000	[120]
atlas_14tev_monojet*	Custom Search for DM in final states with an energetic jet and $\not{E}_T$	5	3000	[121]

Table C.2.: Full list of all CheckMATE analyses used for this study. The column labelled #SR yields the number of signal regions. Entries for the integrated luminosities L_{int} are given in fb^{-1}.

Bibliography

[1] LHC Higgs Cross Section Working Group collaboration, D. de Florian et al., *Handbook of LHC Higgs Cross Sections: 4. Deciphering the Nature of the Higgs Sector*, 1610.07922.

[2] D. Dercks, G. Moortgat-Pick, J. Reuter and S. Y. Shim, *The fate of the Littlest Higgs Model with T-parity under 13 TeV LHC Data*, 1801.06499.

[3] F. Englert and R. Brout, *Broken Symmetry and the Mass of Gauge Vector Mesons*, *Phys. Rev. Lett.* **13** (1964) 321–323.

[4] P. W. Higgs, *Broken Symmetries and the Masses of Gauge Bosons*, *Phys. Rev. Lett.* **13** (1964) 508–509.

[5] G. S. Guralnik, C. R. Hagen and T. W. B. Kibble, *Global Conservation Laws and Massless Particles*, *Phys. Rev. Lett.* **13** (1964) 585–587.

[6] F. Bezrukov, M. Yu. Kalmykov, B. A. Kniehl and M. Shaposhnikov, *Higgs Boson Mass and New Physics*, *JHEP* **10** (2012) 140, [1205.2893].

[7] G. Degrassi, S. Di Vita, J. Elias-Miro, J. R. Espinosa, G. F. Giudice, G. Isidori et al., *Higgs mass and vacuum stability in the Standard Model at NNLO*, *JHEP* **08** (2012) 098, [1205.6497].

[8] S. Alekhin, A. Djouadi and S. Moch, *The top quark and Higgs boson masses and the stability of the electroweak vacuum*, *Phys. Lett.* **B716** (2012) 214–219, [1207.0980].

[9] N. Arkani-Hamed, A. G. Cohen and H. Georgi, *Electroweak symmetry breaking from dimensional deconstruction*, *Phys. Lett.* **B513** (2001) 232–240, [hep-ph/0105239].

[10] N. Arkani-Hamed, A. G. Cohen, T. Gregoire and J. G. Wacker, *Phenomenology of electroweak symmetry breaking from theory space*, *JHEP* **08** (2002) 020, [hep-ph/0202089].

[11] J. F. Gunion, H. E. Haber, G. L. Kane and S. Dawson, *The Higgs Hunter's Guide*, *Front. Phys.* **80** (2000) 1–404.

[12] F. W. J. Koks and J. Van Klinken, *Investigation on β-polarization at low velocities with β-particles from the decay of tritium*, *Nucl. Phys.* **A272** (1976) 61–81.

[13] M. Bardon, P. Norton, J. Peoples, A. M. Sachs and J. Lee-Franzini, *Measurement of the momentum spectrum of positrons from muon decay*, *Phys. Rev. Lett.* **14** (1965) 449–453.

[14] J. G. H. de Groot et al., *Inclusive Interactions of High-Energy Neutrinos and anti-neutrinos in Iron*, *Z. Phys.* **C1** (1979) 143.

[15] P. Langacker, *The standard model and beyond*. 2010.

[16] M. E. Peskin and T. Takeuchi, *Estimation of oblique electroweak corrections*, *Phys. Rev.* **D46** (1992) 381–409.

[17] R. Barbieri, A. Pomarol, R. Rattazzi and A. Strumia, *Electroweak symmetry breaking after LEP-1 and LEP-2*, *Nucl. Phys.* **B703** (2004) 127–146, [hep-ph/0405040].

[18] R. Barbieri, B. Bellazzini, V. S. Rychkov and A. Varagnolo, *The Higgs boson from an extended symmetry*, *Phys. Rev.* **D76** (2007) 115008, [0706.0432].

[19] B. W. Lee, C. Quigg and H. B. Thacker, *Weak Interactions at Very High-Energies: The Role of the Higgs Boson Mass*, *Phys. Rev.* **D16** (1977) 1519.

[20] B. W. Lee, C. Quigg and H. B. Thacker, *The Strength of Weak Interactions at Very High-Energies and the Higgs Boson Mass*, *Phys. Rev. Lett.* **38** (1977) 883–885.

[21] B. Grzadkowski, M. Iskrzynski, M. Misiak and J. Rosiek, *Dimension-Six Terms in the Standard Model Lagrangian*, *JHEP* **10** (2010) 085, [1008.4884].

[22] B. Henning, X. Lu and H. Murayama, *How to use the Standard Model effective field theory*, *JHEP* **01** (2016) 023, [1412.1837].

[23] W. Kilian, *Electroweak symmetry breaking: The bottom-up approach*, *Springer Tracts Mod. Phys.* **198** (2003) 1–113.

[24] C. Degrande, N. Greiner, W. Kilian, O. Mattelaer, H. Mebane, T. Stelzer et al., *Effective Field Theory: A Modern Approach to Anomalous Couplings*, *Annals Phys.* **335** (2013) 21–32, [1205.4231].

[25] W. Buchmuller and D. Wyler, *Effective Lagrangian Analysis of New Interactions and Flavor Conservation*, *Nucl. Phys.* **B268** (1986) 621–653.

[26] H. Georgi, *On-shell effective field theory*, *Nucl. Phys.* **B361** (1991) 339–350.

[27] K. G. Wilson, *Renormalization group and critical phenomena. 1. Renormalization group and the Kadanoff scaling picture*, *Phys. Rev.* **B4** (1971) 3174–3183.

[28] S. Weinberg, *Phenomenological Lagrangians*, *Physica* **A96** (1979) 327–340.

[29] A. Alloul, N. D. Christensen, C. Degrande, C. Duhr and B. Fuks, *FeynRules 2.0 - A complete toolbox for tree-level phenomenology*, *Comput. Phys. Commun.* **185** (2014) 2250–2300, [1310.1921].

[30] W. Kilian, T. Ohl and J. Reuter, *WHIZARD: Simulating Multi-Particle Processes at LHC and ILC*, *Eur. Phys. J.* **C71** (2011) 1742, [0708.4233].

[31] M. Moretti, T. Ohl and J. Reuter, *O'Mega: An Optimizing matrix element generator*, hep-ph/0102195.

[32] B. Chokoufe Nejad, T. Ohl and J. Reuter, *Simple, parallel virtual machines for extreme computations*, *Comput. Phys. Commun.* **196** (2015) 58–69, [1411.3834].

[33] W. Kilian, J. Reuter, S. Schmidt and D. Wiesler, *An Analytic Initial-State Parton Shower*, *JHEP* **04** (2012) 013, [1112.1039].

[34] W. Kilian, J. Reuter and T. Robens, *NLO Event Generation for Chargino Production at the ILC*, *Eur. Phys. J.* **C48** (2006) 389–400, [hep-ph/0607127].

[35] T. Robens, J. Kalinowski, K. Rolbiecki, W. Kilian and J. Reuter, *(N)LO Simulation of Chargino Production and Decay*, *Acta Phys. Polon.* **B39** (2008) 1705–1714, [0803.4161].

[36] T. Binoth, N. Greiner, A. Guffanti, J. Reuter, J. P. Guillet and T. Reiter, *Next-to-leading order QCD corrections to pp –¿ b anti-b b anti-b + X at the LHC: the quark induced case*, *Phys. Lett.* **B685** (2010) 293–296, [0910.4379].

[37] N. Greiner, A. Guffanti, T. Reiter and J. Reuter, *NLO QCD corrections to the production of two bottom-antibottom pairs at the LHC*, *Phys. Rev. Lett.* **107** (2011) 102002, [1105.3624].

[38] B. Chokoufé Nejad, W. Kilian, J. M. Lindert, S. Pozzorini, J. Reuter and C. Weiss, *NLO QCD predictions for off-shell $t\bar{t}$ and $t\bar{t}H$ production and decay at a linear collider*, *JHEP* **12** (2016) 075, [1609.03390].

[39] F. Bach, B. C. Nejad, A. Hoang, W. Kilian, J. Reuter, M. Stahlhofen et al., *Fully-differential Top-Pair Production at a Lepton Collider: From Threshold to Continuum*, 1712.02220.

[40] N. D. Christensen, C. Duhr, B. Fuks, J. Reuter and C. Speckner, *Introducing an interface between WHIZARD and FeynRules*, *Eur. Phys. J.* **C72** (2012) 1990, [1010.3251].

[41] M. Perelstein, *Little Higgs models and their phenomenology*, *Prog. Part. Nucl. Phys.* **58** (2007) 247–291, [hep-ph/0512128].

[42] N. Arkani-Hamed, A. G. Cohen and H. Georgi, *(De)constructing dimensions*, *Phys. Rev. Lett.* **86** (2001) 4757–4761, [hep-th/0104005].

[43] N. Arkani-Hamed, A. G. Cohen, E. Katz and A. E. Nelson, *The Littlest Higgs*, *JHEP* **07** (2002) 034, [hep-ph/0206021].

[44] T. Han, H. E. Logan, B. McElrath and L.-T. Wang, *Phenomenology of the little Higgs model*, *Phys. Rev.* **D67** (2003) 095004, [hep-ph/0301040].

[45] J. Hubisz, P. Meade, A. Noble and M. Perelstein, *Electroweak precision constraints on the littlest Higgs model with T parity*, *JHEP* **01** (2006) 135, [hep-ph/0506042].

[46] M. Schmaltz, *The Simplest little Higgs*, *JHEP* **08** (2004) 056, [hep-ph/0407143].

[47] T. Han, H. E. Logan and L.-T. Wang, *Smoking-gun signatures of little Higgs models*, *JHEP* **01** (2006) 099, [hep-ph/0506313].

[48] S. R. Coleman, J. Wess and B. Zumino, *Structure of phenomenological Lagrangians. 1.*, *Phys. Rev.* **177** (1969) 2239–2247.

[49] C. G. Callan, Jr., S. R. Coleman, J. Wess and B. Zumino, *Structure of phenomenological Lagrangians. 2.*, *Phys. Rev.* **177** (1969) 2247–2250.

[50] S. R. Coleman and E. J. Weinberg, *Radiative Corrections as the Origin of Spontaneous Symmetry Breaking*, *Phys. Rev.* **D7** (1973) 1888–1910.

[51] W. Kilian and J. Reuter, *The Low-energy structure of little Higgs models*, *Phys. Rev.* **D70** (2004) 015004, [hep-ph/0311095].

[52] H.-C. Cheng and I. Low, *TeV symmetry and the little hierarchy problem*, *JHEP* **09** (2003) 051, [hep-ph/0308199].

[53] H.-C. Cheng and I. Low, *Little hierarchy, little Higgses, and a little symmetry*, *JHEP* **08** (2004) 061, [hep-ph/0405243].

[54] C. T. Hill and R. J. Hill, *T^- parity violation by anomalies*, *Phys. Rev.* **D76** (2007) 115014, [0705.0697].

[55] C. T. Hill and R. J. Hill, *Topological Physics of Little Higgs Bosons*, *Phys. Rev.* **D75** (2007) 115009, [hep-ph/0701044].

[56] J. Hubisz and P. Meade, *Phenomenology of the littlest Higgs with T-parity*, *Phys. Rev.* **D71** (2005) 035016, [hep-ph/0411264].

[57] L. Wang, J. M. Yang and J. Zhu, *Dark matter in the little Higgs model under current experimental constraints from the LHC, Planck, and Xenon data*, *Phys. Rev.* **D88** (2013) 075018, [1307.7780].

[58] L. Wu, B. Yang and M. Zhang, *Little Higgs Dark Matter after PandaX-II/LUX 2016 and LHC Run-1*, *JHEP* **12** (2016) 152, [1607.06355].

[59] A. Freitas, P. Schwaller and D. Wyler, *Consequences of T-parity breaking in the Littlest Higgs model*, *JHEP* **09** (2008) 013, [0806.3674].

[60] K. Cheung and J. Song, *Light pseudoscalar eta and H —¿ eta eta decay in the simplest little Higgs mode*, *Phys. Rev.* **D76** (2007) 035007, [hep-ph/0611294].

[61] W. Kilian, D. Rainwater and J. Reuter, *Pseudo-axions in little Higgs models*, *Phys. Rev.* **D71** (2005) 015008, [hep-ph/0411213].

[62] W. Kilian, D. Rainwater and J. Reuter, *Distinguishing little-Higgs product and simple group models at the LHC and ILC*, *Phys. Rev.* **D74** (2006) 095003, [hep-ph/0609119].

[63] M. Tonini, *Beyond the Standard Higgs at the LHC: present constraints on Little Higgs models and future prospects*. PhD thesis, U. Hamburg, Dept. Phys., 2014.

[64] J. Reuter, M. Tonini and M. de Vries, *Littlest Higgs with T-parity: Status and Prospects*, *JHEP* **02** (2014) 053, [1310.2918].

[65] J. Reuter and M. Tonini, *Can the 125 GeV Higgs be the Little Higgs?*, *JHEP* **02** (2013) 077, [1212.5930].

[66] J. Alwall, R. Frederix, S. Frixione, V. Hirschi, F. Maltoni, O. Mattelaer et al., *The automated computation of tree-level and next-to-leading order differential cross sections, and their matching to parton shower simulations*, *JHEP* **07** (2014) 079, [1405.0301].

[67] D. Schmeier, *Automatised Constraints on New Physics at the LHC and Beyond*. PhD thesis, Bonn U., 2016-06-06.

[68] ATLAS collaboration, T. A. collaboration, *Search for supersymmetry with two and three leptons and missing transverse momentum in the final state at $\sqrt{s} = 13$ TeV with the ATLAS detector*, .

[69] ATLAS collaboration, T. A. collaboration, *Search for squarks and gluinos in events with an isolated lepton, jets and missing transverse momentum at $\sqrt{s} = 13$ TeV with the ATLAS detector*, .

[70] ATLAS collaboration, T. A. collaboration, *Search for squarks and gluinos in final states with jets and missing transverse momentum using 36 fb^{-1} of $\sqrt{s} = 13$ TeV pp collision data with the ATLAS detector*, .

[71] ATLAS collaboration, T. A. collaboration, *Search for electroweak production of supersymmetric particles in the two and three lepton final state at $\sqrt{s} = 13$ TeV with the ATLAS detector*, .

[72] S. L. Glashow, J. Iliopoulos and L. Maiani, *Weak Interactions with Lepton-Hadron Symmetry*, *Phys. Rev.* **D2** (1970) 1285–1292.

[73] ATLAS collaboration, G. Aad et al., *Search for new phenomena in final states with large jet multiplicities and missing transverse momentum at $\sqrt{s}$=8 TeV proton-proton collisions using the ATLAS experiment*, *JHEP* **10** (2013) 130, [1308.1841].

[74] ATLAS collaboration, G. Aad et al., *Search for direct third-generation squark pair production in final states with missing transverse momentum and two b-jets in $\sqrt{s} = 8$ TeV pp collisions with the ATLAS detector*, *JHEP* **10** (2013) 189, [1308.2631].

[75] ATLAS collaboration, G. Aad et al., *Search for direct production of charginos and neutralinos in events with three leptons and missing transverse momentum in $\sqrt{s} =$ 8TeV pp collisions with the ATLAS detector*, *JHEP* **04** (2014) 169, [1402.7029].

[76] ATLAS collaboration, G. Aad et al., *Search for direct top-squark pair production in final states with two leptons in pp collisions at $\sqrt{s} = 8$ TeV with the ATLAS detector*, *JHEP* **06** (2014) 124, [1403.4853].

[77] ATLAS collaboration, G. Aad et al., *Search for direct top squark pair production in events with a Z boson, b-jets and missing transverse momentum in $\sqrt{s} = 8$ TeV pp collisions with the ATLAS detector*, *Eur. Phys. J.* **C74** (2014) 2883, [1403.5222].

[78] ATLAS collaboration, G. Aad et al., *Search for supersymmetry at $\sqrt{s}$=8 TeV in final states with jets and two same-sign leptons or three leptons with the ATLAS detector*, *JHEP* **06** (2014) 035, [1404.2500].

[79] ATLAS collaboration, G. Aad et al., *Search for squarks and gluinos with the ATLAS detector in final states with jets and missing transverse momentum using $\sqrt{s} = 8$ TeV proton–proton collision data*, *JHEP* **09** (2014) 176, [1405.7875].

[80] ATLAS collaboration, G. Aad et al., *Search for top squark pair production in final states with one isolated lepton, jets, and missing transverse momentum in $\sqrt{s}$ =8 TeV pp collisions with the ATLAS detector*, *JHEP* **11** (2014) 118, [1407.0583].

[81] ATLAS collaboration, G. Aad et al., *Search for pair-produced third-generation squarks decaying via charm quarks or in compressed supersymmetric scenarios in pp collisions at $\sqrt{s} = 8$ TeV with the ATLAS detector*, *Phys. Rev.* **D90** (2014) 052008, [1407.0608].

[82] ATLAS collaboration, G. Aad et al., *Search for new phenomena in events with a photon and missing transverse momentum in pp collisions at $\sqrt{s} = 8$ TeV with the ATLAS detector*, *Phys. Rev.* **D91** (2015) 012008, [1411.1559].

[83] ATLAS collaboration, G. Aad et al., *Search for direct pair production of a chargino and a neutralino decaying to the 125 GeV Higgs boson in $\sqrt{s} = 8$ TeV pp collisions with the ATLAS detector*, *Eur. Phys. J.* **C75** (2015) 208, [1501.07110].

[84] ATLAS collaboration, G. Aad et al., *Search for new phenomena in final states with an energetic jet and large missing transverse momentum in pp collisions at $\sqrt{s}$ =8 TeV with the ATLAS detector*, *Eur. Phys. J.* **C75** (2015) 299, [1502.01518].

[85] ATLAS collaboration, G. Aad et al., *Search for supersymmetry in events containing a same-flavour opposite-sign dilepton pair, jets, and large missing transverse momentum in $\sqrt{s} = 8$ TeV pp collisions with the ATLAS detector*, *Eur. Phys. J.* **C75** (2015) 318, [1503.03290].

[86] ATLAS collaboration, G. Aad et al., *ATLAS Run 1 searches for direct pair production of third-generation squarks at the Large Hadron Collider*, *Eur. Phys. J.* **C75** (2015) 510, [1506.08616].

[87] ATLAS collaboration, A. Collaboration, *Search for supersymmetry at $\sqrt{s} = 8$ TeV in final states with jets, missing transverse momentum and one isolated lepton*, .

[88] ATLAS collaboration, A. Collaboration, *Search for direct production of the top squark in the all-hadronic ttbar + etmiss final state in 21 fb-1 of p-pcollisions at $\sqrt(s) = 8$ TeV with the ATLAS detector*, .

[89] ATLAS collaboration, T. A. collaboration, *Search for direct-slepton and direct-chargino production in final states with two opposite-sign leptons, missing transverse momentum and no jets in 20/fb of pp collisions at $\sqrt(s) = 8$ TeV with the ATLAS detector*, .

[90] ATLAS collaboration, T. A. collaboration, *Search for strong production of supersymmetric particles in final states with missing transverse momentum and at least three b-jets using 20.1/fb of pp collisions at $\sqrt{s} = 8$ TeV with the ATLAS Detector.*, .

[91] ATLAS collaboration, T. A. collaboration, *Search for strongly produced supersymmetric particles in decays with two leptons at $\sqrt{s} = 8$ TeV*, .

[92] ATLAS collaboration, T. A. collaboration, *Search for an Invisibly Decaying Higgs Boson Produced via Vector Boson Fusion in pp Collisions at $\sqrt{s} = 8$ TeV using the ATLAS Detector at the LHC*, .

[93] ATLAS collaboration, A. Collaboration, *Search for New Phenomena in Monojet plus Missing Transverse Momentum Final States using 10fb-1 of pp Collisions at $\sqrt{s} = 8$ TeV with the ATLAS detector at the LHC*, .

[94] ATLAS collaboration, A. Collaboration, *Search for direct production of charginos and neutralinos in events with three leptons and missing transverse momentum in 21fb^{-1} of pp collisions at $\sqrt{s} = 8$ TeV with the ATLAS detector*, .

[95] ATLAS collaboration, A. Collaboration, *Search for direct top squark pair production in final states with one isolated lepton, jets, and missing transverse momentum in sqrts = 8 TeV pp collisions using 21 fb^{-1} of ATLAS data*, .

[96] ATLAS collaboration, T. A. collaboration, *Search for squarks and gluinos with the ATLAS detector in final states with jets and missing transverse momentum and 20.3 fb^{-1} of $\sqrt{s} = 8$ TeV proton-proton collision data*, .

[97] CMS collaboration, S. Chatrchyan et al., *Search for supersymmetry in hadronic final states with missing transverse energy using the variables α_T and b-quark multiplicity in pp collisions at $\sqrt{s} = 8$ TeV*, *Eur. Phys. J.* **C73** (2013) 2568, [1303.2985].

[98] CMS collaboration, V. Khachatryan et al., *Search for dark matter, extra dimensions,*

and unparticles in monojet events in proton-proton collisions at $\sqrt{s} = 8$ TeV, *Eur. Phys. J.* **C75** (2015) 235, [1408.3583].

[99] CMS collaboration, V. Khachatryan et al., *Search for Physics Beyond the Standard Model in Events with Two Leptons, Jets, and Missing Transverse Momentum in pp Collisions at $\sqrt{s} = 8$ TeV*, *JHEP* **04** (2015) 124, [1502.06031].

[100] CMS collaboration, V. Khachatryan et al., *Search for the production of dark matter in association with top-quark pairs in the single-lepton final state in proton-proton collisions at $\sqrt{s} = 8$ TeV*, *JHEP* **06** (2015) 121, [1504.03198].

[101] CMS collaboration, C. Collaboration, *Search for supersymmetry in pp collisions at $\sqrt{s}$ = 8 TeV in events with two opposite sign leptons, large number of jets, b-tagged jets, and large missing transverse energy.*, .

[102] CMS collaboration, V. Khachatryan et al., *Search for heavy Majorana neutrinos in $e^{\pm}e^{\pm}$+ jets and $e^{\pm}$ $\mu^{\pm}$+ jets events in proton-proton collisions at $\sqrt{s} = 8$ TeV*, *JHEP* **04** (2016) 169, [1603.02248].

[103] ATLAS collaboration, G. Aad et al., *Search for supersymmetry at $\sqrt{s} = 13$ TeV in final states with jets and two same-sign leptons or three leptons with the ATLAS detector*, *Eur. Phys. J.* **C76** (2016) 259, [1602.09058].

[104] ATLAS collaboration, M. Aaboud et al., *Search for new phenomena in events with a photon and missing transverse momentum in pp collisions at $\sqrt{s} = 13$ TeV with the ATLAS detector*, *JHEP* **06** (2016) 059, [1604.01306].

[105] ATLAS collaboration, M. Aaboud et al., *Search for new phenomena in final states with an energetic jet and large missing transverse momentum in pp collisions at $\sqrt{s} = 13$ TeV using the ATLAS detector*, *Phys. Rev.* **D94** (2016) 032005, [1604.07773].

[106] ATLAS collaboration, M. Aaboud et al., *Search for squarks and gluinos in final states with jets and missing transverse momentum at $\sqrt{s}$ = 13 TeV with the ATLAS detector*, *Eur. Phys. J.* **C76** (2016) 392, [1605.03814].

[107] ATLAS collaboration, G. Aad et al., *Search for gluinos in events with an isolated lepton, jets and missing transverse momentum at $\sqrt{s}$ = 13 Te V with the ATLAS detector*, *Eur. Phys. J.* **C76** (2016) 565, [1605.04285].

[108] ATLAS collaboration, G. Aad et al., *Search for pair production of gluinos decaying via stop and sbottom in events with b-jets and large missing transverse momentum in pp collisions at $\sqrt{s} = 13$ TeV with the ATLAS detector*, *Phys. Rev.* **D94** (2016) 032003, [1605.09318].

[109] ATLAS collaboration, M. Aaboud et al., *Search for top squarks in final states with one isolated lepton, jets, and missing transverse momentum in $\sqrt{s} = 13$ TeV pp collisions with the ATLAS detector*, *Phys. Rev.* **D94** (2016) 052009, [1606.03903].

[110] ATLAS collaboration, M. Aaboud et al., *Measurement of the $t\bar{t}Z$ and $t\bar{t}W$ production cross sections in multilepton final states using 3.2 fb^{-1} of pp collisions at $\sqrt{s}$ = 13 TeV with the ATLAS detector*, *Eur. Phys. J.* **C77** (2017) 40, [1609.01599].

[111] T. A. collaboration, *A search for Supersymmetry in events containing a leptonically*

decaying Z boson, jets and missing transverse momentum in $\sqrt{s} = 13$ *TeV pp collisions with the ATLAS detector*, .

[112] T. A. collaboration, *Search for production of vector-like top quark pairs and of four top quarks in the lepton-plus-jets final state in pp collisions at* $\sqrt{s} = 13$ *TeV with the ATLAS detector*, .

[113] ATLAS collaboration, T. A. collaboration, *Search for top squarks in final states with one isolated lepton, jets, and missing transverse momentum in* $\sqrt{s}$ *= 13 TeV pp collisions with the ATLAS detector*, .

[114] ATLAS collaboration, T. A. collaboration, *Search for direct top squark pair production and dark matter production in final states with two leptons in* $\sqrt{s} = 13$ *TeV pp collisions using 13.3* fb^{-1} *of ATLAS data*, .

[115] ATLAS collaboration, T. A. collaboration, *Further searches for squarks and gluinos in final states with jets and missing transverse momentum at* $\sqrt{s}$ *=13 TeV with the ATLAS detector*, .

[116] ATLAS collaboration, T. A. collaboration, *Search for an invisibly decaying Higgs boson or dark matter candidates produced in association with a Z boson in pp collisions at* $\sqrt{s}$ *= 13 TeV with the ATLAS detector*, .

[117] CMS collaboration, C. Collaboration, *Search for new physics in final states with two opposite-sign same-flavor leptons, jets and missing transverse momentum in pp collisions at sqrt(s)=13 TeV*, .

[118] ATLAS collaboration, A. Collaboration, *Prospects for benchmark Supersymmetry searches at the high luminosity LHC with the ATLAS Detector*, Tech. Rep. ATL-PHYS-PUB-2013-011, CERN, Geneva, Sep, 2013.

[119] ATLAS collaboration, A. Collaboration, *Search for Supersymmetry at the high luminosity LHC with the ATLAS experiment*, Tech. Rep. ATL-PHYS-PUB-2014-010, CERN, Geneva, Jul, 2014.

[120] K. Rolbiecki, "Custom Search for Sleptons and Charginos in 2 lepton final states at the high luminosity LHC." `"http://checkmate.hepforge.org/validationNotes/dilepton_HL.pdf"`.

[121] J. S. Kim, O. Lebedev and D. Schmeier, *Higgsophilic gauge bosons and monojets at the LHC*, *JHEP* **11** (2015) 128, [1507.08673].

Acknowledgements

I would like to thank my supervisor, Jürgen Reuter for giving me the opportunity to start this journey as a PhD student in this wonderful research institute DESY, and for all the productive discussions. I also thank Gudrid Moortgat–Pick for agreeing to co-supervise my thesis and for all her kind cheering words. I am also grateful to Christophe Grojean, Gregor Kasieczka and Caren Hagner for being part of the disputation committee.

I am grateful to Daniel Dercks for comments on my thesis and for unofficial training exercises, `So`. I am also thankful to Stefan Liebler, Markus Ebert, Shruti Patel and Jim Talbert for comments on my thesis. I thank Marco Tonini for his Mathematica legacy.

I would also like to thank Stefan Liebler, Markus Ebert, and Johannes Michel for being nice or funny office mates and for big and small tasks you have done for me. During all lunch and coffee times and beyond I enjoyed to be with all other DESY 1b penthouse residents: Markus Diehl, Zoltan Nagy, Frank Tackmann, Goutam Das, Lais Sarem Schunk, Riccardo Nagar, Johannes Michel, Jim Talbert, Ibrahim Akal, Thibaud Vantalon, Stefan Liebler, Markus Ebert, Piotr Pietrulewicz, Marco Tonini, Maarten Buffing, Florian Domingo, Jonathan Gaunt, Peter Drechsel, Maximilian Stahlhofen, Lorena Rothen, Shruti Patel and Shireen Gangal. Moreover I thank other colleagues and friends from the DESY theory group and the WHIZARD collaboration: Anne Ernst, Jan Peter Carstensen, Bijan Chokoufe, Christian Weiss, Vincent Rothe, Pascal Stienemeier, Wolfgang Kilian.

I am grateful to Stefan Liebler, for making the isolated town, in particular our common ex-neighborhood, less boring. Also, I thank `trio infernale` for Shimperator.

I wish to thank my family, Nam, Ki-In and Sim, Young-Jin, for their love and absolute support for every decision I have made.

Eidesstattliche Erklärung

Hiermit erkläre ich an Eides statt, dass ich die vorliegende Dissertationsschrift selbst verfasst und keine anderen als die angegebenen Quellen und Hilfsmittel benutzt habe.

Declaration on oath

I hereby declare, on oath, that I have written the present dissertation by my own and have not used other than the acknowledged resources and aids.

Hamburg, den 16. März 2018 So Young Shim